AD-A073 477 WRIGHT AIR DEVELOPMENT CENTER WRIGHT-PATTERSON AFB OH F/G 18/3
OPERATION UPSHOT-KNOTHOLE NEVADA PROVING GROUND, MARCH-JUNE 195--ETC(U)
OCT 55 E SEVIN

UNCLASSIFIED WADC-TR-55-420 DASA-WT-722 NL

1 OF 2

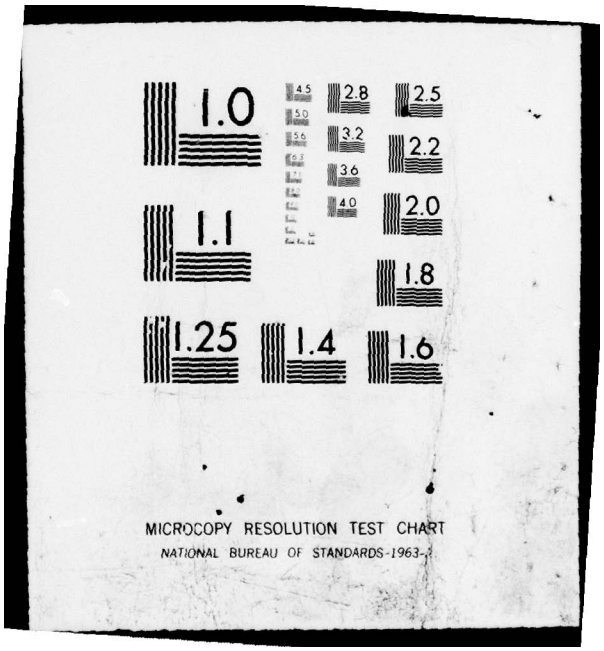
1.0
1.1
1.25
1.4
1.6
1.8
2.0
2.2
2.5
2.8
3.2
3.6
4.0
4.5
5.0
5.6
MICROCOPY RESOLUTION TEST CHART
NATIONAL BUREAU OF STANDARDS-1963-A

AD A073477

DDC ACCESSION NUMBER

DATA SHEET

PHOTOGRAPH

THIS SHEET

II
LEVEL

1
INVENTORY

WT-722
DOCUMENT IDENTIFICATION

DISTRIBUTION STATEMENT A
Approved for public release;
Distribution Unlimited

per telecon w/Betty Fox (DNA Tech Libr, Chief), the classified references contained herein may remain.
D. LaChance (DDA-2)
9-5-79

Accession For
NTIS GRA&I [X]
DDC TAB [ ]
Unannounced [ ]
Justification per Doc.
By
Distribution/
Availability Codes
Dist | Avail and/or special
A

DISTRIBUTION STAMP

DDC
RECEIVED
SEP 5 1979
E

DATE ACCESSIONED

79 08 21 049

DATE RECEIVED IN DDC

PHOTOGRAPH THIS COPY

WT-722

Copy No. 186 A

Operation UPSHOT-KNOTHOLE

NEVADA PROVING GROUNDS

March - June 1953

Project 3.3

TESTS ON THE LOADING OF HORIZONTAL CYLINDRICAL SHAPES

[redacted]

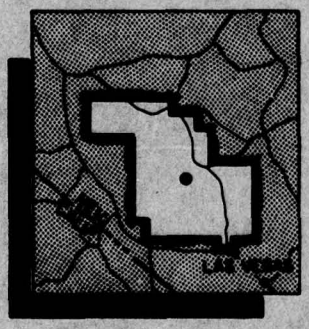

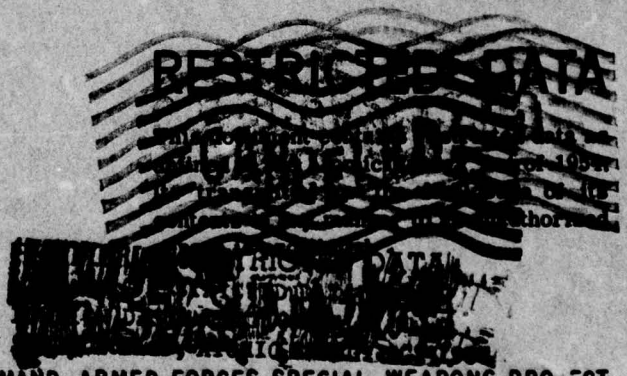

HEADQUARTERS FIELD COMMAND, ARMED FORCES SPECIAL WEAPONS PROJECT
SANDIA BASE, ALBUQUERQUE, NEW MEXICO

[redacted]

Reproduced Direct from Manuscript Copy by
AEC Technical Information Service
Oak Ridge, Tennessee

Inquiries relative to this report may be made to

Chief, Armed Forces Special Weapons Project

Washington, D. C.

[redacted]

UNCLASSIFIED

WT-722

This document consists of 114 pages

No. 186 of 274 copies, Series A

OPERATION UPSHOT-KNOTHOLE

Project 3.3

TEST ON THE LOADING OF HORIZONAL CYLINDRICAL SHAPES

REPORT TO THE TEST DIRECTOR

by

Eugene Sevin

October 1955

WADC-TR-55-420

U. S. Air Force
Wright Air Development Center
Wright-Patterson Air Force Base
Dayton, Ohio

Contract No. AF33(038)-30029

[redacted]

UNCLASSIFIED

ABSTRACT

This report deals with pre- and post-test work on Air Force Structures Program, Project 3.3, Tests on the Loading of Horizontal Cylindrical Shapes. The general objective of this test was to increase the knowledge of blast loadings on structures of cylindrical shape. The specific objectives were to determine the effect of (1) shock strength, (2) size (i.e., scaling), (3) ground proximity, and (4) three-dimensionality.

Five horizontal cylinders of various size and distance above ground were situated in the Mach region of both Shots 9 and 10. Instrumentation consisted of pressure gages and strain gages, the latter representing the output of a net force measurement system.

Most of the test objectives could not be realized. The majority of the pressure data exhibited a considerable and generally random behavior which obscured the effects being studied. In addition, the strain data did not yield any quantitative results; however, it appears to be mainly due to an inability to interpret the data properly. While the methods of data reduction employed have been rather unsuccessful, they by no means constitute an exhaustive study of this problem. Accordingly, it was not possible to reach a definite conclusion as to the feasibility of net force measurement systems whose output represent the response of a complicated dynamic system to an input which is itself the desired information.

The pressure-time distribution was obtained on a cylinder one radius above the ground. The results indicate the build up and clearing times to be essentially the same as for a cylinder in free space, except for a somewhat longer clearing time on the front face.

The analysis of pressure gage data obtained from a vertical cylindrical storage tank, included as part of Air Force Project 3.26.1. Test of the Effects on POL Installations (WT-736), is presented in this report. These results indicate that the finite size of the tank did not affect the front face loading appreciably; the loading on the back side built up somewhat more rapidly than predicted for a two-dimensional cylinder.

FOREWORD

This report is one of the reports presenting the results of the 78 projects participating in the Military Effects Tests Program of Operation UPSHOT-KNOTHOLE, which included 11 test detonations. For readers interested in other pertinent test information, reference is made to WT-782, Summary Report of the Technical Director, Military Effects Program. This summary report includes the following information of possible general interest.

a. An over-all description of each detonation, including yield, height of burst, ground zero location, time of detonation, ambient atmospheric conditions at detonation, etc., for the 11 shots.

b. Compilation and correlation of all project results on the basic measurements of blast and shock, thermal radiation, and nuclear radiation.

c. Compilation and correlation of the various project results on weapons effects.

d. A summary of each project, including objectives and results.

e. A complete listing of all reports covering the Military Effects Tests Program.

PREFACE

In a letter dated 12 March 1952, the Air Materiel Command was requested by Air Research and Development Command to submit for testing in Operation UPSHOT-KNOTHOLE existing requirements for a structures program which would be based on the needs of the Air Force for target analysis and indirect bomb damage assessment information. Within the Air Materiel Command, the responsibility for designing and executing such a program was delegated to the Special Studies Office, Engineering Branch of the Installations Division. The requirements which were submitted and approved became part of Program 3 of the operation and were designated as Projects 3.1, 3.3, 3.4, 3.5, 3.6 and 3.26.1. Mr. B. J. O'Brien of the Special Studies Office was appointed Project Officer and, as such, coordinated and successfully directed the planning and operational phases of five of the six projects. Due to the similarity in test objectives involving railroad equipment, the projects proposed by the Transportation Corps, U. S. Army, and the U. S. Air Force were combined into Project 3.6 with Lt. Colonel Donald G. Dow, TC, USA, as Project Officer and Mr. O'Brien as Assistant Project Officer.

Armour Research Foundation (ARF) of the Illinois Institute of Technology was awarded a contract to assist the Special Studies Office in planning and designing the experiments, and in analysis and reporting of test results. During the period of planning, close liaison was maintained with other interested Air Force agencies, particularly the Physical Vulnerability Division, Directorate of Intelligence, Headquarters, USAF. Many valuable suggestions were contributed by Colonel John Weltman, USAF, Lt. Colonel John Ault, USAF, Messrs. R. G. Grassy and S. White, Dr. F. Genevese and others of that Division, and by Mr. Louis A. Nees, Chief of the Engineering Branch, Installations Division, AMC.

Personnel of the Special Studies Section who were intimately connected with the program were Mr. Eric H. Wang, Chief, Special Studies Office, who was the technical and scientific monitor for the Air Force Program, Mr. Arthur Stansel, and Mrs. Maisie G. Ridgeway, secretary to Mr. Wang. Other members of the Office who were associated with the program were Messrs. R. R. Birukoff, P. A. Cooley, J. C. Noble, and Lts. T. M. Murray and G. A. Rockwell, USAF.

Most of the introduction section of this report was taken from the preface of the Preliminary Report, Operation UPSHOT-KNOTHOLE, Project 3.3, authored by Eric H. Wang and Bernard J. O'Brien.

The responsibility within the Air Force for execution of the six projects was transferred from the Special Studies Office, Installations Division, Air Materiel Command to Blast Effects Research, Mechanics Branch, Aeronautical Research Laboratory, Wright Air Development Center, on 15 November 1954.

ACKNOWLEDGMENTS

This report covers the activities of the Armour Research Foundation in connection with the Air Force Structures Program, Project 3.3, Tests on the Loading of Horizontal Cylindrical Shapes, of Operation UPSHOT-KNOTHOLE. The work reported herein was technically monitored by the Special Studies Office of the Installations Division of the Air Materiel Command, Wright-Patterson Air Force Base, Dayton, Ohio, under the terms of Air Force Contract AF33(038)-30029. It was sponsored by Wright Air Development Center.

ARF personnel who have contributed to this report include: R. L. Calvin, S. J. Fraenkel, K. C. Gandy, A. K. Hawkes, R. L. Janes, E. L. McDowell, K. E. McKee, R. W. Sauer, E. Sevin, A. Sherman, T. Schiffman, L. A. Schmidt, M. R. Smith, A. H. Wiedermann and T. A. Zaker.

CONTENTS

ILLUSTRATIONS

TABLES

CHAPTER 1

INTRODUCTION

1.1 PURPOSE OF AIR FORCE TEST PROGRAMS

The series of tests conducted by the Air Force in Operation UPSHOT-KNOTHOLE is part of a continuing Air Force program designated as "Determination of Blast Effects on Buildings and Structures." The United States Air Force is mainly interested in the offensive aspects of such research.

The UPSHOT-KNOTHOLE projects sponsored by the Air Force and their specific objectives cannot be fully understood without some knowledge of the general objectives of the over-all program. The research results emanating from these studies and experiments conducted by the Air Force are used by a number of government agencies to improve their own systems of determining blast effects, or to further their own research.

One of these agencies is the Directorate of Intelligence, Headquarters, USAF, which feeds results as they are obtained into its own system of vulnerability classes, thereby making it possible to analyze prospective enemy targets with greater accuracy, and to recommend the desired ground zero. Another principal user of the research results is the Strategic Air Command, which applies them toward improvement of an existing indirect bomb damage assessment system. The purpose of this system is to make it possible to dispense with the usual reconnaissance after a strike, using instead, information on the actual ground zero, height of burst, and yield of the weapon which is brought back to the operational base by the strike aircraft to determine the damage inflicted.

The task of determining the effect of blast on various types of building structures and tactical equipment is a rather formidable one. However, its difficulty is somewhat relieved by the fact that, for the offensive purposes in which the Air Force is interested, it is not necessary to determine the effect of transient loads on these items with the same accuracy as would normally be employed for static design purposes. In fact, even if it were possible to solve the dynamic problems satisfactorily, Intelligence information would be far too sketchy to furnish the information necessary to justify the use of an accurate analysis for items located in prospective enemy countries. From the experience that is so far available it is expected that it will be

possible within the foreseeable future to determine blast damage within broad limits with sufficient accuracy for planning as well as for operational purposes.

In view of the complex phenomena attending shock waves emanating from various types of atomic blasts and the uncertainties inherent in determining significant parameters, an investigator's first idea would be to obtain solutions through a long series of very elaborate and properly designed full-scale tests. However, neither funds nor time will allow such an approach. It has therefore been the objective of the agencies involved to obtain sufficiently accurate results by judicious use of theoretical analyses, laboratory tests, high-explosive field tests, and a small number of full-scale atomic tests.

Three of these research projects have involved full-scale atomic testing. The first was GREENHOUSE, the second was JANGLE (the first underground burst of an atomic weapon to which an Air Force structures program was subjected) and the third the UPSHOT-KNOTHOLE program.

From previous analysis, laboratory tests, and full-scale tests (the latter especially as conducted in GREENHOUSE), methods of damage prediction have been developed by Armour Research Foundation (ARF) and others. These prediction methods have attempted to describe the character of the blast loads acting on a variety of items. Response computations based on the predicted loadings permit, in turn, an estimate of physical damage. However, the relation between the deflection or movement of a body and significant military damage has never been clearly established except for extreme cases, e.g., total destruction or no destruction. Another aim of these tests is, therefore, to establish the relationship between deflection and functional damage. A full-scale test also affords an excellent opportunity to determine scaling check points for laboratory tests.

In addition to the scientific aspects of the tests, most of the results of the Air Force projects can be used by other government agencies such as the Directorate of Intelligence to furnish "rough and ready" experimental answers to the behavior of various kinds of structures under blast. In many cases there is a statistically significant number of items involved which, added to previous experimental data such as those gathered at Hiroshima and Nagasaki, will help round out the present vulnerability picture. In other cases, mathematical analysis may have to rely on ad hoc information to furnish parameters which cannot be obtained in any other way.

The foregoing remarks are designed to furnish the background necessary for a full understanding of the objectives of this and other of the Air Force projects. The full significance and value of the results of each test will be realized only when they are correlated with results of past, current, and future analyses, laboratory tests, high-explosive field tests, and full-scale atomic investigations.

1.2 SPECIFIC OBJECTIVES

Knowledge of the blast loading on circular cylindrical bodies is required in connection with the prediction of damage to certain items

of target interest. Fuel storage tanks, tank cars, chimneys, and penstocks are but a few items which are idealized as cylinders for the prediction of blast loading.

Existing load-prediction theories are based, for the most part, on small-scale model studies conducted in a shock tube. Thus, a great deal of interest concerns the validity of scaling shock tube data to full-scale field conditions. Cylinders of target interest are often supported at varying distances above the ground or other reflecting surfaces. Shock tube studies of this configuration, (Air Force Planning Program Final Pretest Report, Part I, Oil Storage and Equipment Tests)1/ have indicated an increase in total force due to multiple reflections between the undersurface of the cylinder and the ground. It is therefore desirable to establish whether or not this phenomenon occurs under field conditions, and the extent to which it may be predicted.

Since most shock tube studies have to date been conducted on two-dimensional cylinders, it is also of interest to compare these results with the loading on finite (i.e., three-dimensional cylinders).

The purpose of this test is to obtain information on the above items by determining the blast loads on nondeformable right circular cylinders supported horizontally at various distances above the ground. The specific test objectives are to determine the influence of the following parameters on the blast loading of cylinders:

1. Shock strength
2. Size
3. Ground proximity
4. Three-dimensionality

The aim of this test is thus to obtain information which can provide the proper scale relationships for continuing shock tube and high-explosive studies on the blast loading of circular cylinders. This information can be ultimately incorporated in suitable damage prediction schemes for items of this type.

1.3 RESPONSIBILITIES

Armour Research Foundation (ARF) was retained by the Air Materiel Command (AMC) of the United States Air Force to carry out the following work:

A. Consultation on the selection of the test items.

B. Design of the test items.

C. Specification of instrumentation requirements.

D. Location of the structures at the test site.

E. Supervision of construction of the test items.

1/ Complete reference concerning publications mentioned in parentheses may be found in the Bibliography at the end of this report.

F. Theoretical and experimental analyses concerning pretest predictions of blast loading and response of the test items where required.

G. Analysis of the test results.

H. Submission of reports accounting for the Foundation's activities pursuant to the objectives of the program.

Detailed statements of the duties and obligations of the contracting parties can be found in the Statement of Work section of Air Force Contract AF33(038)-30029.

Preparation of the construction drawings for most of the test items was subcontracted by the Foundation to the firm of Holabird and Root and Burgee. A member of this organization supervised the actual construction under the general direction of ARF. As-built drawings of all the test items were prepared by the Silas Mason Company.

All instrumentation was installed and operated by the Ballistic Research Laboratories (BRL) under UPSHOT-KNOTHOLE Project 3.28.1 (Structures Instrumentation, WT-738). BRL was also responsible for the reduction and presentation of the instrument records.

CHAPTER 2

GENERAL DESCRIPTION OF TEST

2.1 TEST ITEMS

Five horizontal cylinders, closed at both ends and supported at varying distances above the ground, were located at two stations in both Shots 9 and 10. Four of the cylinders were identical in size and shape; the fifth was a quarter-scale model of the other four. A schedule of the cylinder dimensions is shown in Fig. 2.1; as-built construction drawings are shown in Fig. 2.2.

The basic cylinder was 6 ft in diameter and 20 ft long. Each cylinder was oriented so that the shock wave would be normal to its longitudinal axis. All five were fabricated from 1/2-in. steel plate with reinforced end sections. All seams were butt-welded so that surfaces of interest would be smooth. The cylinders were supported on specially designed sensor bars welded to the end plates. The sensors, in turn, were bolted to piers of reinforced concrete construction set in the ground (see Fig. 2.2).1/ The design was such that no permanent deformation or gross motion of the cylinder was expected at the intended overpressures. Photographs of the quarter-scale cylinder (3.3b) and an end view of a typical 6-ft diameter cylinder are shown in Figs. 2.3 and 2.4. A summary of the cylinder properties is given in Table 2.1.

An analysis of the pressure gage data obtained from a vertical cylindrical storage tank, included as part of UPSHOT-KNOTHOLE Project 3.26.1 (Tests of the Effects on POL Installations, WT-736), is presented in this report. The tank (3.26bd) was of 1/4-in. welded steel plate construction, 15 ft in diameter and 10 ft high. The roof had a slope of approximately 10 degrees and consisted of a 1/16-in. sheet steel cover on twelve 1-by-4-in. wooden rafters. The rafters were toe-nailed to a 4-by-4-in. wooden centerpost and were strengthened by bridging. The tank was filled with water to a level of 7 ft. A photograph of the tank is shown in Fig. 2.5.

TABLE 2.1 - Properties of Test Cylinders

Property	Units	Cylinder	
		3.3a, c, d, e	3.3b
Cross-sectional area	$in.^2$	112	27.5
Mass per Unit Length (Neglecting End Plates)	$lb\ sec.^2/in.$	0.0824	0.0202
Total Mass (Including End Plates)	$lb\ sec.^2/in.$	28.5	1.71
Moment of Inertia of Cross Section About Diameter	$in.^4$	71.8×10^3	1.05×10^3
Stiffness of Sensor Supports*	lb/in.	2.5×10^6 5.5×10^6	1.6×10^6 2.7×10^6

* "Stiffness" refers to the load per unit deflection of the sensor bar assembly in the plane of the sensor bar frame. Due to the geometry involved, the stiffness of the frame is independent of the orientation of the load and, hence, is given by the load per unit deflection of a single sensor bar loaded axially (stiffness due to bending of the bars is neglected throughout). The larger value of stiffness is based on the unsupported sensor bar length; the lower value on the total length between center of the cylinder and base plate. (The actual value of stiffness is intermediate to these two extremes.) See Fig. 2.2 for dimensions of the cylinders and sensor frames.

2.2 INSTRUMENTATION

2.2.1 General

It was desired to measure net forces on the cylinder as well as local forces on certain portions of the cylinder (e.g., on the surface facing the ground). Instrumentation consisted of both pressure gage and strain gage measurements. Six air-pressure gages were mounted on the circumference of each cylinder at mid-length. The gage locations are shown schematically in Fig. 2.1, and in the as-built construction drawings of Fig. 2.2. The pressure data were to provide the desired local effects and, when averaged, the net force on the cylinder. The geometry of the cylinder was such that the gages at mid-length would provide the loading on an essentially two-dimensional body, at least during the initial period of loading (see Section 3.1).

Strain gages were mounted on the front and back of each sensor support, and connected in series electrically to cancel out bending strains. Corresponding sensor bars on opposite sides of the cylinder were averaged, so that a total of two instrumentation channels per cylinder were employed for strain measurements. The strain data provides a measure of the net force acting on the cylinder. However, it should be recognized that the strain data as such does not necessarily give a direct measure of the applied blast loading, but rather the response of the cylinder-sensor system to this loading. In effect the cylinder is being utilized as a dynamometer, and a suitable analysis of the strain data is required in order to determine the desired information.

Soil stabilization was provided for a distance of 150 ft in front of the cylinders at the intended 4900-ft location. The purpose of the stabilization was to increase the probability of obtaining a clean pressure wave at that location. No stabilization was provided for the cylinders at the farther location.

Six air-pressure gages were placed on the roof and sides of the UPSHOT-KNOTHOLE Project 3.26.1 (Tests of the Effects on POL Installations, WT-736) vertical storage tank. The location of these gages is shown schematically in Fig. 2.6.

2.2.2 Air-Pressure Measurements

All air-pressure - versus - time measurements were obtained by the use of Wiancko-type gages; a differential inductance bridge actuated by a pressure-sensitive Bourdon tube. The gage output was fed into modified Webster-Chicago magnetic tape recorders. The circuitry is described as a phase-modulated system.

The pressure gages were calibrated statically in conjunction with the recording system just prior to each shot. A regulated air-pressure system was used for positive pressures and a vacuum pump for negative pressures. Accurately known steps of pressure were applied in increments of 10 per cent of full-scale deflection for each gage. The resulting record was then played back and a calibration established.

The accuracy of the pressure values is estimated by the Ballistic Research Laboratories to be 3 per cent2/ of full-scale readings. The time resolution is in all cases within one millisecond. Complete details of the pressure gage installations is contained in the final report on UPSHOT-KNOTHOLE Project 3.28.1 (Structures Instrumentation, WT-738).

2.2.3 Strain Measurements

Standard SR4 strain gages were used in a four active arm bridge configuration to measure axial strain. The output of each bridge was fed into a Webster-Chicago recording system through a coupling unit and

2/ This is not felt to be a realistic error estimate insofar as the uncertainty associated with information obtained from the pressure data is concerned. In fact, ARF believes that it is impossible to assign a rational bound to the probable error in pressure magnitudes.

recorded on magnetic tape. The electrical calibration of the strain gages was accomplished by shunting the proper arm of each gage installation with an accurately known resistance to simulate actual strain.

Complete details of the strain gage installations are contained in the report on UPSHOT-KNOTHOLE Project 3.28.1 (Structures Instrumentation, WT-738).

2.2.4 Instrument Records

The Ballistic Research Laboratories handled all of the instrumentation on this program. The output of the pressure and strain gages was recorded initially on magnetic tape and later played back onto oscillographic paper. The resulting records had nonlinear ordinate scales and were undesirable for purposes of interpretation and comparison. Thus, all the records were converted into linear form.

The BRL reduced, calibrated, and plotted to linear scales all of the instrument records. The records, as presented to ARF, were in the form of plots made up of the points at which the records were read. The ARF was responsible for fairing curves through these points. The BRL also submitted tabulated listings of the points, as well as copies of the original playbacks.

The numerical data-reduction scheme employed on the strain records required that the data be given at equal time intervals. Accordingly, the BRL made a separate linearization of selected strain records at equal time intervals of about 4 ms, and supplied these results on IBM punched cards.

2.3 LOCATION OF TEST STRUCTURES

The location of the cylinders at the test site is shown in Fig. 2.7. Ground range from intended and actual ground zero is given in Chapter 4, Table 4.1. The measured overpressure levels are also listed in that table. The orientation effects resulting from the bombing error are considered to be negligible. The test, as conducted, did not significantly deviate from the test specifications given in the final pretest report (Air Force Planning Program, Final Pretest Report, Part VI, Tests on Horizontal Cylinders, with the exception that pretest planning anticipated participation in only one shot.

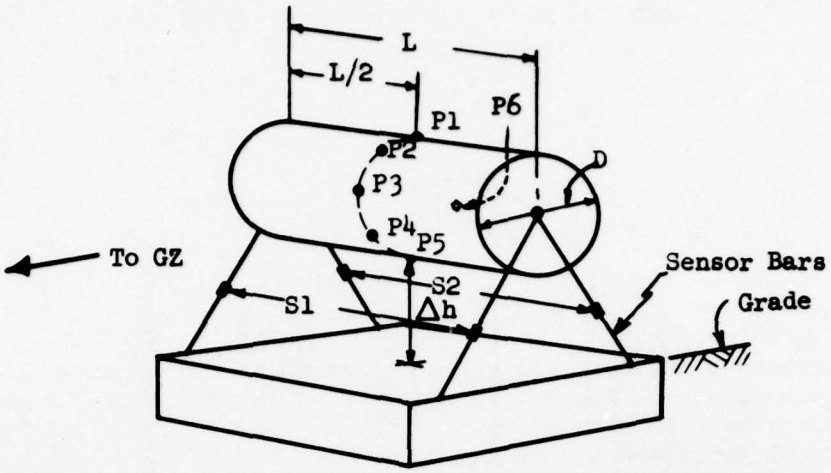

a. Typical Cylinder Showing Pressure and Strain Ag ge Locations

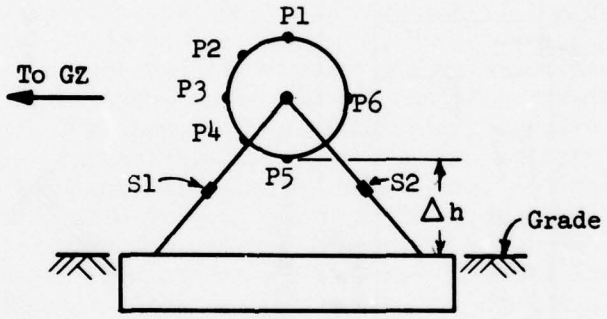

b. Section at L/2 Showing Location of Pressure Gages

Cylinder Schedule (Nominal Dimensions)			
Item	D	L, feet	Δh, inches
3.3a	6' - 0"	20	36
3.3b	1' - 6"	5	9
3.3c	6' - 0"	20	36
3.3d	6' - 0"	20	18
3.3e	6' - 0"	20	4

Fig. 2.1 Schematic Detail and Dimensions of Horizontal Cylinders

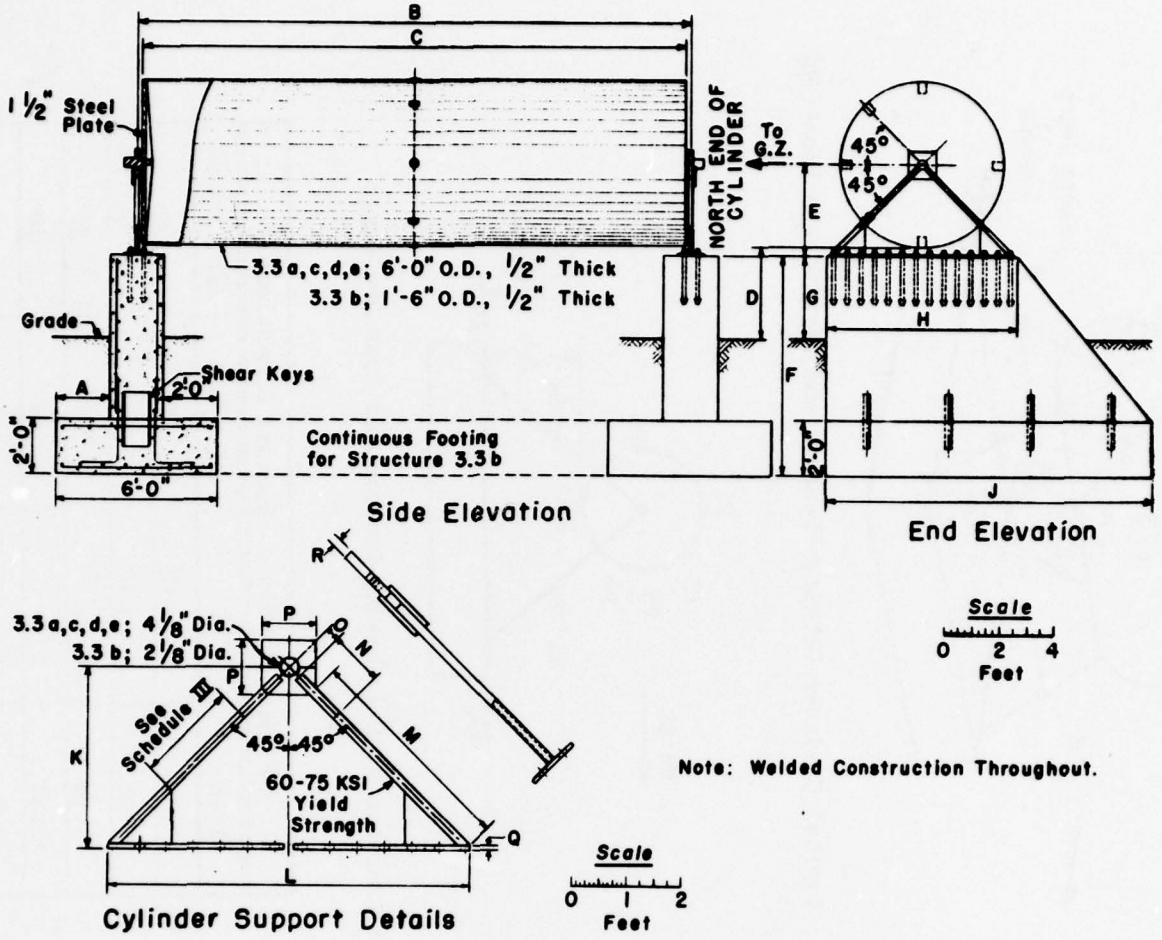

Note: Welded Construction Throughout.

Fig. 2.2 As-Built Construction Drawings

~~SECRET RESTRICTED DATA~~

UNCLASSIFIED

I - Dimensions									
Structure	A	B	C	D	E	F	G	H	J
3.3a	2'-0"	20'-4-1/4"	19'-11-5/8"	3'-0"	3'-4"	8'-6"	2'-8"	7'-0"	12'-0"
3.3b	0'-9"	5'-2-1/2"	5'-0-1/8"	0'-10-1/2"	1'-4"	5'-7"	0'-3"	3'-0"	6'-0"
3.3c	2'-0"	20'-4-7/8"	19'-11-5/8"	2'-11-5/8"	3'-4"	8'-5-5/8"	2'-7-5/8"	7'-0"	12'-0"
3.3d	2'-0"	20'-4-7/8"	19'-11-1/2"	1'-6"	3'-4"	8'-6"	1'-2"	7'-0"	12'-0"
3.3e	2'-0"	20'-4-1/2"	19'-11-5/8"	0'-3"	3'-4"	8'-5"	-0'-1"	7'-0"	12'-0"

Structure	K	L	M	N	O	P	Q	R
3.3a, c, d, and e	3'-4"	6'-8"	4'-0-3/4"	1'-0"	0'-3"	1'-0"	0'-1"	0'-2"
3.3b	1'-4-1/2"	2'-9-1/2"	1'-7-3/8"	0'-5"	0'-2"	0'-6"	0'-1/2"	0'-1"

II - Location of Pressure Gages											
Structure	P1 - P2	P2 - P3	P3 - P4	P4 - P5	P1 - P6	Location from North End of Cylinder					
						P1	P2	P3	P4	P5	P6
3.3a	2'-4-3/8"	2'-4"	2'-4-5/16"	2'-4-5/16"	4'-8-7/8"	10'-0-3/16"	10'-0-1/4"	10'-0"	9'-11-7/8"	10'-0"	9'-11-5/8"
3.3b	0'-7-5/16"	0'-7-7/32"	0'-7"	0'-7-3/16"	1'-2-7/16"	2'-5-7/8"	2'-6"	2'-6"	2'-5-3/4"	2'-6"	2'-5-7/8"
3.3c	2'-4-1/16"	2'-4-1/2"	2'-4-3/16"	2'-4-13/16"	4'-8-5/8"	10'-0"	9'-11-3/8"	9'-11-1/2"	9'-11-1/4"	9'-11-5/8"	10'-0"
3.3d	2'-4-3/16"	2'-4"	2'-4-1/2"	2'-4-1/8"	4'-8-7/8"	10'-0"	10'-0-1/8"	9'-11-3/4"	10'-0-1/8"	9'-11-7/8"	9'-11-3/4"
3.3e	2'-4-5/8"	2'-4-9/16"	2'-4"		4'-8-3/16"	10'-0"	10'-0-1/4"	10'-0"	10'-0-1/16"		9'-11-1/2"

III - Unsupported Sensor Bar Lengths				
Structure	S. E. Leg	S. W. Leg	N. E. Leg	N. W. Leg
3.3a	2'-10"	1'-9-11/16"	1'-9-3/4"	1'-9-7/8"
3.3b	0'-11-1/2"	0'-11"	0'-11-1/4"	0'-11-3/8"
3.3c	1'-9-1/2"	1'-9-3/4"	1'-9-1/2"	1'-9-1/4"
3.3d	1'-9-5/8"	1'-9-5/8"	1'-9-1/2"	1'-9-1/2"
3.3e	1'-9-5/8"	1'-9-3/8"	1'-9-1/2"	1'-9-1/2"

Schedule for Fig. 2.2

Fig. 2.3 1-1/2 ft Diameter Cylinder, 3.3b

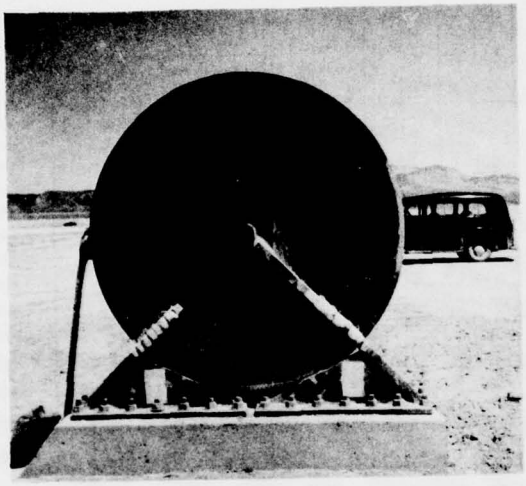

Fig. 2.4 End View of Typical 6 ft Diameter Cylinder

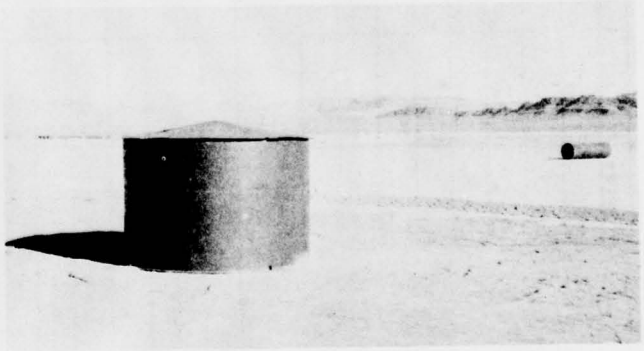

Fig. 2.5 Project 3.26.1 Vertical Storage Tank

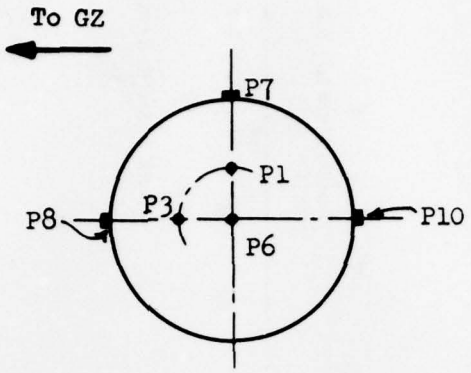

a. Plan View

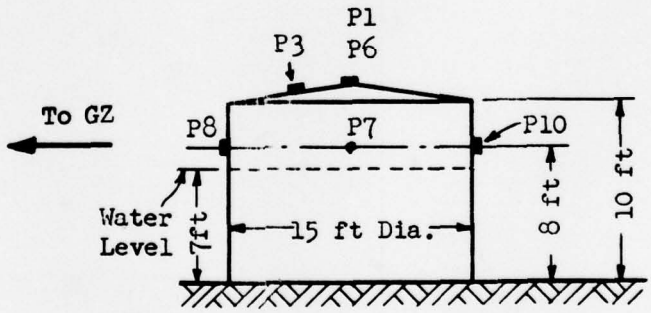

b. Side Elevation

Fig. 2.6 Pressure Gage Locations on Project 3.26.1 Vertical Storage Tank (3.26bd)

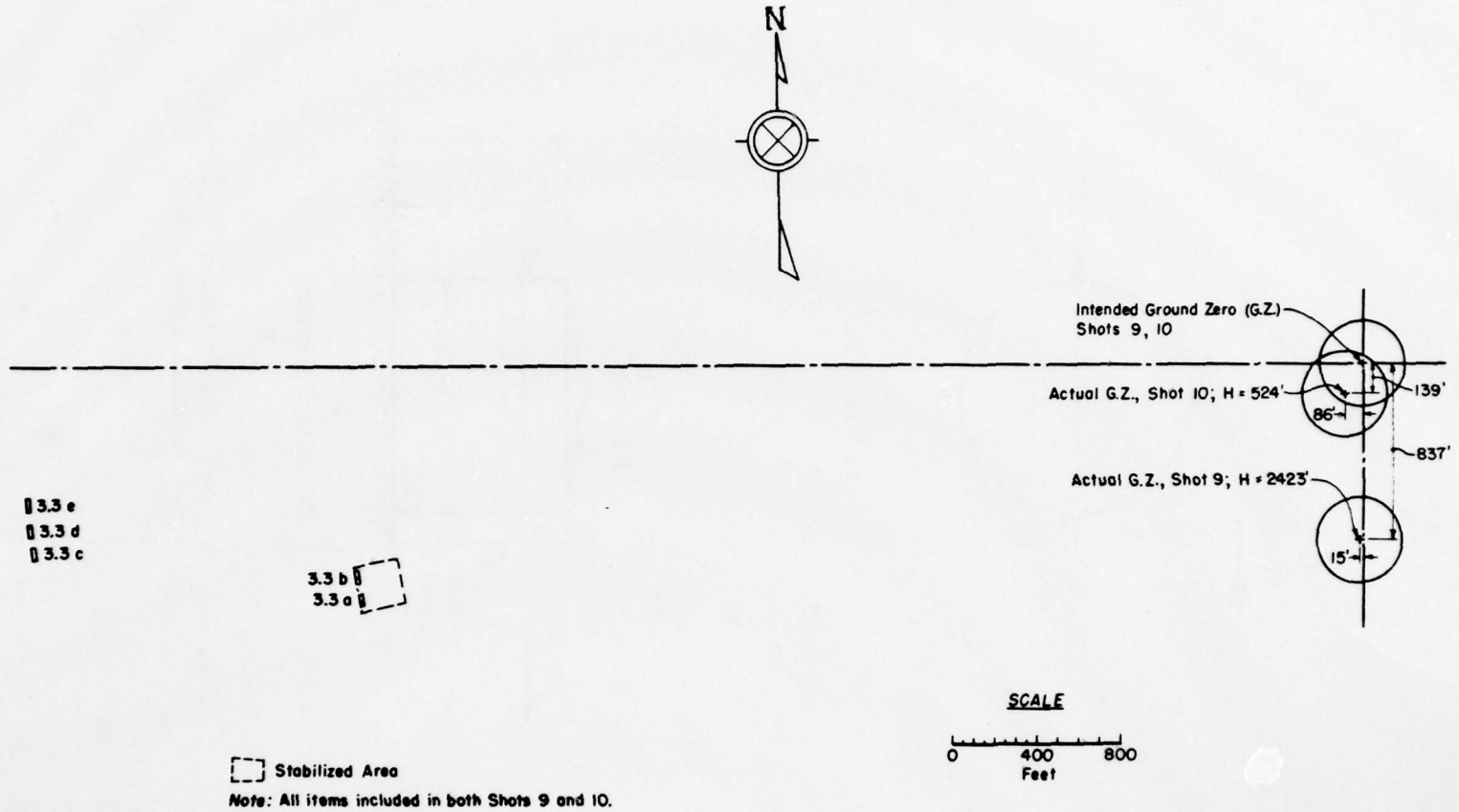

Fig. 2.7 Location of Cylinders at Test Site

CHAPTER 3

PRETEST CONSIDERATIONS

3.1 SELECTION OF TEST ITEMS

The number and location of the cylinders were chosen so as to achieve the test objectives with the minimum possible number of cylinders. In designing the test, the following items were taken into consideration.

Shock tube experiments at Princeton University (Bleakney, W. Diffraction of Shock Waves Around Obstacles, Technical Report II-3) indicate that the character of the loading on the top of two-dimensional cylinders of square cross section is dependent on the strength of the shock. This is apparently due to the dependence of the formation of vortices with shock strength, and it is quite possible that a similar effect occurs in the case of circular cylinders. This effect was investigated in the test by placing two cylinders of the same size in overpressure regions differing by about a factor of 2 (Cylinders 3.3a and 3.3c). It was felt that any vortex effects dependent on shock strength should be discernible for this variation in pressure.

Shock tube experiments indicate that the time details of the loading during the diffraction phase scale linearly with the absolute size of the geometry under consideration. This dependence of size was investigated by placing two cylinders of the same diameter-to-length-to-ground proximity ratio, but differing in absolute size by a factor of 4, in the same overpressure region (Cylinders 3.3a and 3.3b). A scale ratio of 4-to-1 was felt to be sufficient in order to point out this effect of size.

In addition to the scaling of time details during the diffraction period, the loading during the drag phase is also dependent upon the absolute size of the cylinder. The total horizontal steady-state drag coefficient for cylinders is known to vary between 1 and 1/3 in the range of Reynolds numbers (based on diameter) between 10^5 and 7×10^5, and then remain essentially constant at 1/3 for larger Reynolds numbers (see Aerodynamic Drag by S. F. Hoerner). Under transient flow conditions such as in the field, the Reynolds number itself will vary with time. For the test cylinders, the Reynolds number is supercritical initially (i.e., greater than 7×10^5) and will, of course, vanish when

the particle velocity goes to zero. There is considerable interest in the behavior of the drag loading under these circumstances. However, there is some question as to whether the pressure gage instrumentation is adequate to determine this effect of size. That is, under test conditions the drag pressures are expected to be small - of the order of uncertainty in the pressure datum itself. Therefore, information of this nature, while highly desirable is considered to be of bonus value.

Tests conducted in the ARF 4-in. shock tube showed that the pressure on the underside of a cylinder depends markedly on the proximity of the cylinder to a reflecting surface such as the ground (Air Force Planning Program, Final Pretest Report, Part I, Oil Storage and Equipment Tests). It is believed that a systematic study is in order to determine quantitatively both the magnitude of this pressure build up and the scaling relationships which hold between full-scale and model tests. Three cylinders of the same size but at different distances above the ground, subject to the same loading, were to provide the desired information (Cylinders 3.3c, 3.3d, and 3.3e).

It is felt that a reasonable comparison of two- and three-dimensional loadings could be had by comparing the net loads as determined by the pressure data (two-dimensional loading) and by the strain data (three-dimensional loading). The ratio of cylinder length to diameter is believed to be sufficiently great (L/D = 3.33) so that the pressure gages located at mid-length will read essentially two-dimensional data, at least for the initial period of the loading. The pressure gages should represent two-dimensional loading exactly for the first 3r/U units of time (r = radius of cylinder, U = velocity of the shock front), since it would take a disturbance signal at least this length of time to travel from one end of the cylinder to the center. Moreover, it is believed that such signals are sufficiently weak, so that the observations made at mid-length represent the two-dimensional load on the cylinder for the entire duration of the loading. The data obtained from the strain gages, on the other hand, are indicative of the net loading on a finite cylinder and, as such, represent the three-dimensional loading case. All of the test cylinders may be said to contribute to this objective.

3.2 LOAD PREDICTIONS

Theories concerning the influence of ground proximity on the blast loading on cylindrical shapes are practically nonexistent. For a circular cylinder in free space (i.e., infinitely removed from the ground) the situation is more satisfactory. Prediction methods for this case are discussed in detail in the final pretest report (Air Force Planning Program, Final Pretest Report, Part VI, Tests on Horizontal Cylinders), and the results are presented in Chapter 5 of this report (see Fig. 5.13). The tall chimney included in Operation JANGLE (Air Force Structures Program 3.3, Final Report, Vol. I) affords a check between measured and predicted loads for this case.

The pretest work on load predictions was concerned primarily with an estimate of the peak pressure on the underside of the front portion of a cylinder as a function of ground proximity. No attempt was made to predict the subsequent pressure distribution as the shock spills over the rear of the cylinder. This work was based primarily on the results of shock tube studies (see Bleakney, W. The Diffraction of Shock Waves Around Obstacles, Technical Report II-3, Princeton University and Air Force Planning Program, Final Pretest Report, Part I, Oil Storage and Equipment Tests). The limiting case for which the cylinder touches the ground has been solved analytically from an approximate point of view. This condition was assumed to be equivalent to the pressure build up occurring when a shock impinges upon a re-entrant corner (Air Force Planning Program, Final Pretest Report, Part V, Regular Reflection on Cubical Structures). The other limiting case is, of course, for the cylinder in free space. Inasmuch as these predictions are rather crude and no comparison with test results proved possible, the work is not repeated here.

3.3 NET FORCE MEASUREMENTS

3.3.1 Sensor Design

Effort was expended during the planning phase of the program to devise a method for direct measurement of the net applied blast forces acting on the test cylinders. Ideally, a direct measurement system would be one whose output is either proportional to the net blast loads acting over the entire structure, or whose output can be converted to net loads in a straightforward fashion. This requirement for a so-called net force measurement system is meant to exclude pressure gage instrumentation, at least in the present case. While there are certain types of structures for which net forces (over the entire structure) can be adequately determined by means of combining and averaging individual pressure gage data, there are many structures of interest where such averaging is either subject to considerable uncertainty or is totally impractical. There are also cases where the presence of pressure gages may sufficiently alter the flow conditions around the test item, so as to rule out this means of force measurement. In the present case, where an averaging procedure was possible, it was not practical to provide the necessary additional pressure gage instrumentation. Thus, an alternative force measurement system had to be devised.

The force measurement or sensor system finally adopted consisted of supporting the cylinders on either end as shown in Fig. 2.2, and measuring the forces in these supports by means of resistance-type strain gages. While other supporting schemes were considered (e.g., a ballistic pendulum arrangement utilizing accelerometer output) the present scheme was resorted to, since an identical system was utilized in connection with the UPSHOT-KNOTHOLE Project 3.4 (Tests on the Loading of Truss Systems Common to Open-Framed Structures, WT-723). In this latter program the end-support scheme appeared to be the only practical approach.

In the present setup, the test cylinder was utilized in the sense of a dynamometer. That is, the cylinder and sensor arrangement as a whole constituted the gaging device. The output of the strain gage system (i.e., the force in the sensor bars) was thus dependent upon the dynamic characteristics of the cylinder-sensor system as well as upon the applied blast force. In order for the strain data to be utilized as a direct measure of the applied blast loadings, it is necessary that the frequency response of the cylinder be considerably greater than that of the sensor supports alone and, in turn, that the fundamental period of the system as a whole be sufficiently less than the significant time-details of the applied blast loading. In this case the response is essentially that of a single-degree-of-freedom system (i.e., a rigid cylinder on flexible supports) and, with suitable damping, the strain data could be interpreted much as are the pressure data - simply by inspection. Unfortunately, it did not appear possible to satisfy these conditions. While the rigidity of the cylinders could have been increased considerably, the frequency response of the sensor bars was limited in two ways. First, was the requirement that a sufficiently great strain be produced to yield a reliably measurable signal from the strain gages throughout most of the loading period. Second, the sensor arrangement was designed on the basis of there being no provision for pretest field calibration of the entire setup (and there was none). This necessitated a rather longer sensor bar than might otherwise have been utilized (and, hence, a lower frequency), since it was imperative that the measured surface strain be an inadequate measure of the actual force in the bar.1/

Details of the sensor bar construction are shown in the as-built drawings of Figs. 2.2 and in the photograph of Fig. 2.4. Briefly, the end supports consisted of a rigid right-angle frame of welded construction whose vertex was attached at the axial center of the cylinder. On the 6-ft diameter cylinders, the bars were 2 in. square and approximately 22 in. long between welds (i.e., the unsupported sensor bar length); on the quarter-scale cylinder (3.3b), the bars were 1 in. square and approximately 11 in. long. High-strength steel was used for all sensor bars. The geometry of the supports was such that each sensor bar could be considered as a two-force member.2/ This would, of course, be the case if the frame were ideally pin-connected, but a rigid frame was more desirable from the construction viewpoint.

1/ That is, the sensor bar had to be sufficiently long so that the stress distribution at the cross section being gaged was essentially uniform.

2/ An analysis of the maximum error introduced by the assumption of pin-ends was carried out in the final pretest report (Air Force Planning Program, Final Pretest Report, Part VI, Tests on Horizontal Cylinders). The error in the magnitude of the force was found to be less than 6 per cent, and about 1.5 degrees in direction relative to the centerline of the bars.

3.3.2 Interpretation of Strain Measurements

The final sensor design was such that the measured forces in the cylinder support would most likely be influenced by the dynamic characteristics of the entire test structure and, thus would not be a direct measure of the applied blast force. This situation necessitated a data-reduction system that was capable of taking this influence into account and providing the desired net applied forces. In essence, the problem here is the inverse of the conventional dynamic response problem. That is, the usual problem is "given the dynamic system and the input, find the output" — here the problem is "given the dynamic system and the output, find the input."

The solution to the inverse problem is generally the more complicated but in principle can be achieved, at least for linear dynamic systems, provided the response of the system to a given input is known. However, the present problem is made more difficult by the fact that the characteristics of the dynamic system itself are not known with any certainty. That is, the system is sufficiently complicated that the response (i.e., the force in the sensor bars) to a known input cannot be computed with sufficient accuracy to justify a solution to the inverse problem by standard methods.

A data-reduction scheme referred to as "transient analysis" was developed during the course of the pretest work and was believed to be adequate for the needs of this program. In principle, the method of transient analysis is applicable to the determination of the time variation of an input function (the magnitude of the input can be determined only within an arbitrary scale factor) from a known output function, even when the equations of motion of the system are not known in detail. The method is restricted to dynamic systems characterized by linear second-order differential equations with constant coefficients, and input functions which can adequately be represented by finite sums of exponential functions (i.e., "e" functions), all of whose coefficients and exponents are real numbers. In effect, this last requirement limits the input functions to those having no harmonic components, which seemed a reasonable enough assumption in the case of blast loading functions. A further restriction is that the forcing functions associated with the various modes of the system be either zero or timewise proportional.

The restrictive assumptions which permit the valid use of transient analysis as a technique for data reduction in the present application were considered to be satisfied during the pretest planning period. However, as discussed in Chapter 5, the application of transient analysis to the strain data was unsuccessful. The analysis is developed in Appendix A of this report, which also contains a critical discussion of the method.

3.3.3 Relationship Between Strains and Forces

The relationship between strain and total force in the sensor bars per unit projected area of the cylinder is given by

$$S = (A_s/A_c)E\epsilon \tag{3.1}$$

where,

S = unit force in one sensor bar, psi

A_s = cross-sectional area of the bar, $in.^2$

A_c = projected area of the cylinder along a diameter, $in.^2$

E = Young's modulus for the sensor bars, psi

ϵ = strain measured in one sensor bar, in./in.

Assuming pin connections, the horizontal and vertical components of total load per unit projected area acting on the cylinders is given in terms of the force in the sensor bars as:

$$F_h = \frac{2}{\sqrt{2}}(S_1 - S_2)$$

$$F_v = \frac{2}{\sqrt{2}}(S_1 + S_2) \tag{3.2}$$

The unit horizontal force, F_h, is taken to be positive acting downstream, and the unit vertical force, F_v, positive acting upward. The subscripts "1" and "2" refer to the forces in the upstream and downstream sensor bars, respectively, which are assumed positive in tension. In terms of the measured strains, F_h and F_v are given numerically as,

$$\left.\begin{aligned} F_h &= 9.82 \times 10^{-3}(\epsilon_1 - \epsilon_2), \text{ psi} \\ F_v &= 9.82 \times 10^{-3}(\epsilon_1 + \epsilon_2), \text{ psi} \end{aligned}\right\} \text{ for the 6-ft diameter cylinders, 3.3a, c, d, and e} \tag{3.3a}$$

$$\left.\begin{aligned} F_h &= 39.3 \times 10^{-3}(\epsilon_1 - \epsilon_2), \text{ psi} \\ F_v &= 39.3 \times 10^{-3}(\epsilon_1 + \epsilon_2), \text{ psi} \end{aligned}\right\} \text{ for the 1.5-ft diameter cylinder, 3.3b} \tag{3.3b}$$

where the strains are given in μ in./in.($= 10^{-6}$ in./in.), and a value of $E = 30 \times 10^6$ psi has been used for Young's modulus.

CHAPTER 4

EXPERIMENTAL RESULTS

4.1 FIELD CONDITIONS

The specifications for the flow conditions, as established during the pretest planning period, were not substantially violated during the test. The cylinders were located in the Mach reflection region in both Shots 9 and 10, and the incident shock waves were clean and well-developed in each case. The error in ground zero on Shot 9 changed the range and orientations of the cylinders, and resulted in somewhat different overpressures than were intended. (Shot 10 was not anticipated during the planning phase.) The field conditions are summarized in Table 4.1, and the blast wave parameters are given in Table 4.2.

4.2 PRESSURE GAGE DATA

Of the thirty pressure gages used in Shot 9, four did not yield pressure-time observations, whereas of the thirty gages used in Shot 10 only one failed to yield any observations. The records lost on Shot 9 were from Gages P2 and P3 of Cylinder 3.3c and from Gage P5 on Cylinder 3.3d and 3.3e. The only record lost on Shot 10 was from Gage P5 of Cylinder 3.3e. (See Fig. 2.1 for pressure gage locations.)

In general, the original pressure-time observations which were obtained appeared to be quite good on first inspection; that is, the noise level was reasonably low and the records were relatively free from extraneous pips, etc. These data are considered in more detail in Chapter 5. Typical pressure-time records are shown in Fig. 5.1.

4.3 STRAIN GAGE DATA

Of the twenty strain gages (ten each on Shots 9 and 10), all but one provided records of some sort in each shot. The records were played back by BRL at two speeds; a slow speed which in most cases gave information during and beyond the positive loading period, and a fast speed which indicated greater detail of the response during the first 200 ms. or so after shock arrival. The extent of these two playbacks is

TABLE 4.1 - Summary of Field Conditions

Test Item	Shot No.	Ground Range (ft)		Orientation (Degree from normal)		Overpressure (psig)		Actual Duration* (sec.)
		Intended	Actual	Intended	Actual	Intended	Actual	
3.3a	9	4900	4780	0	9-1/2	8	6.7	0.90
	10	4900	4750	0	1	-	3.5	0.90
3.3b	9	4900	4780	0	9-1/2	8	6.7	0.90
	10	4900	4750	0	1	-	3.5	0.90
3.3c	9	6375	6280	0	7-1/2	5.2	4.6	0.95
	10	6375	6290	0	1	-	2.0	0.95
3.3d	9	6375	6280	0	7-1/2	5.2	4.6	0.95
	10	6375	6290	0	1	-	2.0	0.95
3.3e	9	6375	6280	0	7-1/2	5.2	4.6	0.95
	10	6375	6290	0	1	-	2.0	0.95

Ambient preshot conditions: Shot 9 air pressure P_o = 13.2 psi;
air temperature = 16.7° C.
Shot 10 air pressure P_o = 13.2 psi;
air temperature = 14.8° C.

*Duration of the Positive Phase of the Blast Wave.
Data obtained from Summary Report of the Technical Director, WT-782.

TABLE 4.2 - Summary of Blast Wave Parameters

Parameter	Symbol	Units	Shot 9		Shot 10	
			3.3a / 3.3b	3.3c,d and e	3.3a / 3.3b	3.3c,d and e
Ambient Pressure	P_o	psi	13.2	13.2	13.2	13.2
Ambient Temperature	T_o	°F	62	62	59	59
Ambient Sound Velocity	c_o	fps	1121	1121	1118	1118
Ambient Density	ρ_o	lb/ft^3	0.0683	0.0683	0.0683	0.0683
Peak Overpressure	$p_\sigma(0)$	psi	6.7	4.6	3.5	2.0
Shock Strength	ξ	-	1.51	1.35	1.26	1.15
Reflected Pressure	p_r	psi	16.1	10.6	7.67	4.09
Reflected Pressure Ratio	$p_r/p_\sigma(0)$	-	2.40	2.30	2.23	2.06
Duration of Positive Phase	t_o	sec	0.90	0.95	0.90	0.95
Density Behind Shock	ρ_1	lb/ft^3	0.0916	0.0841	0.0800	0.0752
Temperature Behind Shock	T_1	°F	127	107	93	78
Particle Velocity Behind Shock	u	fps	342	247	188	112
Shock Front Velocity	U	fps	1341	1280	1234	1185
Peak Drag Pressure	$p_d(0)$	psi	1.13	0.53	0.30	0.11
Viscosity	$\mu \times 10^7$	lb/ft sec.	133	129	127	125
Reynolds Number (based on Diameter)	$R_{eD} \times 10^{-6}$	-	14.2 / 3.52	9.65	7.08 / 1.77	4.02

Notes: Ambient conditions, overpressure and duration obtained from Summary Report of the Technical Director, WT-782.
Other quantities computed from the conventional Rankine-Hugoniot relationships applicable across the shock front.

TABLE 4.3 - Summary of Strain Gage Data

Strain Record	Remarks (see notes at end of table)	
	Shot 9	Shot 10
3.3aS1	$s > t_o$; $f(NL) \simeq 180$ ms $EC_1 \neq EC_2$	$s > t_o$; $f \simeq 145$ ms $EC_1 = EC_2$
3.3aS2	$s(L) > t_o$; $f \simeq 140$ ms $EC_1 \simeq EC_2$	$s < t_o$; $f \simeq 300$ ms $EC_1 = EC_2$
3.3bS1	No record	$s < t_o$; $f \simeq 190$ ms $EC_1 \simeq EC_2$
3.3bS2	$s > t_o$; $f \simeq 200$ ms $EC_1 \simeq EC_2$	$s(L) > t_o$; $f \simeq 210$ ms f and s do not agree initially $EC_1 \simeq EC_2$
3.3cS1	$s < t_o$; $f \simeq 300$ ms $EC_1 \neq EC_2$	$s > t_o$; $f(NL) \simeq 350$ ms $EC_1 \neq EC_2$
3.3cS2	$s < t_o$; $f \simeq 320$ ms $EC_1 \simeq EC_2$	No record
3.3dS1	$s \simeq t_o$; $f \simeq 260$ ms $EC_1 \neq EC_2$	$s > t_o$; $f \simeq 260$ ms $EC_1 \simeq EC_2$
3.3dS2	$s < t_o$; $f \simeq 270$ ms $EC_1 \simeq EC_2$	$s > t_o$; $f \simeq 260$ ms $EC_1 \simeq EC_2$
3.3eS1	$s > t_o$; $f \simeq 270$ ms $EC_1 \neq EC_2$	$s < t_o$; $f \simeq 380$ ms $EC_1 \simeq EC_2$
3.3eS2	$s < t_o$; $f \simeq 300$ ms $EC_1 = EC_2$	$s > t_o$; $f \simeq 240$ ms $EC_1 = EC_2$

Notes:
1. See Fig. 2.1 for explanation of strain gage code.
2. The term "s" refers to slow record playback. "s(L)" indicates a linearized plot, otherwise "s" plots not linearized, "$s > t_o$" indicates "s" plot extends beyond duration of positive loading period, otherwise "$s < t_o$".
3. "f" refers to fast record playback. "f(NL)" indicates "f" plot not linearized, otherwise all "f" plots linearized. "$f \simeq 180$ ms" indicates "f" plot extends to about 180 ms after shock arrival.
4. EC_1, EC_2 refer to pretest electrical calibrations (see text).

indicated in Table 4.3, which summarizes all the strain gage data. Only two of the slow playbacks were linearized (3.3aS2, Shot 9, and 3.3bS2, Shot 10), whereas all but two of the fast playbacks were linearized.

The entries in Table 4.3 labeled EC_1 and EC_2 refer to electrical calibration marks; EC_1 is a field calibration just prior to shot time, and EC_2 is an earlier calibration taken some time before the tests. No postshot calibrations were made. As is seen, these marks are generally only approximately equal, and in those cases marked "not equal," the difference was of the order of the strain calibration jumps. The linearizations were made on BRL's best estimate of the proper calibration; where EC_1 differed appreciably from EC_2, the possible error was not estimated by BRL. As far as could be told, the baselines appeared to be good in that no drift from the preshot position could be noted by visual inspection.

As indicated in Table 4.3, the magnitude of initial peaks on record 3.3bS2, Shot 10, do not agree between the fast and slow playbacks. This was the only case in which a discrepancy between a linearized plot and the original playback could not be resolved. However, not evident in the table is the fact that many similar discrepancies arose. For example, three linearized plots were originally discarded, since they appeared to provide data for less than 35 ms, until it was noted that the time scales were in error by a factor of 10. Additional discussion of the reliability of the strain data is given in Chapter 5. Typical strain records are shown in Fig. 5.28.

CHAPTER 5

DISCUSSION OF RESULTS

5.1 PRESSURE MEASUREMENTS

5.1.1 Reliability of Data

Spot-checking the original record playbacks with the BRL linearizations showed some discrepancies. These consisted mainly of extraneous pips in the linearizations and were easily corrected by comparing them with the original playbacks. However, several not so obvious irregularities were noted, and it is probable that some of these were carried through the analysis. A typical example of this type of discrepancy is seen by comparing Figs. 5.2a and b. Figure 5.2a is a partial tracing of the original playback on Record 3.3eP3, Shot 10; Fig. 5.2b is the linearized plot of the same record. As can be seen, the magnitudes of the first and second maximums and the first minimum are not consistent between these records; after about 15 ms, however, the two compare favorably.

A more serious criticism of the records is that the magnitudes of the pressures, in general, are lower than expected. The difference is apparent in the few instances where lower bounds can be established for the pressures. For example, at the position of Gage P3 (the head-on gage position) the pressure should rise instantaneously to the normal reflected pressure, p_r, and then decay to its pseudo-steady-state value. As seen in Fig. 5.5, this gage on Cylinders 3.3a and 3.3c, Shot 10, recorded peak pressures of between $1.6p_\sigma(0)$ and $1.7p_\sigma(0)$, whereas the expected values (listed in Table 4.2) were about $2.2p_\sigma(0)$ and $2.1p_\sigma(0)$, respectively. On Cylinder 3.3a, Shot 9, Gage P3 gave a value of $p_r/p_\sigma(0) = 2.1$, which is 12 per cent lower than the expected value of 2.4.

At the head-on gage position, the pseudo-steady-state value is always greater than the free-stream pressure, $p_\sigma(t)$, since the drag coefficient is positive at that point. The free-stream pressure-time curves (obtained from Summary Report of the Technical Director, WT-782) are presented in Fig. 5.9 for about the first 125 ms after shock arrival. For convenience, these curves have been normalized in

terms of peak side-on pressure and r/U time units, where r = 3 ft is the radius of the larger cylinders. A comparison of Figs. 5.5 and 5.9 shows that the pressures recorded by Gage P3 on Cylinders 3.3a, Shot 9, and 3.3c, Shot 10, are slightly greater than free-stream pressure at the time t = 30 r/U as expected, while the same gage on Cylinder 3.3a, Shot 10, reads just slightly less than free-stream pressure.

The initial pressure at the positions of Gages P2 and P4 (see Fig. 2.1) should also be of the order of the reflected pressure, p_r, whereas the pseudo-steady state value of the pressure at Gage P2 should be approximately $p_\sigma(t)$, since the drag coefficient at that position is approximately zero. As seen in Fig. 5.4, Gage P2 indicates a peak value less than $1.7p_\sigma(0)$ for Cylinder 3.3a, Shots 9 and 10, and for Cylinder 3.3c, Shot 10. At a time of 30 r/U units, Gage P2 reads less than free-stream pressure in both shots; the same gage on Cylinder 3.3c, Shot 10, is approximately equal to free-stream pressure at this time. Gage P4 on Cylinder 3.3a, Shot 9 (Fig. 5.6), appears reasonable in Shot 9 and probably somewhat low in Shot 10. However, this gage on Cylinder 3.3c reads a peak value less than the incident free-stream pressure in both shots. While it is possible that the gage system did not respond to the initial peak pressures, this seems unlikely and would not account for the lower pseudo-steady-state values noted above.

The recording systems were electrically calibrated twice: once some time before the test (mark EC_2 in Fig. 5.2a) and again just prior to the test (mark EC_1 in Fig. 5.2a). These calibration steps did not match in approximately half of the records; however, the majority of the deviations were small. Thus, the same uncertainties found in the strain data calibrations noted in Chapter 4 are present here.

The original data appeared to contain also some shifts in baseline. The combination of the baseline shifts and calibration errors affect the magnitudes of the pressure records, and since the scales were nonlinear, these errors can affect, to a small degree, the shape of the records. The time scales, however, seem to be quite reliable.

There is some question of data reliability regarding overpressures, since the actual overpressures were lower than the intended overpressures (see Table 4.1). This resulted in pressure deflections on the recorder which were less than full scale, and hence, the recorder and calibration errors were effectively enlarged. BRL estimated the accuracy of the pressure data to be 3 per cent of full-scale deflection.1/

To facilitate analysis of the relatively large number of pressure-time records, the linearized form of the data was replaced by a "simplified" pressure-time curve. Typical examples are shown in Fig. 5.1. A series of straight lines were drawn through the linearized data, conserving the essential features of the curves and neglecting the oscillations which were due to the dynamic effects of the recording system. The accuracy of this procedure, of course, depends upon the analyst's understanding of the basic flow phenomenon as well as the

---

1/ See footnote on page 19.

dynamic recording system. These simplified curves were plotted in a normalized form, using the variable $p/p_\sigma(0)$ for the unit of pressure and r/U for the unit of time, where p is measured pressure, $p_\sigma(0)$ is the peak incident overpressure, r is the radius of the cylinder, and U is the velocity of the shock wave. This final form of the data was then used to evaluate the flow phenomenon and to check the validity of the pretest predictions in an attempt to achieve the objectives of this program.

5.1.2 Correlation of the Data

5.1.2.1 Effect of Shock Strength

One of the test objectives was to determine the effect of shock strength on the loading of a cylinder supported horizontally near the ground. Test items 3.3a and 3.3c were used to achieve this objective and, with both Shots 9 and 10, yielded four sets of data. These test items were identical in size (6-ft diameter) and elevation (3 ft above the ground). The values of the shock strengths obtained were: ξ = 1.51 and 1.35 for Shot 9, and ξ = 1.26 and 1.15 for Shot 10 on items 3.3a and 3.3c, respectively. These values of shock strength represent a reasonable spread in this variable for loading comparisons. (The maximum intended shock strength was approximately ξ = 1.6.) The basic blast wave parameters for all the test items are presented in Table 4.2.

The pressure data were plotted in normalized form, as discussed previously, and in general indicate that (a) the data were not sufficiently accurate to determine any effects of shock strength, even during the diffraction period, and (b) the pressure magnitudes in many cases appear to be from 10 to 50 per cent low. The first conclusion is borne out by examining the normalized plots presented in Figs. 5.3 through 5.8. It was not possible to observe any consistent or interpretable trend with increasing shock strength from these pressure-time plots. This randomness of behavior prevailed on all correlations which were made. However, in only a few cases did the plots for a given gage position differ basically in shape.

The second conclusion follows directly from the discussion in Section 5.1.1 concerning the reliability of the data. In view of the fact that the strain gage data provided no quantitative results (see Section 5.2), the test objective dealing with the effect of shock strength could not be realized.

Since the effect of shock strength could not be ascertained from the pressure records, the data were averaged and further reduced to yield what is believed to be the best possible estimate of the loading on a cylinder one radius above the ground (i.e., $\Delta h/D = 0.5$). The data of Figs. 5.3 through 5.8 were averaged linearly in most cases; erratic portions of the records were ignored. These average pressure-time records were also modified slightly in order to be consistent with corresponding or neighboring records. The resultant plots are presented in Fig. 5.10 and can be considered to represent the loading

on a cylinder one radius above the ground and struck by a shock of strength ξ = 1.32 (average value of the four sets of data).

The average pressure-time plots were used to construct pressure distributions acting on the cylinder at various times after shock arrival. This procedure was carried out in steps of one r/U unit up to a normalized time of 20 r/U units (approximately 50 ms). A few typical pressure distributions are presented in Fig. 5.11. These pressure distribution plots were then used to compute the average pressure in the horizontal and vertical directions (i.e., ratio of total force to projected area). The net horizontal and vertical loads are presented in Fig. 5.12. The magnitudes found are questionable; however, it is believed that the time details of the loadings are correct.

The significant information obtained from these loadings are the clearing and buildup times for the respective surfaces (arcs). These build up and clearing times are essentially the same as for a two-dimensional cylinder in free space, with the exception of the clearing time on the front face. The predicted loadings for a two-dimensional cylinder in free space based on average test conditions is given in Fig. 5.13. A plot of the reflection coefficient referred to in Fig. 5.13 is shown in Fig. 5.14. With reference to the experimental results of Fig. 5.10, the clearing time on the front face of a cylinder located one radius above the ground is estimated to be between 8 and 10 r/U time units. As seen from Fig. 5.13, however, the predicted value for this time on a cylinder in free space is less than 5 r/U units. This increase is reasonable, however, when one considers the increase in pressure due to ground proximity as well as the greater effective clearing distance of the cylinder. The clearing distance of the cylinder varies from the order of r for $\Delta h/D = \infty$ (i.e., in free space) to 2r for $\Delta h/D = 0$ (i.e., touching the ground).

5.1.2.2 Effect of Size

Another test objective deals with the effect of size of the cylinder on the loading. Contributing toward this objective were Cylinders 3.3a and 3.3b, both located at the same ground range and struck by identical shock waves (ξ = 1.51 for Shot 9 and ξ = 1.26 for Shot 10). These cylinders were identical in geometry but differed in absolute size by a factor of 4. Cylinder 3.3a was 6 ft in diameter and located 3 ft above the ground, whereas 3.3b was 1.5 ft in diameter and located 9 in. above the ground. The initial Reynolds numbers based on the cylinder diameters are shown in Table 5.1. 2/

2/ These Reynolds numbers apply to flow just behind the shock front; the flow parameters given in Table 4.2 have been computed from the conventional Rankine-Hugoniot theory relating the state variables across the shock front.

Table 5.1 - Initial Reynolds Numbers for Test Cylinders

Cylinder 3.3a	$R_{eD} = 14.2 \times 10^6$	for Shot 9
	7.1×10^6	for Shot 10
Cylinder 3.3b	$R_{eD} = 3.5 \times 10^6$	for Shot 9
	1.8×10^6	for Shot 10

According to steady-state concepts (see Aerodynamic Drag by S. F. Hoerner), these Reynolds numbers are sufficiently large to make the drag coefficient relatively independent of the Reynolds number (critical Reynolds number $\cong 7 \times 10^5$.

The simplified pressure-time plots for these two cylinders are presented in Figs. 5.15 through 5.20. The records do not show any large deviations in the drag coefficient due to a size effect; however, there is a considerable and generally random spread in the values of the pressures. This spread is typical of all the pressure-time records obtained for this program. The actual value of the drag coefficient could not be determined from these pressure-time records.

If one applies a correction factor to the pressure scales of Fig. 5.15 such that the peak pressure equals 1.82 $p_\sigma(0)$ (i.e., the predicted value for a free cylinder), then the drag coefficient on the front face is approximately -1, and the drag coefficient on the back face is less than -4. These values are, of course, not realistic. If, on the other hand, one assumes that the pressure scale of Fig. 5.12a is correct, then the drag coefficients are even more unrealistic.

It must be concluded, therefore, that even when averaged, the pressure data do not yield any information about the actual value of the drag coefficient. While it was realized at the outset that the pressure data might not prove sufficiently accurate to determine drag pressures (see Section 3.1), this is nonetheless unfortunate. Equally unfortunate is the fact that if the pressure data obtained in this test are as reliable as one can expect from field operations, the determination of drag pressures associated with relatively weak shocks is not practical by means of direct pressure measurements at the present time.

The observations on test item 3.3b tend to indicate that the occurrence of events (i.e., time) scale is as predicted. The response of the recording system was just sufficient to detect this scaling. See Figs. 5.15 through 5.20 for these trends. The magnitude of one r/U unit for the smaller cylinder, 3.3b, ($r/U \simeq 0.6$ ms) was too small to determine clearly the exact time ($\pm 2r/U$) of a particular event.

5.1.2.3 Effect of Ground Proximity

A third, and perhaps the most important, objective of this test was to determine the effect of ground proximity. The test items used to study this effect were 3.3c, 3.3d, and 3.3e. These cylinders were identical in size (6-ft diameter) and were elevated 3 ft, 1.5 ft, and 4 in. above the ground, respectively, resulting in $\Delta h/D$ values of 0.5, 0.25, and 0.055. The test items were located at the same ground range and were subjected to essentially identical blast waves (ξ = 1.35 for Shot 9 and ξ = 1.15 for Shot 10). The simplified pressure-time records are presented in Figs. 5.21 through 5.26 for these cylinders.

The effect of ground proximity on the loading of a horizontal cylinder was not determined as a result of this test. Determination could not be made for two primary reasons. First, a majority of the pressure records (Gages P4 and P5, Fig. 2.1) which would contribute most to this effect were either lost or invalidated. The records at gage position P5 (directly facing the ground) were lost for test items 3.3d, Shot 9, and 3.3e, Shots 9 and 10, whereas the pressure-time record on test item 3.3d, Shot 10, was obviously in error since it recorded a pressure of the order of $4p_o(0)$ for a considerable length of time (approximately 200 ms). The second reason is that these particular gage records were generally poor, both with respect to the magnitude of the pressure as well as the form of the pressure-time curves. (See Figs. 5.21 through 5.26.) This is borne out if comparisons are made of the records from Gages P1, P2, P3, and (possibly) P4 during the initial portion of the loading where the effect of the reflecting surfaces has not yet influenced the pressure at these gages. Negative pressures were observed initially (see Fig. 5.26) at the position of Gage P6 on Cylinder 3.3e during both Shots 9 and 10; it does not seem possible that the initial pressure signal could actually have been negative. There are many corrections or processes that one can apply to the data in order to make them appear more realistic (i.e., by changing scale factors or by shifting time scales, etc.). However, in all cases, the pressure values would become arbitrary and controversial, and, it is felt, this procedure would not increase the meaningfulness of the test results.

5.1.2.4 Effect of Three-Dimensionality

The remaining test objective concerned three-dimensional effects on the loading (i.e., the effect of finite size). This objective was to have been achieved by comparing the net forces obtained from the pressure data with those obtained from the strain gage data. The pressure data would have provided two-dimensional results, at least during the initial loading period, whereas the strain data would provide the three-dimensional results. As discussed in later sections, the strain data did not yield the necessary quantitative information to effect such a comparison and, hence, this objective could not be achieved. This is indeed unfortunate, since the results of the strain would have contributed equally as well to all test objectives.

5.1.3 Results of Project 3.26.1 Pressure Gages

A portion of UPSHOT-KNOTHOLE Project 3.26.1 (Tests on Effects of POL Installations, WT-736), is related to the present program inasmuch as both deal with the loading on structures of cylindrical shape. There was one vertical cylindrical storage tank in Project 3.26.1 (test item 3.26bd) which was instrumented with six pressure gages in Shot 9. (A photograph of the tank is shown in Fig. 2.5; the pressure gage locations are indicated in Fig. 2.6. A description of the tank is given in Chapter 2.)

The tank was at an actual ground range of 6560 ft in Shot 9 and was struck by a clean and well-developed shock wave. The peak overpressure was 4.2 psi and the positive phase duration was approximately one second. All of the pressure-time records exhibited an appreciable amount of "noise" prior to shock arrival, and it must be assumed that the noise level did not change thereafter. Typical linearized gage records (fast playbacks) are shown in Fig. 5.27. These pressure-time observations were not considered in the final report on Project 3.26.1 and are discussed in this section.

The roof of the tank collapsed and fell into the tank shortly after shock arrival. This time has been estimated to be about 100 ms from motion picture films taken of the tank. Thus, the observations were invalidated for use in the verification of loading methods on rigid three-dimensional cylinders at the time the geometry changed radically. In addition to the change in geometry, the pressure records from the side gages show many disturbances which are not considered to be due to flow phenomenon and may well have resulted from fragments of the roof striking the gage cables.

In general, the magnitudes of the pressures appear to be low; however, the form of the pressure-time curves for the gages on the side of the tank are reasonable. Pressure Gage P8, which was facing the blast wave, shows a large initial peak value which decays rapidly to a pseudo-steady-state value. While the magnitudes were probably low, the ratio of the magnitudes was approximately correct. The peak-reflected pressure cleared in approximately 15 ms, which is nearly $3r/U$ time units and agrees with the clearing time for a free cylinder (see Fig. 5.13). This gage was located near the top edge of the cylinder and indicates that the three-dimensionality of this structure does not affect the front loading appreciably.

Pressure Gage P10, which was on the back side of the tank, indicated a build up somewhat more rapid than predicted. However, this is reasonable since the gage was located relatively close to the edge on the tank, i.e., the shock wave swept around from the side in addition to sweeping over the top edge. This record also shows a vortex of moderate strength (approximately $0.4p_{\sigma}(0)$) sweeping past the gage at approximately $6r/U$ time units after the shock wave had reached the back of the tank. The observations on the back of the Project 3.3 cylinders indicate a vortex of approximately the same strength sweeping past at from 4 to 5 r/U time units. Pressure Gage P7, which was located on the side of the tank, also indicates the existence of

a vortex of moderate strength (approximately $0.5p_{\sigma}(0)$) at the time $4r/U$. This agrees quite well with the observations made at that point on the Project 3.3 cylinders. Pressure Gage P7 did not indicate a small initial peak which, it is believed, should have existed.

The records of roof Gages P1, P3, and P6 do not seem to be realistic, and since the roof failed early, the records do not provide useful information, even in the very early stages prior to roof failure.

5.2 STRAIN MEASUREMENTS

5.2.1 Introduction

The analysis and discussion of the strain data is presented in the following sections. Section 5.2.2 is concerned with a discussion of the frequency response of the cylinder-sensor system, and an attempt is made to identify the physical origin of the various frequencies observed in the records. It appears likely that a well-defined low-frequency oscillation found in practically all records may be due to a rigid-body motion of the cylinder foundation in the soil. In any event, the frequency response of the test items is considerably more complicated than originally anticipated, and it is not considered feasible to determine the response of this system to even a known input by analytical means.

A comparison of peak horizontal force as computed from the strain data and pressure data, together with the predicted values for an isolated cylinder, is given in Section 5.2.3. Based on this comparison, the strain data yield results which are in all cases lower than expected, and in some cases lower than is reasonable. The vertical force acting at the time of maximum horizontal force indicates a random directional behavior. That is, in some cases the vertical force appears to act upwards; and in others, downwards. The fact that an initial downward force is considered unrealistic points to either an uncertainty in the measured peak strains of about 30 per cent or more, or the fact that this interpretation of the records is invalid.

The magnitude and time-details of the incident blast loading could not be adequately determined from visual inspection of the strain records alone. That this might be the case was anticipated from the outset, and a numerical method of analysis designed to determine the input (i.e., the blast loading) from the known output (i.e., the strain data) was devised during the pretest planning phase. This method of data reduction, referred to as transient analysis, was applied to all strain data which appeared reasonable, but for one reason or another, the results of this analysis proved largely unsatisfactory. The development of the method of transient analysis, together with a critical discussion of its general applicability as it is currently understood, is presented in Appendix A; the actual work carried out and the results obtained are given in Section 5.2.4.

A first application of the method of transient analysis proved inconclusive. A second application was begun but, since it did not seem as if the necessary additional work required to prove or disprove the method in the present application would be consistent with the scope of the program, this work was not completed. Thus, no definite conclusions have been reached as to the feasibility of this method in general, although it must be admitted that much has been learned regarding certain aspects of the analysis and the general complexity of the computational procedures which was not at all appreciated at the outset. And it must further be admitted and recognized that the problem of data-reduction stemming from so-called net force measurement systems such as in the present case (i.e., where the test items represent a fairly complicated dynamic system) is still largely an unsettled issue.

In view of the unsuccessful results of the numerical data-reduction scheme, it was necessary to follow another approach in an effort to obtain the desired information from the strain data. The method adopted, which can be called only a qualitative approach to the problem, was an attempt to remove the harmonic components of the response by inspection and thereby yield at least the shape of the forcing function. A discussion of this work and the rather conflicting results obtained is given in Section 5.2.4.

In connection with the qualitative approach indicated above, a brief effort was directed toward utilization of the ARF analog computer as a curve-fitting device. The work is described in Section 5.2.6. While no conclusive results were obtained, the technique appears to be a promising one.

5.2.2 Frequency Response of Cylinders

A typical strain-time record is shown in Fig. 5.28a. Even a brief inspection of this record is sufficient to point out that the cylinder-sensor arrangement did not respond as what could be termed a simple dynamic system. Quite the contrary, as at least four principal frequencies can be identified in the majority of the records. An attempt is made in this section to identify these various frequencies so as to interpret better the strain data.

Average values of the principal periods as determined from a visual inspection of the strain records are shown in Table 5.2. Where no periods are shown, either no usable record was obtained (see Table 4.3), or the periods were not clearly defined. While the results of Table 5.2 could no doubt be improved by a statistical approach to the data (the autocorrelation function was calculated for one set of data), these approximate values are adequate for the present discussion. It might also be mentioned that a much lower frequency of about 5 cps (a period of 200 ms or greater) not shown in Table 5.2 was evident in a number of the original record playbacks. The discrepancies noted in frequencies for the same cylinder in the two shots may either be due to the inadequacy of determining these values by inspection, or to the differences in excitation brought about by the difference in orientation of the shock.

TABLE 5.2 - Principal Periods Observed in Strain Records

Cylinder and Sensor	Average Period T (mspc)	
	Shot 9	Shot 10
3.3aS1	14, 3-4	14, 3-4
3.3aS2	16	14
3.3bS1	-	15, 5-6, 2
3.3bS2	7, 2-5	35, 6-7
3.3cS1	38, 15, 8-12	3-4
3.3cS2	46, 15	-
3.3dS1	42, 16, 6-12	38, 18, 6-4
3.3dS2	22, 6-12	19, 14
3.3eS1	35	49, 20, 9-10
3.3eS2	30, 3-4	25

Average for Cylinder 3.3a, c, d, e, Shots 9 and 10:

T = 41, 16, 8, 4 mspc

Average for Cylinder 3.3b, Shots 9 and 10:

T = 35, 15, 6, 2 mspc

Note: mspc = milliseconds per cycle

The strain records are direct evidence of the highly involved response of the cylinder-sensor system, which is that of a relatively thin circular shell with restrained ends on flexible supports. A detailed dynamic analysis of this system was not carried out in view of the technical difficulties and uncertainties involved. In fact, it is precisely one's lack of ability to characterize adequately the response of the test setup that makes the analysis and interpretation of the strain records such a formidable problem. For the purpose of identifying the principal frequencies, however, it is possible to consider certain idealized response modes of the cylinder-sensor system individually. Several such idealized response modes and associated frequencies (and periods) are indicated in Table 5.3. The entries in this table are discussed in the following paragraphs.

If the cylinder were sufficiently rigid, it is reasonable to expect that the principal symmetrical response mode of the system would be translation of the cylinder parallel to the plane of the sensor supports. If the bending resistance of the sensor bars is neglected as compared to their axial stiffness, this motion can be idealized as that corresponding to a single-degree-of-freedom mass-spring system. This is the first mode listed in Table 5.3, the required data are given in Chapter 2, Table 2.1. Two extreme values for the period of this mode are given for both the 6- and 1.5-ft diameter cylinders. This variation is due to the uncertainty regarding the effective length of the sensor bars in this motion (see note in Table 2.1). The higher frequency corresponds to the unsupported length of the bars; the lower frequency is based on the over-all length of the bars (see Fig. 2.2).

The second mode considered is that of simple beam vibration of the cylinder with the sensors acting as rigid supports, but providing no end moment restraint.3/ This frequency is computed from the well-known relation for a simply supported beam and incorporates first-order corrections for shear deformation (see Vibration Problems in Engineering by S. Timoshenko). The frequencies associated with this mode are about twice as great as the rigid cylinder motion.

Another idealized mode is that of the vibration of an isolated thin circular shell. In the present case this is a rather complicated problem, even if the influence of the sensor supports is neglected, since the effect of the end plates is to maintain a fixed diameter. Solutions for the vibration of a thin cylindrical shell of finite length whose ends remain circular but otherwise unrestrained are available (see Mathematical Theory of Elasticity by A. E. H. Love). The frequencies

3/ The frequencies of vibration of a beam mounted on the same type of sensor supports and including the flexibility and moment restraint of the supports was carried out in connection with a pretest analysis on Operation TEAPOT Air Force Project 3.2 (Study of Drag Loading of Structures in and out of the Precursor Zone, WT-1124). The results obtained did not differ too greatly from the frequencies of a conventional simply supported beam.

TABLE 5.3 - Summary of Frequency Response of Cylinders

Assumed Mode of Response	Frequency f: Period T	
	Cylinders 3.3a, c, d, e	Cylinder 3.3b
1. Rigid Cylinder on Flexible Supports	67 < f < 99 cps 10 < T < 15 mspc*	153 < f < 199 cps 5 < T < 7 mspc
2. Cylinder as Simple Beam on Rigid Supports	f = 122 cps T = 8 mspc	f = 480 cps T = 2 mspc
3. Cylinder as Thin Circular Shell		
(a) Extensional Modes	f = 746 cps T = 1.4 mspc	
(b) Inextensional Modes 1st Mode	f = 10 cps T = 1000 mspc	f = 154 cps T = 6.5 mspc
4th Mode	f = 85 cps T = 12 mspc	
4. Rigid Body Motion in Soil		
(a) Rotational Mode	f = 16 cps T = 62 mspc	
(b) Vertical Translational Mode	f = 12.8 cps T = 78 mspc	
(c) Horizontal Translational Mode	f = 6.5 cps T = 155 msps	

*mspc = milliseconds per cycle

corresponding to both extensional and inextensional vibrations are shown in Table 5.3 for this simplified case. The extensional frequency shown (i.e., longitudinal, torsional or radial deformation) is the lowest of two possible frequencies according to this solution; the other one is only slightly higher (about 1000 cps for the 6-ft diameter cylinder). The fundamental inextensional frequency (the cross section assumes the shape of an ellipse) is only 10 cps, which is considerably lower than any of the modes considered previously; the frequency of the fourth mode (see Table 5.3), is of the order of the rigid-cylinder motion. Only the first mode need be considered for the quarter-scale cylinder, 3.3b. It should be kept in mind, however, that these frequencies are undoubtedly low, inasmuch as they neglect all end effects.

The higher frequency modes are easily identified from a comparison of Tables 5.2 and 5.3. Periods of around 15 mspc or less appear to be due to some combination of beam flexure and rigid-body motion on flexible supports. The identification of the lowest frequency (with periods of about 40 mspc and possibly larger) is definitely less clear-cut. While it could easily be explained by inextensional shell vibrations, the numerical values shown in Table 5.3 are in considerable doubt, as indicated above.

In an attempt to investigate further the occurrence of the low-frequency response, an analysis was conducted in which the cylinder and supporting foundation (see Fig. 2.2) was considered to vibrate in the soil; the soil acting as an elastic restoring medium. The cylinder plus foundation was represented by a rigid lamina (i.e., a plane problem) and frequencies corresponding to rotation about the center of mass, and horizontal and vertical translations of the center of mass were computed for the 6-ft diameter cylinder.

The soil constant was assumed to be 100 lb/in., which represents a considered engineering guess for soil conditions at the Nevada test site. The results of these computations (the analysis is not included in the present report as it is a straightforward problem) are shown in the fourth entry in Table 5.3, and it is seen that this motion could indeed account for the observed period of around 40 mspc or greater, as well as the much higher period of about 200 mspc (not shown in Table 5.2). This type of analysis is admittedly a rather gross idealization of actual conditions. The assumption of an ideally elastic soil is certainly questionable, as is the selection of a particular elastic constant. However, in support of such motion it should be noted that recent static pull tests on a test item included in UPSHOT-KNOTHOLE Project 3.4 (and included as part of Operation TEAPOT Project 3.2, Study of Drag Loading of Structures in and Out of the Precursor Zone, WT-1124), which is similar in most respects to the cylinder setup, shows that appreciable motion of the foundation most likely did occur in the present test. Also, in the case of the quarter-scale cylinder, shell vibrations do not account for the lowest frequency observed; this frequency is, however, consistent with rigid motion of the foundation in the soil.

5.2.3 Comparison of Peak Transmitted Forces

It is of considerable interest to determine the peak forces acting on the test cylinder as indicated by the strain records. The initial peak strains were read directly from the linearized strain records and converted to total force per unit projected area of the cylinder transmitted to the sensor bars according to Equation 3.3. These results, in the form of horizontal and vertical force components, along with the peak strain data, are shown in Table 5.4. It might be noted that the strain gage system was apparently wired so that a tensile force in the sensor bars was recorded as a negative strain. These signs have been reversed in Table 5.4 so that a positive F_h indicates a horizontal force directed downstream, and a positive F_v indicates a vertical force directed upward.

According to Equation 3.3 the strains in the front and rear sensor bars should be numerically equal (but of opposite sign) in the absence of a vertical force component for the static case. The majority of the strain records do indeed show a well-defined initial peak strain which is of the same order of magnitude for both front and rear sensors of the same cylinder. Thus, in those cases where the data from only one sensor bar were obtained, the peak horizontal force indicated in Table 5.4 is based on the assumption that the same magnitude strain occurred in the other sensor bar. Due to the uncertainty of this assumption, however, the vertical force component which depends on the difference of the magnitudes of peak strains was not computed unless records from both sensor bars were obtained.

The measured reactions (i.e., F_h and F_v) in general cannot be compared directly with the applied force due to the influence of the dynamic characteristics of the cylinder-sensor system on these reactions. In the present case, however, the appearance of well-defined initial peaks suggests the following approximate scheme for deducing the peak applied force from the measured peak reactions. It is assumed that during the first half-cycle of motion (i.e., in the time of rise to the initial peak) the cylinder acts as a single-degree-of-freedom system with period equal to twice the observed rise time. Knowing this period and assuming undamped motion initially, it is possible to relate the dynamic overshoot of the system to the peak applied loading by means of the so-called dynamic load factor (DLF)[4] for the appropriate type of forcing function.

The average rise time for the 6-ft diameter cylinders was found from the strain records to be about 8 ms, indicating an initial period of about 16 mspc; for the quarter-scale cylinder, this period was found to be about 6 mspc (note from Table 5.2 that such periods were found throughout the entire history of the motion). According to the pretest load prediction scheme for a cylinder in free space (see Fig. 5.13), the net horizontal load during the diffraction phrase rises linearly from zero to a maximum in one r/U unit (about 2.4 and 0.6 ms for the 6- and 1.5-ft diameter cylinders, respectively) and then decays linearly

---

[4] Peak dynamic response = DLF x (static response to peak applied load).

TABLE 5.4 - Summary of Peak Horizontal Forces Acting on Cylinders

	Cylinders	ϵ_1 (μ in./in.)	ϵ_2 (μ in./in.)	F_h (psi)	F_v (psi)	$\frac{F_h}{(DLF)}$ (psi)	F_h Pressure Data (psi)	F_h Predicted (psi)	$p_\sigma(0)$ (psi)
Shot 9	3.3a	-	-285	5.6	-	3.7	8.7	12.6	6.7
	3.3b	-	-59	5.0	-	3.8	8.7	12.6	6.7
	3.3c	297	-262	5.5	0.34	3.7	6.0	8.5	4.6
	3.3d	293	-348	6.3	-0.54	4.2		8.5	4.6
	3.3e	175	-330	5.0	-1.5	3.3		8.5	4.6
Shot 10	3.3a	33	-13	0.45	0.20	0.3	4.5	6.3	3.5
	3.3b	26	-37	2.5	-0.43	1.9	4.5	6.3	3.5
	3.3c	180	-	3.5	-	2.3	2.6	3.5	2.0
	3.3d	170	-220	3.8	-0.49	2.5		3.5	2.0
	3.3e	220	-140	3.5	0.79	2.3		3.5	2.0

Notes: ϵ_1 ... strain in sensor S_1 (upstream sensor)

ϵ_2 ... strain in sensor S_2 (downstream sensor)

F_h, F_v computed from Equation 3.3

DLF = 1.5 for 3.3a, c, d and e; DLF = 1.3 for 3.3b

"Measured" $F_h = 1.3p_\sigma(0)$ for 3.3a, b, c (see Fig. 5.15)

"Predicted" F_h computed from Equation 5.1

See Table 2.1 for description of cylinders

to pseudo-steady-state in between 4 and 5r/U units. Inasmuch as this decay time is somewhat less than the initial periods, it is sufficient to consider only this triangular diffraction loading in estimating the desired DLF. From solutions available in the literature (Elastic Structures Under Rapidly Applied Loading - III, Mechanical World and Engineering Record, No. 2574), it is found that DLF = 1.5 for the 6-ft diameter cylinder and DLF = 1.3 for the 1.5-ft cylinder for both shots. Accordingly, the column labeled F_h/DLF in Table 5.4 represents the estimated peak applied horizontal force as indicated by the strain records.

The measured values of F_h shown in Table 5.4 are taken from the results of Fig. 5.12a for the cylinder configuration $\Delta h/D = 0.5$, where the peak pressure was found to be about $1.3p_\sigma(0)$. The predicted values of F_h shown in the table were computed from the relation

$$\frac{F_h}{p_\sigma(0)} = 0.63 \left[C_{\text{cyl hor}} - 1 \right] + 1 \qquad (5.1)$$

which is applicable to a cylinder in free space (see Fig. 5.13). A plot of the average reflection coefficient, $C_{\text{cyl hor}}$, is given in Fig. 5.14.

With reference to Table 5.4, it is seen that the peak force as determined by the strain gage data, in every case, appears to be low; in most cases, even less than the side-on pressure acting at that time. The values of F_v (i.e., the vertical force component at the time the peak F_h occurs) also appear to be unrealistic. More often than not, the results indicate a net vertical force acting downward on the cylinder, which is contrary to all previous experience. And there is no consistency in the apparent direction of F_v between the results of Shots 9 and 10. Although the magnitude of F_v increases with increasing Δh, as would be expected, this trend is not consistent between the two shots.

In view of the low values of F_h, as computed from the strain data, and the randomness in sign of F_v, it appears that either the association between the measured strains and the applied forces is invalid, or that the magnitudes of the strain data are unreliable. It is impossible to assess fully the validity of converting the peak measured strains to applied forces short of undertaking a comprehensive dynamic analysis of the system. As long as the cylinder-sensor system responds initially in only one mode, the use of a DLF is valid. While the proper value of the DLF is open to some question, even a lower bound value of DLF = 1 5/ results in peak forces which are still considered low. However, it is possible that certain harmonic components of the dynamic system act so as to appreciably distort the initial time details of the loading. In such case, the initial peak strain might no longer be proportional to the applied load, and the comparison of Table 5.4 would be invalid. At later times in the response, however, these components may be damped out, and the shape and magnitude of the applied force might be readily obtained.

5/ DLF = 1 is a lower bound value for the periods and duration of diffraction loading considered here.

The strain data for Cylinder 3.3a, Shot 10, tend to support this view. As indicated in Table 5.4, the peak recorded force of 0.45 psi is felt to be low by a factor of 10 or more. However, as discussed in Section 5.2.4, after about 20 ms the strain data appear quite realistic and, in fact, supports steady-state wind-tunnel results for drag coefficients. Similarly, the randomness in behavior of most of the other cylinders could be explained in terms of a complicated response. In Shot 9, identical Cylinders 3.3a and c were in regions of different shock strength, yet the measured peak strains were practically identical. Cylinders 3.3c, d and e had decreasing $\Delta h/D$ in the order given (see Fig. 2.1) and were exposed to the same loading. However, the peak horizontal force does not show a trend consistent with the variation in $\Delta h/D$, in that the intermediate cylinder, 3.3d, in both Shots 9 and 10 indicated the higher loading. From the other point of view, however, the results for Cylinders 3.3c and d in Shot 9, and 3.3d and e in Shot 10 show extremely well-defined initial peaks (see Fig. 5.28) and it seems reasonable that the present interpretation is valid, at least in these cases.

As seen in Table 5.4, the peak strains in the two sensor bars differ in one case by as little as 11 μ in./in. and in another by 35 μ in./in. Under static load conditions the reliability of the SR-4 strain gages used in the test is only about $\pm 20\mu$ in./in. Thus the inconsistency in the vertical force could be explained in part by reasonable inaccuracies in the strain data. Of course, it is possible that errors in strain or strain calibration could account for all the uncertainty noted here. It would then follow from a consideration of F_v that the uncertainty in strain magnitude is of the order of 30 per cent — or an uncertainty in pressure of from 1 to 2 psi. However, it should be noted that the magnitude of the vertical force shown in Table 5.4 in some cases is not inconsistent with what was found from the pressure gage data. For example the results of Fig. 5.12b (applicable to Cylinder 3.3c) indicate a net upward force of about 0.7 psi for that cylinder (in Shot 9) at the time the peak horizontal force occurred. Considering the fact that there will be some time lag in the response of the cylinder to this load, a measured value of 0.34 psi is not unrealistic.

There is an alternative explanation to the apparent error in sign of F_v and low values of the maximum horizontal force. This is that the recording equipment may have missed the initial peak strain in some cases, and what has been accepted as the first maximum of the strain is in reality the first minimum which occurs one-half cycle later. Not only would this account for the low values of F_h, but it would imply a change in sign of F_v, since what was assumed to be positive strain now takes on a negative value. (The signs would then agree with BRL's sign convention on the original playbacks.) However, in view of the rated response time of the recording equipment as well as in inspection of the original record playback, this explanation does not appear to be realistic.

To summarize, the maximum recorded strains point to a general randomness and inconsistency in behavior when the results are taken as a whole. Whether the interpretation of these data is invalid due to the complexity of the dynamic system, or whether there exists a large uncertainty in the records themselves due to errors in magnitude or calibration, cannot definitely be stated; some evidence is presented for either reason.

In retrospect it is now evident that in field tests of this nature, as much information as possible should be obtained regarding the dynamic systems being tested. A minimum of such information would consist of pretest and post-test static pull tests which would serve to define the linear range of the system and check out the strain gage system and calibration. Some sort of dynamic tests should also be considered in order to determine the principal frequencies and damping of the cylinder-sensor system. Information of this type would undoubtedly have aided in the study and interpretation of the strain data.

5.2.4 Graphical Analysis of the Strain Records

The results of a rather comprehensive visual inspection of the individual strain records is presented in this section. For lack of a better name, the approach followed is referred to as graphical analysis, and it should be emphasized at the outset that the method and results obtained are only meaningful in a qualitative sense. Briefly, the method consisted of combining the two strain records for each cylinder into horizontal and vertical components (where possible), and constructing what appeared to be the most reasonable median curve about which the combined records appeared to be oscillating. This median curve was obtained by first estimating the envelopes to the record and then constructing a curve which passed midway between the upper and lower bounds. This procedure was repeated several times until a reasonably smooth, nonoscillating curve was obtained; this curve was then taken as representing the general shape of the forcing function being considered. In effect, the graphical approach filters out the harmonic components of the response and, in principle, accomplishes what was intended with the method of transient analysis.

Before considering the results obtained, there are several points to be mentioned in connection with the method of analysis and the records themselves. The method of transient analysis (discussed in the following section and in Appendix A) was applied to individual strain records, since a preliminary inspection of the data indicated some uncertainty in the strain calibration and in the location of shock arrival time. It was decided to base the present approach, however, on the combined data, (i.e., horizontal and vertical strain components) inasmuch as a direct comparison with the results of the pressure gage analysis and predicted values was desired.

As discussed in connection with the strain data for Cylinder 3.3a on Shot 10, the results obtained do not appear to be seriously affected within the range of uncertainty in locating a consistent zero time between the two strain records for a particular cylinder.

In those cases where well-defined initial peak strains occurred, a common zero time was established by matching these peaks on the two records. In those cases where the initial peaks were not well-defined, the zero time was determined in a somewhat arbitrary fashion. In any event, the results are not believed to be materially affected by errors in the location of zero time. With respect to possible errors or inconsistencies in the strain calibration, little can be said. However, as mentioned in connection with a comparison of peak force values, the general inconsistency of the results obtained may in part reflect on the validity of the strain data itself.

As indicated in Table 4.3, the majority of the linearized strain plots extended to only about 300 ms after shock arrival. Since the duration of the blast was about 1 sec for all cylinders, the linearized data provide information for only about the first third of the loading period. However, in view of the nature of the results obtained, this is not felt to be a serious limitation, inasmuch as the (nonlinear) slow playbacks provide adequate information in those cases where details at later times are of interest.

Normalized overpressure and dynamic pressure-time curves for Shots 9 and 10 are shown in Fig. 5.29. The overpressure curves are based on the commonly accepted empirical relationship:

$$p_\sigma(t) = p_\sigma(0)\, e^{-ct/t_0} (1 - t/t_0) \qquad (5.2)$$

where $p_\sigma(0)$ is the incident overpressure, t_0 is the duration of the positive phase of the blast, and c is an empirically determined constant. In general, c is known to depend on both scaled height-of-burst and ground range (UPSHOT-KNOTHOLE Project 3.1, Tests on the Loading of Building and Equipment Shapes, WT-721). However, for the present discussion, c = 2 and c = 1 are found to represent adequately the overpressure wave form at both test locations in Shots 9 and 10, respectively.

While the relationship between dynamic pressure and overpressure at the shock front is well-known, the wave form of the dynamic pressure curve is considerably less certain, and adequate measurements are not available at the test locations. In the past, it has been commonly assumed that the Rankine-Hugoniot conditions applicable at the shock front, apply throughout the wave. For small shock strengths, as in the present case, this is tantamount to taking the dynamic pressure time-curve proportional to the square of the overpressure time-curve. While the validity of this approach may be questioned, the dynamic pressure curves shown in Fig. 5.29 are based on such an assumption. Inasmuch as the application of these curves is for a qualitative comparison with the results of the analysis discussed in this section, the present approach is considered acceptable.

The results obtained by the so-called method of graphical analysis for the six sets of strain data considered are summarized in Table 5.5, which briefly indicates the character of the forcing functions so determined.

TABLE 5.5 - Summary of Results Obtained by Graphical Analysis

Cylinder	General Shape of Forcing Function	
	Horizontal Component, F_h	Vertical Component, F_y
3.3c, Shot 9 (See Figs. 5.36, 5.37) $\Delta h = \frac{D}{2}$ $p_\sigma(0) = 4.6$ psi	Force directed upstream after about 30 ms. At 280 ms force is about 0.6 psi; dynamic pressure at this time is about 0.08 psi. Apparently a serious baseline shift.	Force directed upward which tends to about 0.6 psi at about 280 ms. If baseline shift of this amount were included, F_v would appear to oscillate about zero.
3.3d, Shot 9 (See Figs. 5.38, 5.39) $\Delta h = \frac{D}{4}$ $p_\sigma(0) = 4.6$ psi	Shape of F_h uncertain between 20 to 100 ms. Indicates peak unit force of about one psi directed upstream at 60 ms. Between 100 and 200 ms, F_h oscillates about curve having approximate wave form as dynamic pressure curve; "drag coefficient" about 1.5 during this time.	Force oscillating about zero or possibly a slightly negative (i.e., upward) value.
3.3a, Shot 10 (See Figs. 5.42, 5.43, 5.44) $\Delta h = \frac{D}{2}$ $p_\sigma(0) = 3.5$ psi	No appearance of initial peak force. (See Table 5.4.) Indicates wave form practically parallel to dynamic pressure curve from about 15 to 150 ms. Average "drag coefficient" is about 0.27.	Upward force gradually increasing from zero to about 0.15 psi at 40 ms and tends to about 0.21 psi in 140 ms. Dynamic pressure about 0.17 psi at latter time. Rate of initial rise may be more rapid depending on choice of zero time.
3.3b, Shot 10 $\Delta h = \frac{D}{2}$ $p_\sigma(0) = 3.5$ psi	Inconclusive; no indication of sustained initial peak. F_h appears to oscillate about zero or possibly a slightly negative (i.e., upstream) value.	F_v very similar to that of 3.3a, Shot 10; rises to about 0.16 psi in 30 ms and tends to about 0.23 psi in 160 ms. Dynamic pressure is about 0.15 psi at latter time.
3.3d, Shot 10 (See Figs. 5.40, 5.41) $\Delta h = \frac{D}{4}$ $p_\sigma(0) = 2.0$ psi	F_h very similar in shape to that obtained for same cylinder in Shot 9. Shape uncertain between about 30 and 100 ms. Between about 140 and 240 ms, F_h appears to be well defined, indicating a curve which decays somewhat more rapidly than does the dynamic pressure curve during this time; the "drag coefficient" varies from about 5.0 at 160 ms to 1.4 at 230 ms.	Indicates force oscillating about zero.
3.3e, Shot 10 (See Figs. 5.45, 5.46) $\Delta h = \frac{D}{18} = 0.33$ $p_\sigma(0) = 2.0$ psi	F_h similar to 3.3d, Shot 10, although decay of curve between about 100 and 200 ms not as well defined. The average "drag coefficient" appears to be about 6.	Initial rise not well defined. Decays to about 0.15 psi at 160 ms along a curve reasonably parallel to dynamic pressure curve, between about 80 to 160 ms; magnitude of F_v is from 2.5 to 3 times the dynamic pressure during this time.

Referring to Table 5.5 and Fig. 5.30, the results for Cylinder 3.3c, Shot 9, indicate a strong possibility that an appreciable baseline shift occurred in the strain record. The original playback of one strain gage (3.3cS1) suggests a baseline shift at about 200 ms after shock arrival; the other record shows no peculiarities at this time. However, since both slow playbacks end at about 600 ms after shock arrival (i.e., prior to the duration of the blast) no information is available regarding the condition of the baseline at later times. In view of the fact that F_h as determined from the data appears to be the only reasonable interpretation, especially at later times, the data for this cylinder are considered to be erroneous. While the response during the initial loading period may well be meaningful, it is not possible to deduce the necessary detail of the loading function by the present method.

Referring to Table 5.5 and Fig. 5.31, the results for Cylinder 3.3d, Shot 9 appear more or less reasonable. While the horizontal force indicates a negative (upstream) value between about 30 and 100 ms, it is by no means certain that such is actually the case. But, of course, this is precisely the uncertainty involved in the present approach. At later times, the curve appears to oscillate with relatively low frequency about the dashed line indicated in Fig. 5.31a. This curve is approximately parallel to the dynamic pressure curve shown in Fig. 5.29, and is of the order of magnitude of the dynamic pressures acting at this time. The ratio of these two pressures, or "drag coefficient"[6] is about 1.3. Insofar as the vertical force F_v is concerned, the results of Fig. 5.31b can only be interpreted as indicating a mean value of zero.

The results for the same cylinder in Shot 10, Fig. 5.32, are similar to those described above. The extent of the negative portion of F_h is practically identical and the peak negative values are in the same ratio as the incident overpressure. Beyond about 160 ms, both the shape and magnitude of F_h seems to be well-defined. This portion of the curve is compared with the approximate dynamic pressure curve in Fig. 5.32a, and it is seen that F_h decays more rapidly than does the dynamic pressure curve. Specifically, the "drag coefficient" decreases from about 5 at 160 ms to 1.4 at 230 ms. That the drag pressures appear to be unrealistically high stands in marked contrast to the fact that initial peak forces are found to be low. This would tend to support the contention that initial peak forces cannot be obtained from the strain data in what might be termed a direct manner. However, an alternate interpretation is suggested below. The net vertical force again indicates a mean value of zero with no initial peak observable.

Inspection of the original playback for the cylinder on Shot 10 indicates a well-defined frequency of about 5 cps, which is also evident in the results for F_h and F_v. The fact that this frequency extends beyond the duration of the blast suggests the possibility that, rather than indicating the shape of the pseudo-steady-state loading, the results

6/ Quotation marks are used to emphasize the qualitative nature of these results, both with regard to the determination of F_h and the particular choice of the dynamic pressure curve.

of Fig. 5.32 simply represent a portion of this low-frequency oscillation. In such cases, F_h would then appear to be oscillating about zero as a mean, and the difference in "drag coefficient" noted in Shots 9 and 10 would be due entirely to the differences in amplitude of this motion. No conclusions can be drawn regarding these choices of interpretation.

With reference to Table 5.5 and Figs. 5.33a and b, the results for Cylinder 3.3a, Shot 10, deserve special mention. The strain data for this cylinder were orginally discarded, since the strain calibration appeared to be in error by a factor of about 10. However, the results of the graphical analysis indicate, beyond about 20 ms, a horizontal force practically parallel to the dynamic pressure curve, and whose magnitude yields an average "drag coefficient" of around 0.27; this is close to steady-state experimental data of about 0.35. That the peak force appears to have been missed, of course, can be attributed to the complexity of the dynamic system noted earlier. But it is surprising that nearly all other cylinders showed a predominant initial peak – even if somewhat low.

The results obtained for the vertical force, F_v, are also of interest. As can be seen from Fig. 5.33b, F_v appears to increase from zero to a constant value at about 150 ms; the pressure at this time is slightly in excess of the dynamic pressure. The trend indicated here for F_v appears to be the only reasonable interpretation of the data by the present method, and stands in contrast to all expectations. It might be noted that Cylinder 3.3d, which indicated a zero net vertical force in both Shots 9 and 10, was closer to the ground than Cylinder 3.3a.

The data for Cylinder 3.3a, Shot 10, were such that some uncertainty arose in establishing a common zero time in constructing the horizontal and vertical strain components. This uncertainty amounted to a relative time shift of about 5 ms and, accordingly, F_h and F_v were constructed on the basis of two different zero positions. While the resultant strain record differed to some extent in phasing, the median curves were consistent within the expected accuracy of the method. The principal difference occurred in the shape of F_v where the initial rise time appeared to vary by about 20 ms, depending upon the choice of zero time. The results obtained for F_h are indicated in Fig. 5.33c where F_h as determined from one choice of zero time, is superimposed on the strain record constructed according to the second choice in zero time. A comparison of the two strain records can be seen between Figs. 5.33a and c.

Cylinder 3.3b is the quarter-scale model of Cylinder 3.3a discussed previously. The results for Shot 10 shown in Table 5.5 tend to support the shape of F_v found above, but are definitely not consistent with the horizontal force found for Cylinder 3.3a. As well as can be seen, F_h appears to be oscillating about zero as a mean, and does not indicate a shape similar to dynamic pressure curve. The shape of F_v, however, is practically identical to that found above, which must lend support to the validity of this result.

As discussed in Section 5.2.6 some work was done on the use of the ARF analog computer as a curve-fitting device in connection with the present data reduction problem. Preliminary results obtained with one strain record on Cylinder 3.3b, Shot 10, indicate a forcing function approximately parallel to the dynamic pressure curves (see Fig. 3.37), and nearly identical to the shape of F_h, as found for Cylinder 3.3a, Shot 10 by the present method. The fact that this trend was not found by means of graphical analysis might be due to uncertainties in locating the common zero time, although, as discussed above, this source of error appeared to be negligible in other cases.

Cylinder 3.3e was the nearest to the ground of the items tested. As indicated in Table 5.5 and Fig. 5.34, the shape of F_h is consistent with that found for Cylinder 3.3d in both Shots 9 and 10. The initial portion of F_v is not well-defined but beyond about 80 ms the curve is practically parallel to the dynamic pressure curve. Due to the qualitative nature of the analysis, the shape of F_v found here may not be inconsistent with those found for Cylinders 3.3a and b, Shot 10. The larger vertical force indicated for Cylinder 3.3e is certainly reasonable, but shows a somewhat smaller influence of ground proximity than had been anticipated.

5.2.5 Application of Transient Analysis

A numerical data-reduction scheme referred to as transient analysis was developed during the pretest planning phase of the program. The development and critical discussion of the method is presented in Appendix A. The present section is concerned with the specific application of the method to the strain data.

The method of transient analysis was designed to determine the input or forcing function to a linear system whose transfer functions[7] are not known but whose output or response function is known. In general, for a multi-degree-of-freedom system the solution to this problem is not unique; that is, a given response in a particular mode of the system may result from more than one combination of forcing functions in the various modes. In the original development of the method, it was believed that uniqueness stemmed from the fact that, in the present application, both the unknown forcing and transfer functions could be adequately represented by a particular class of analytic functions. Specifically, the forcing function was represented by a finite sum of exponential terms (i.e., "e" functions), all of whose exponents and coefficients were real, and the transfer function was represented by a similar series, all of whose exponents and coefficients occurred in complex conjugate pairs. (This is equivalent to assuming a forcing function that has no harmonic components, and a transfer function consisting of damped sinusoids.) Based on this particular representation, the method in brief, consists of curve-fitting the known response to

---

[7] The transfer function refers to the response of the system in one mode due to a unit impulse applied in another mode (see Appendix A).

a similar exponential series, and then identifying those coefficients and exponents which belong to the forcing function. (In the process the transfer function is determined also.)

In the present application of the method, the known response was fitted to a five-term exponential series as described in Appendix A. It was hoped that the fifth-order polynomial resulting from this curve fitting would have three real roots and two complex conjugate roots. If so, the analysis would yield a forcing function consisting of three exponential terms, and a transfer function containing a single frequency. However, as it turned out in the majority of cases, the analysis provided only a one-term approximation to the forcing function and two frequencies. The results obtained are shown in Table 5.6, only a relative scale being indicated for the magnitude of the forcing function.

The two cases for which three terms in the forcing function were obtained are plotted in Fig. 5.35; the shape of the dynamic pressure curve from Fig. 5.29 is indicated for comparison. The result for Cylinder 3.3c, Shot 9 (Fig. 5.35a), shows no pronounced peak, but indicates a rate of decay nearly identical to the dynamic pressure curve. (It will be recalled that the results of the previous section for this cylinder indicated a strong baseline shift.) The result for Cylinder 3.3e, Shot 10 (Fig. 5.35b), is unrealistic. In general, the results indicated in Table 5.6 are not believed to be an adequate interpretation of the strain data and, as such, it must be concluded that the present application of transient analysis was unsatisfactory. In an attempt to understand just why the analysis failed, a rather detailed post-test reappraisal of the method was undertaken. Much of the critical discussion presented in Appendix A is a result of this further study.

The failure of this first attempt can be explained in terms of the poor fit obtained for the known response by means of the five-term exponential series. Whether it was due to computational errors or simply an inadequate number of terms in the approximating series, the fact remains that the determination of the forcing function was based on an analytical expression that was not an adequate representation of the measured strain-time curve.8/

As discussed in Appendix A, the valid application of transient analysis is limited to linear systems where the forcing functions associated with each mode are either zero or timewise proportional. When the forcing functions are not all timewise proportional, the results of the analysis probably cannot be given physical meaning. (This limitation of the method was not fully appreciated at the outset.) The results obtained in the previous section indicate that,

---

8/ The method of transient analysis was applied to the strain data obtained in UPSHOT-KNOTHOLE Project 3.4 (Tests on the Loading of Truss Systems Common to the Open-Framed Structures, WT-723) with equally unsatisfactory results. The analysis was repeated, based on better curve-fitting of the data, but the work was not completed and no conclusive results were obtained. However, indications were that the analysis was capable of providing meaningful results, in at least this case.

TABLE 5.6 - Results of Transient Analysis; Coefficients and Exponents of Forcing Function, f(t)

$$f(t) = F_1 e^{\alpha_1 t} + F_2 e^{\alpha_2 t} + F_3 e^{\alpha_3 t} \quad (t \text{ in ms})$$

Strain Record	Shot	Numerical Constants					
		F_1	F_2	F_3	α_1	α_2	α_3
3.3aS1	10	1			-0.017		
3.3aS2	10	1			-0.067		
3.3bS1	10	1	0.47	-0.63	-0.146	-0.664	-1.032
3.3bS2	10	1			-0.013		
3.3cS1	9	1	-0.95	0.44	-0.007	-0.188	-0.093
3.3cS2	9	1			-0.147		
3.3dS1	9	1			-0.124		
3.3dS2	9	1			-0.113		
3.3dS1	10	1	0.51	-0.67	-0.086	-0.177	-0.498
3.3dS2	10	1			-0.124		
3.3eS1	9	1			-0.038		
3.3eS2	9	1			-0.088		
3.3eS1	10	1			-0.314		
3.3eS2	10	1	-0.72	0.90	-0.080	-0.505	-0.136

at least initially, the time details of the horizontal and vertical force components differ considerably. Hence, there is a strong indication that at least two modes of vibration are excited by timewise dissimilar forces. The fact that, initially, the method of transient analysis may be invalid in the present application, may also explain the unsatisfactory results obtained.

5.2.6 Analog Computer Method

Work was initiated toward the end of the post-test period on use of the ARF Analog Computer to deduce the desired input functions from the strain records. The method of solution consists of simulating a dynamic system on the computer which yields displacements similar to the strain record under consideration, and then adjusting the circuit parameters so that the two displacement-time curves are essentially the same. The system equations are taken to be a series of linear second-order differential equations with constant coefficients, an assumption which is also basic to the method of transient analysis. The forcing function may be represented by a variety of analytical or graphical functions on the computer but to-date only decaying exponential terms have been utilized, again as in the method of transient analysis.

On first thought this approach might seem rather hopeless in view of the large number of unknown quantities involved; i.e., the constants of the system equations and the parameters of the forcing function. However, the method appears to be quite practical and, while not carried sufficiently far as to provide any conclusive results, gives indications of being an advantageous approach. The feasibility of the method in practice stems from the fact that the strain record to be matched can be plotted on graph paper and the displacement arising from the simulated system can be plotted automatically by means of an "x-y recorder" on the same sheet of paper. This allows a visual estimate of the accuracy of the matching, and permits much more judgment on the part of the operator in carrying out the solution than is possible using a numerical method. This advantage, together with the brief time required for varying parameters and obtaining solutions, permits the matching to be completed in a relatively short time. A block diagram for a simulated system incorporating two modes of oscillation (i.e., two frequencies in the transfer function) is shown in Fig. 5.36. (In the actual analog circuit the damping coefficients and the frequencies can be varied by single adjustments.)

This analog curve-fitting process based on a two-term exponential representation of the forcing function was applied to strain record 3.3bS2, Shot 10. The resulting displacement curve and forcing function are shown in Fig. 5.37; the original strain record is shown in Fig. 5.38 for comparison. The results shown in Fig. 5.37 are only of a preliminary nature and do not necessarily represent the best possible match between the two curves which can be obtained by the present method. Even so, a comparison of Figs. 5.37 and 5.38 indicates that a reasonable fit has been obtained. It will be noticed that the phase

of the simulated displacement differs somewhat from the actual record. This can be corrected by introducing a third component to the forcing function having a finite value at zero time (positive or negative), and which decays to zero quite rapidly. This additional forcing component would not affect the displacement record after about 50 ms where the fit is quite reasonable. It would, of course, be difficult, if not impractical, to match the actual strain record identically over the entire time range of interest, since the actual system may have initially excited modes which cannot be observed sufficiently well and thus cannot be simulated.

The derived forcing function is compared with the dynamic pressure curve in Fig. 5.37, and it is seen that the wave form is approximately the same for both curves. It will be recalled that the graphical approach described in Section 5.2.4 provided no conclusive results in this case; if anything the horizontal force appeared to oscillate about zero as a mean.

The present discussion is by no means intended as a comprehensive study of the application of the analog computer to the present problem of data reduction, inasmuch as this technique was only initiated toward the end of the post-test period. However, this preliminary work has indicated a reasonable expectation of ultimate success, and it is strongly recommended that this work be pursued further as part of an over-all study into the data-reduction problems associated with net force measurement systems.

One advantage of the analog approach which concerns the forcing function approximation should be emphasized. It is not necessary in the analog scheme to be restricted to an exponential approximation of the forcing function (as is the case in transient analysis), since it is possible to generate many other functions on the computer. For example, one form of representation which could be handled easily is a series of straightline sections during the initial loading period followed by either a linear or exponential decay to zero. In fact, existing load prediction schemes could be generated on the computer and the response of the simulated system compared with the actual response data.

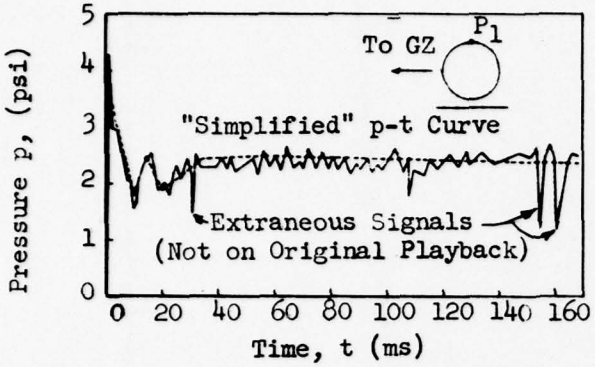

a. Cylinder 3.3a, Gage P1, Shot 10

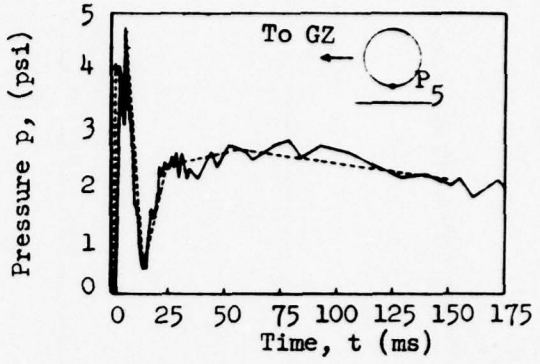

b. Cylinder 3.3e, Gage P5, Shot 9

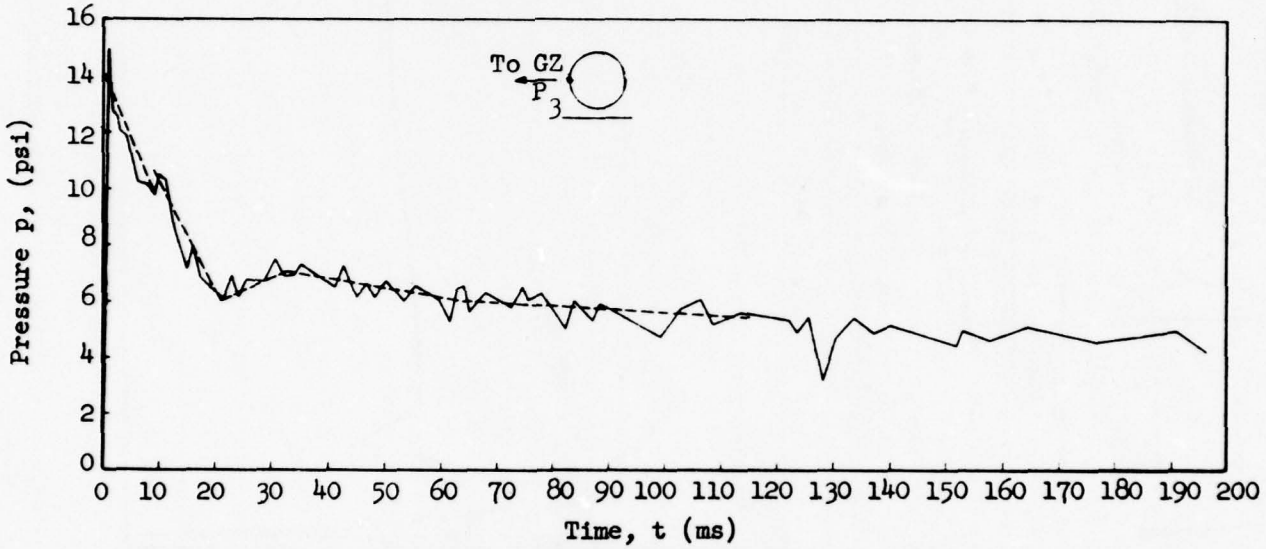

c. Cylinder 3.3a, Gage P3, Shot 9

Fig. 5.1 Typical Linearized Pressure-Time Records

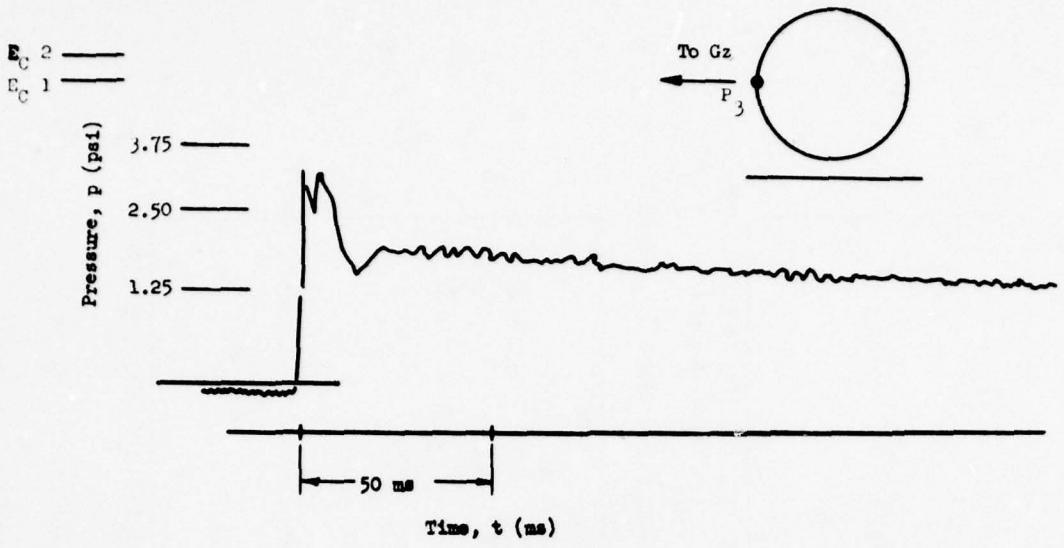

a. Original Record

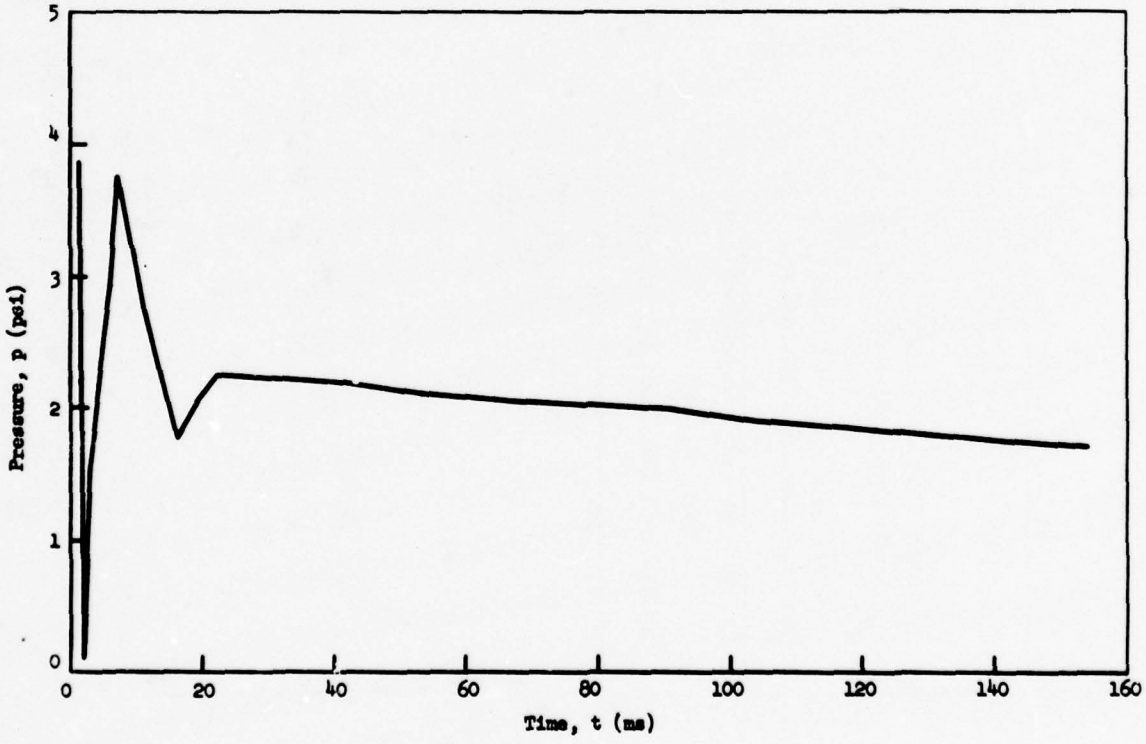

b. Linearized Record

Fig. 5.2 Original and Linearized Pressure-Time Records (3.3e P3, Shot 10)

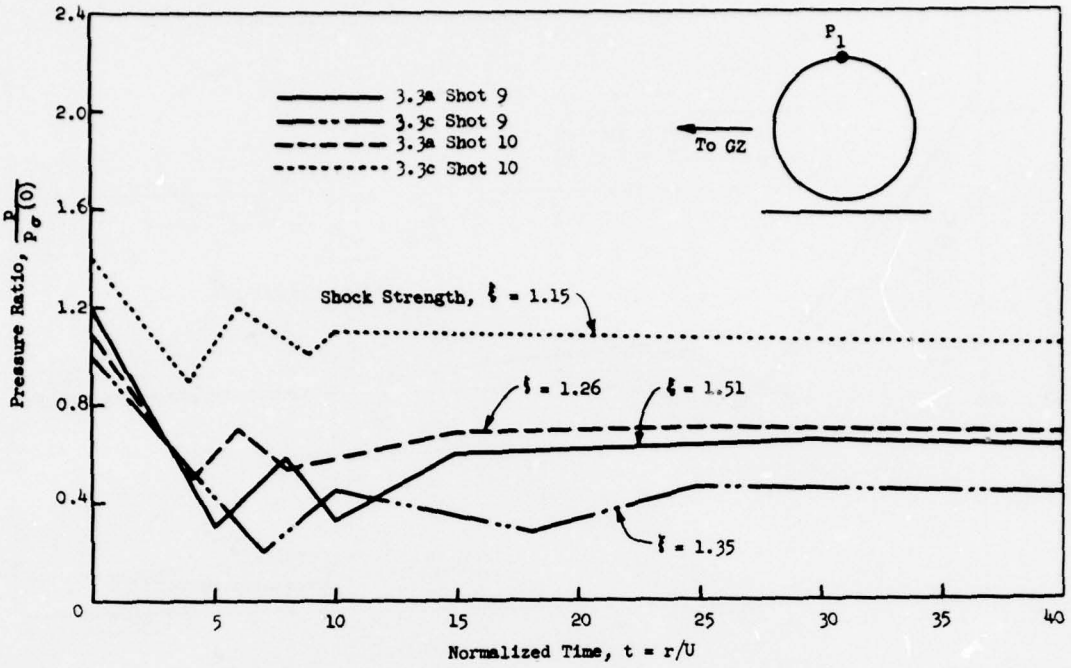

Fig. 5.3 Effect of Shock Strength, Gage P1 (Δ h/D = 0.5)

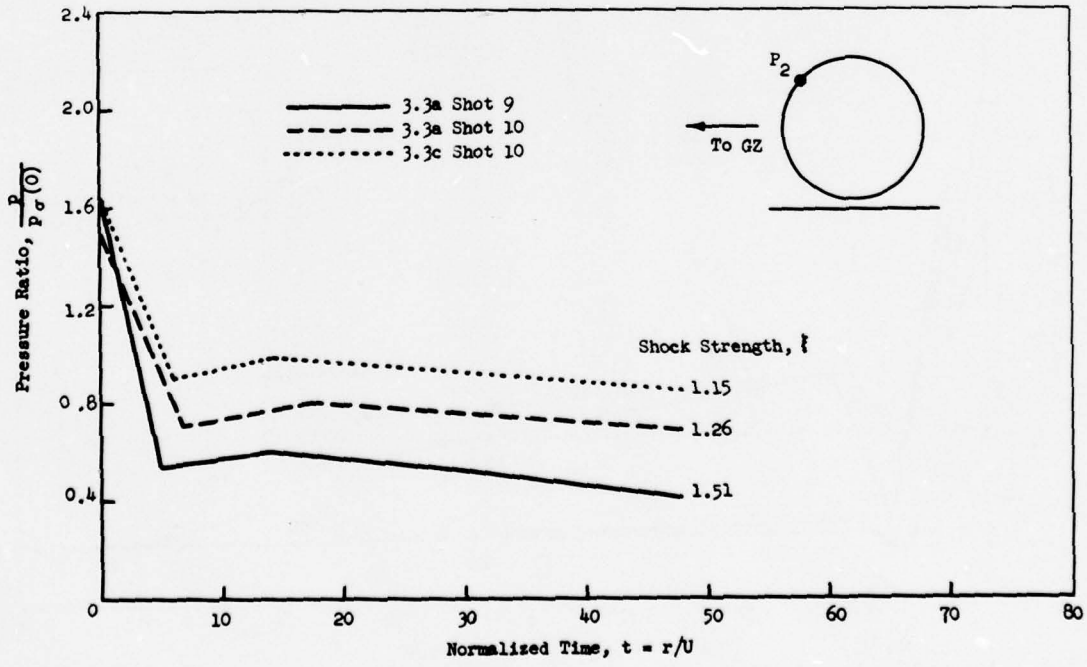

Fig. 5.4 Effect of Shock Strength, Gage P2 (Δ h/D = 0.5)

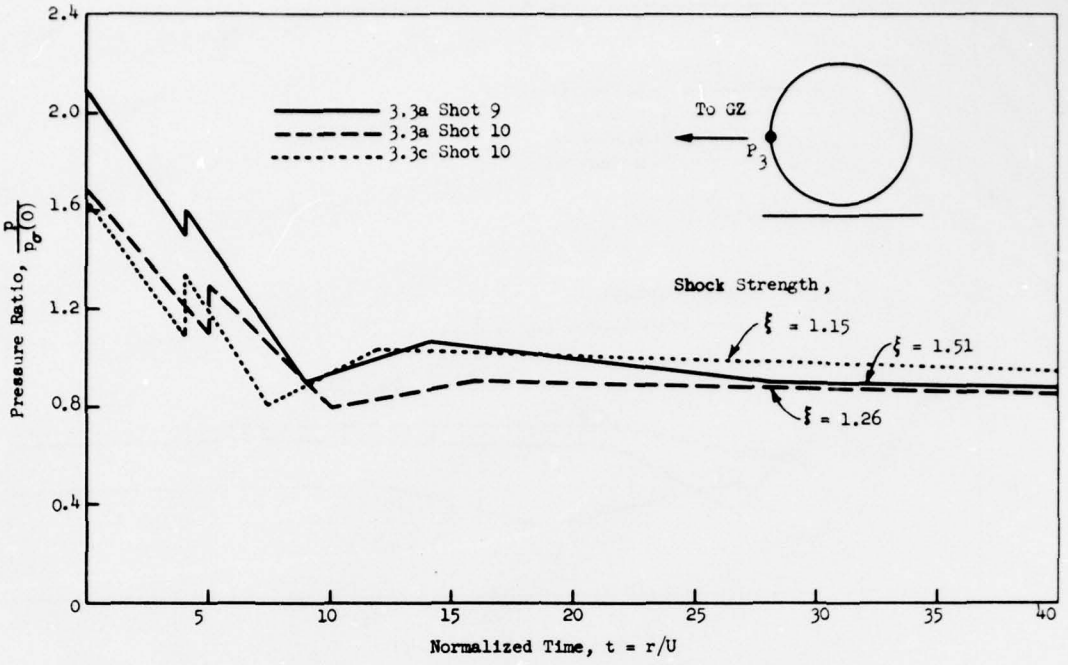

Fig. 5.5 Effect of Shock Strength, Gage P3 (Δ h/D = 0.5)

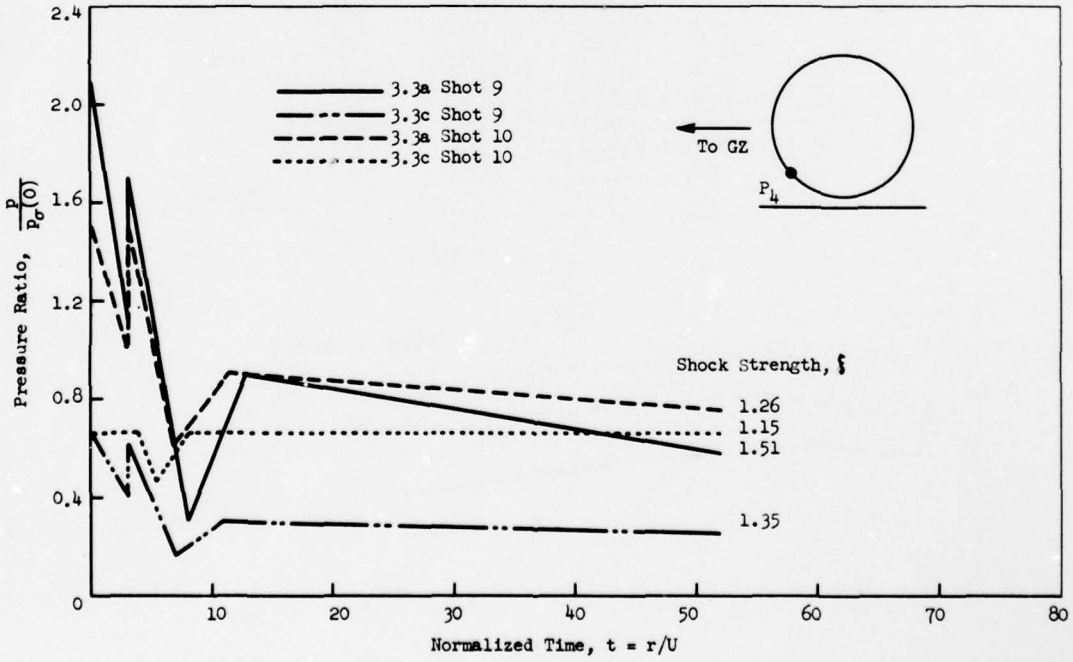

Fig. 5.6 Effect of Shock Strength, Gage P4 (Δ h/D = 0.5)

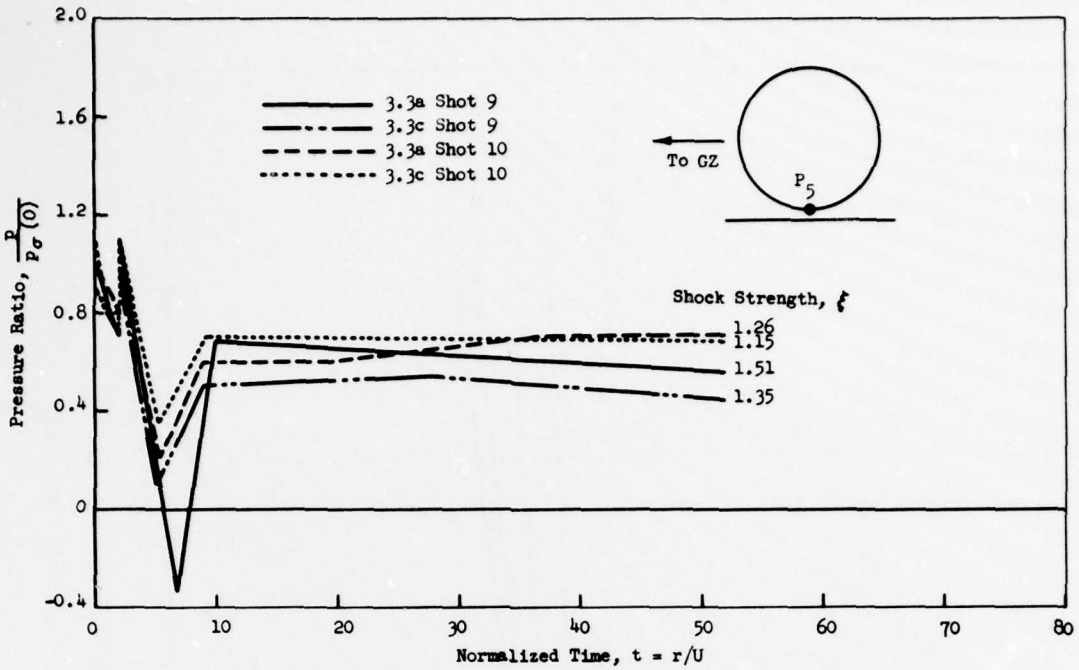

Fig. 5.7 Effect of Shock Strength, Gage P5 ($\Delta h/D = 0.5$)

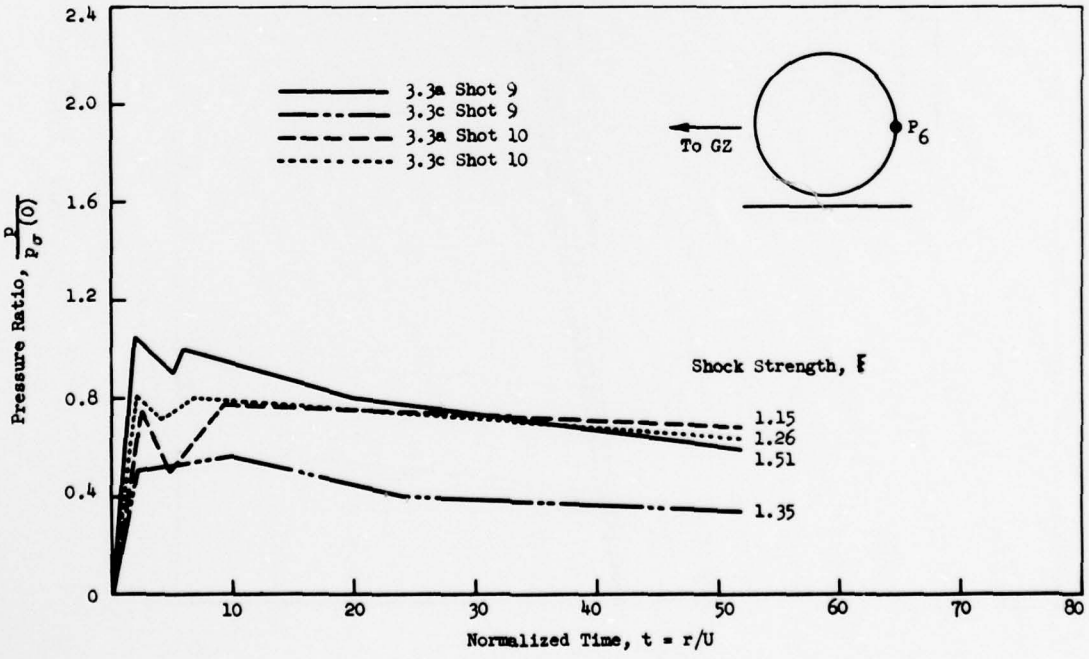

Fig. 5.8 Effect of Shock Strength, Gage P6 ($\Delta h/D = 0.5$)

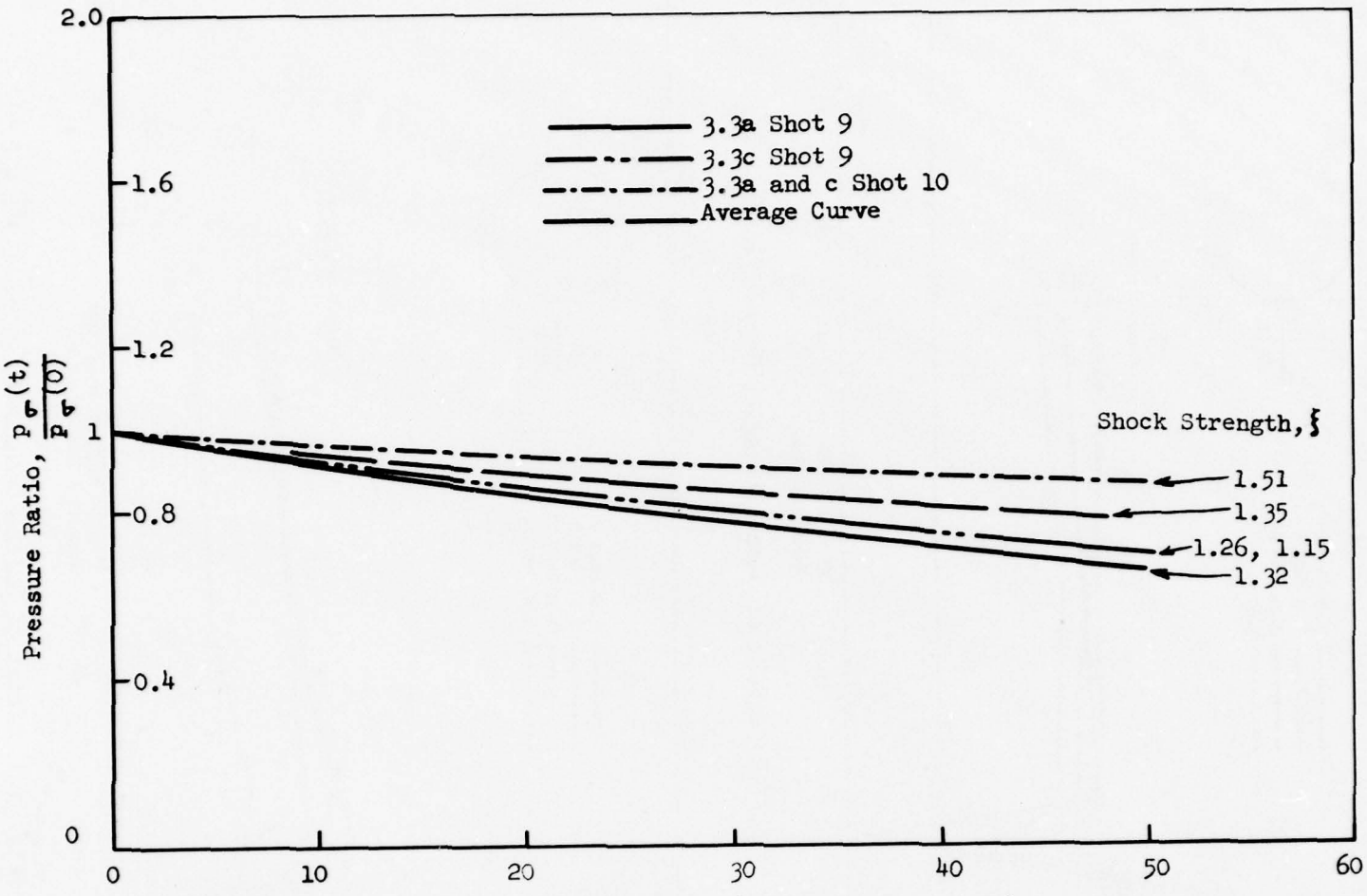

Fig. 5.9 Normalized Free-Stream Pressure-Time Curves

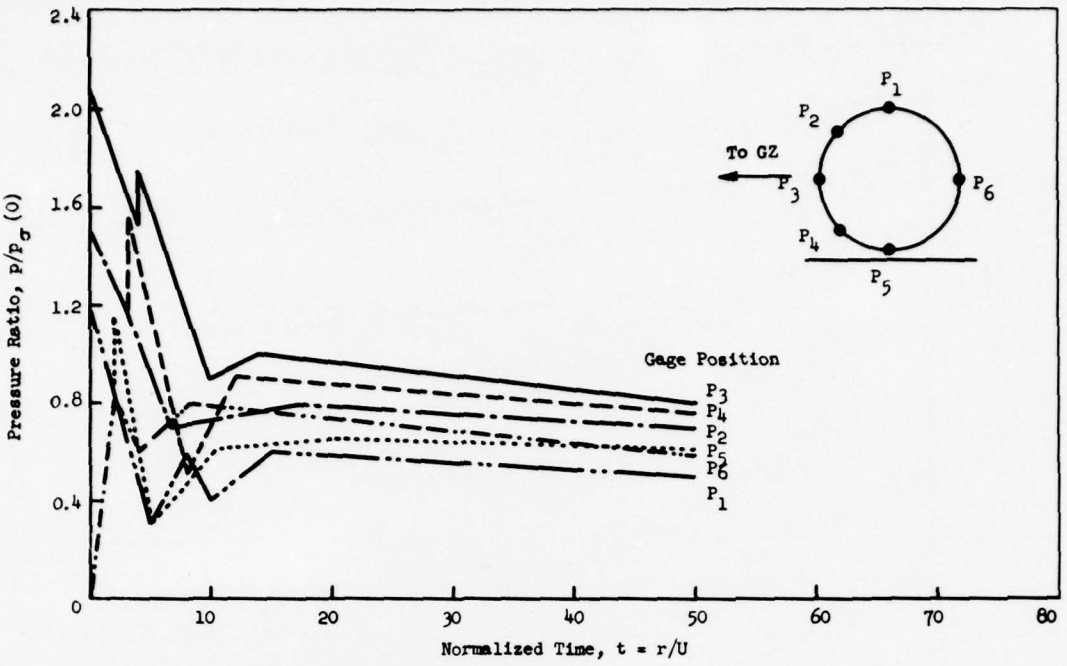

Fig. 5.10 Pressure-Time Curves, Averaged Data (ζ = 1.32, $\Delta h/D$ = 0.5)

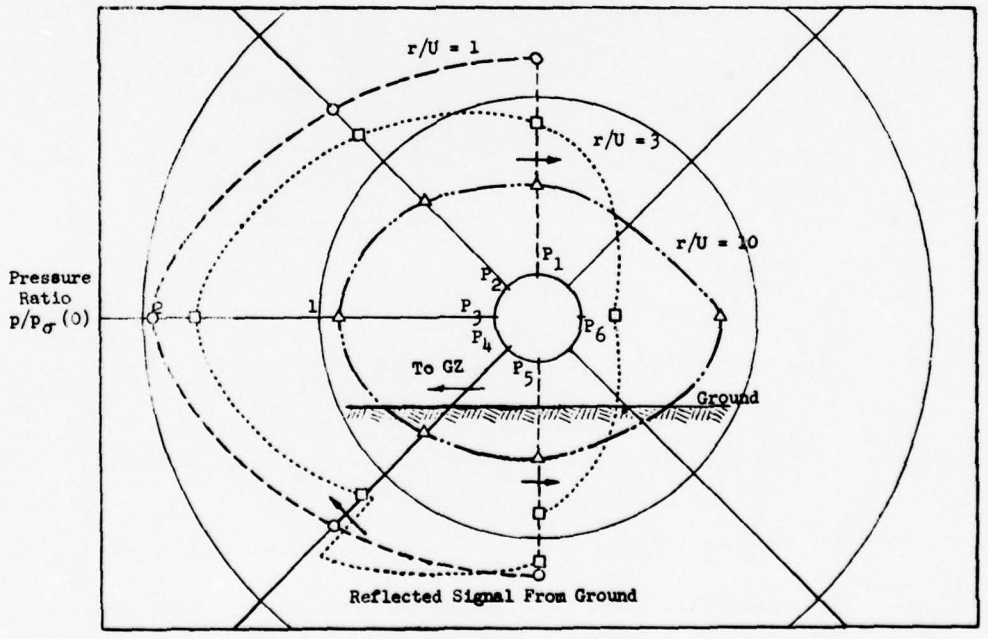

Fig. 5.11 Pressure Distribution on Cylinder, Averaged Data ($\Delta h/D$ = 0.5)

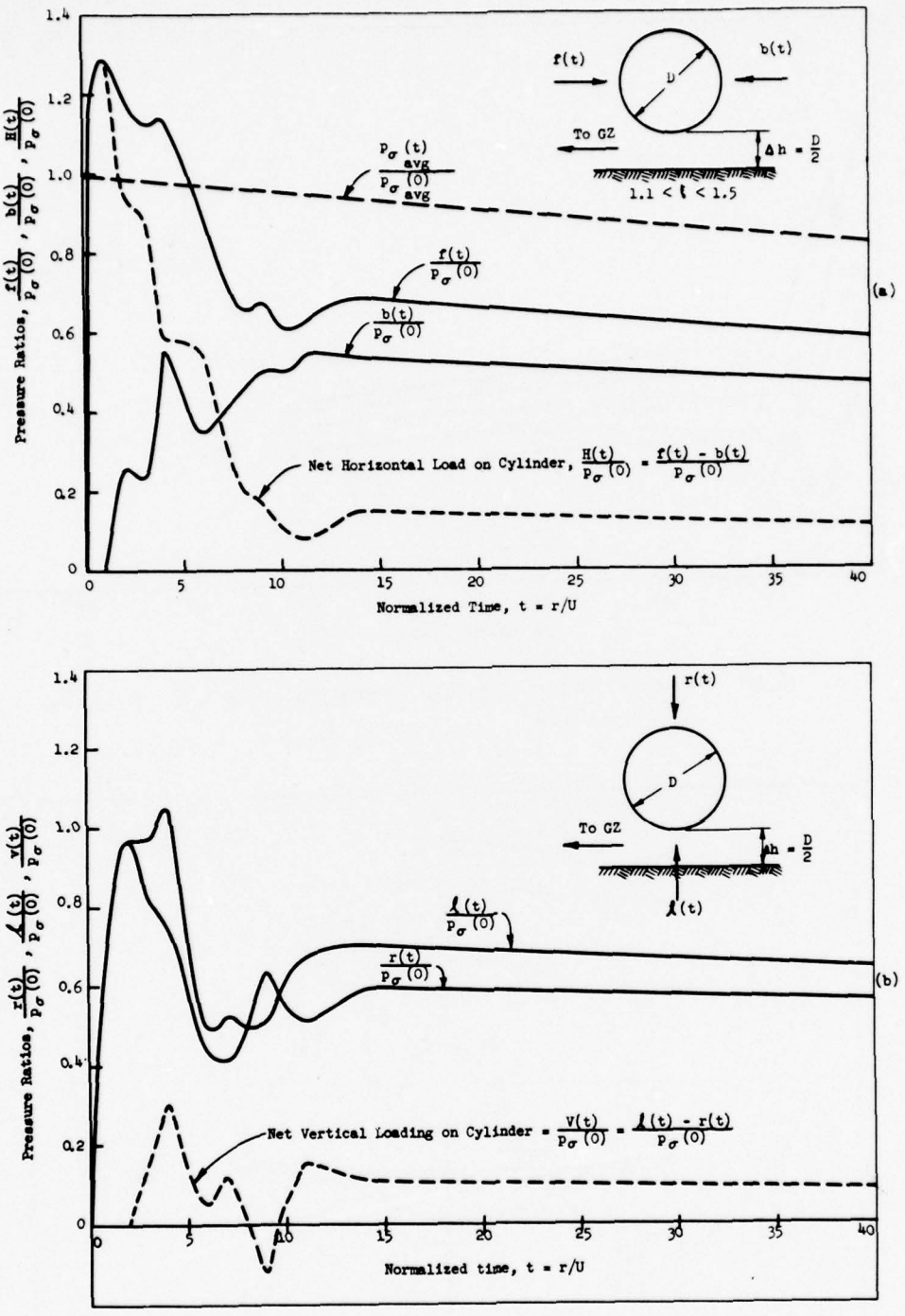

Fig. 5.12 Pressure-Time Curves Showing Horizontal and Vertical Loadings on Cylinder, Average Data ($\Delta h/D = 0.5$). (a) Horizontal Loading; (b) Vertical Loading

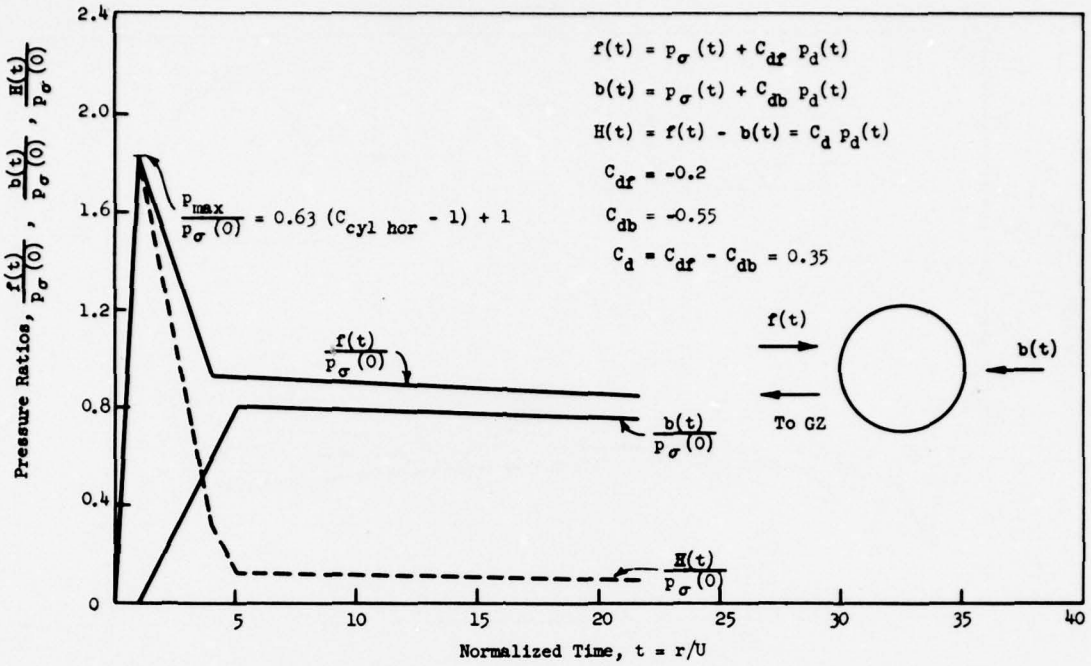

Fig. 5.13 Predicted Loading on Two-Dimensional Cylinder in Free Space, Averaged Data

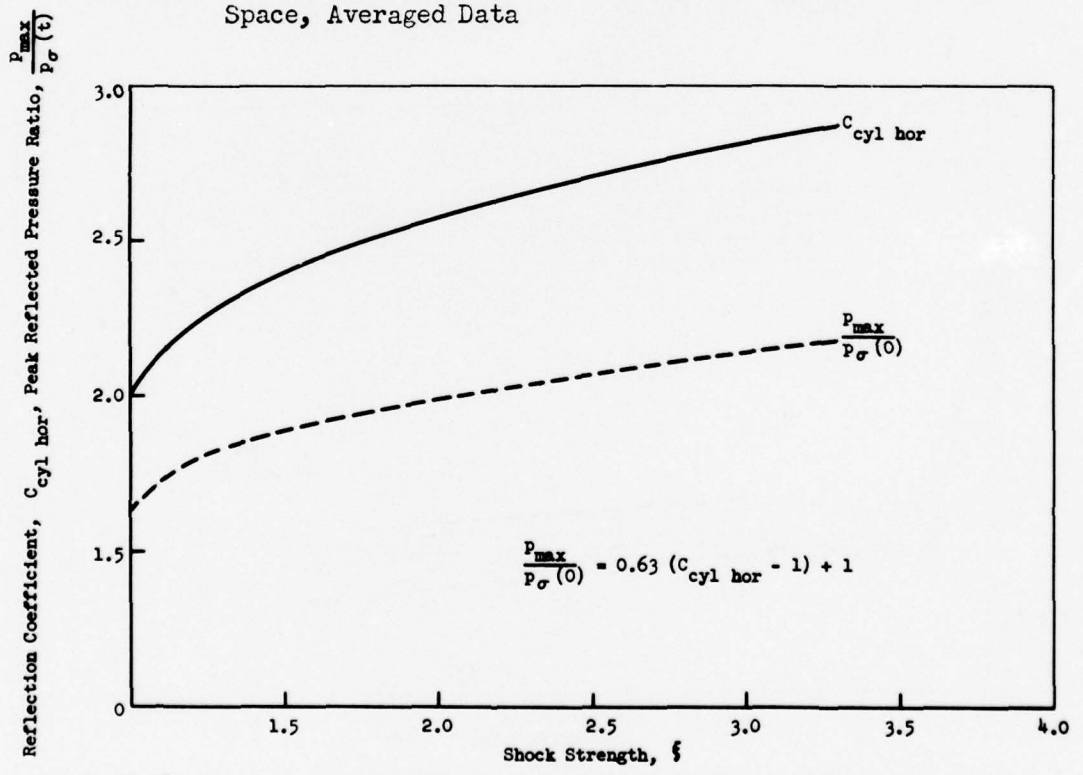

Fig. 5.14 Reflection Coefficient and Peak-Reflected Pressure Ratio as a Function of Shock Strength

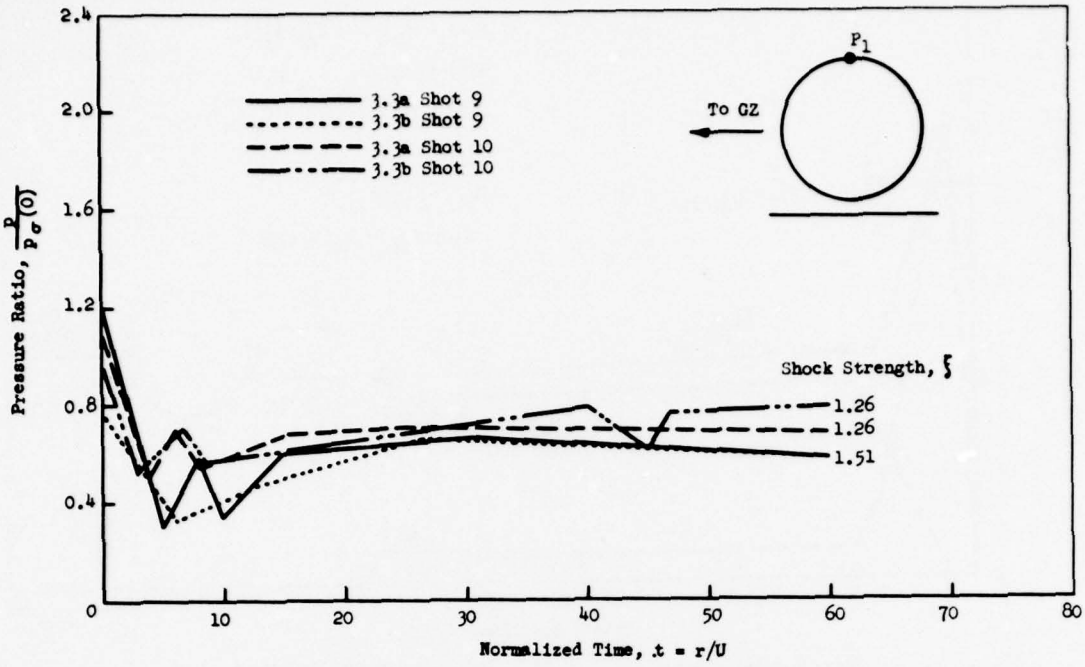

Fig. 5.15 Effect of Size, Gage P1 (Δ h/D = 0.5)

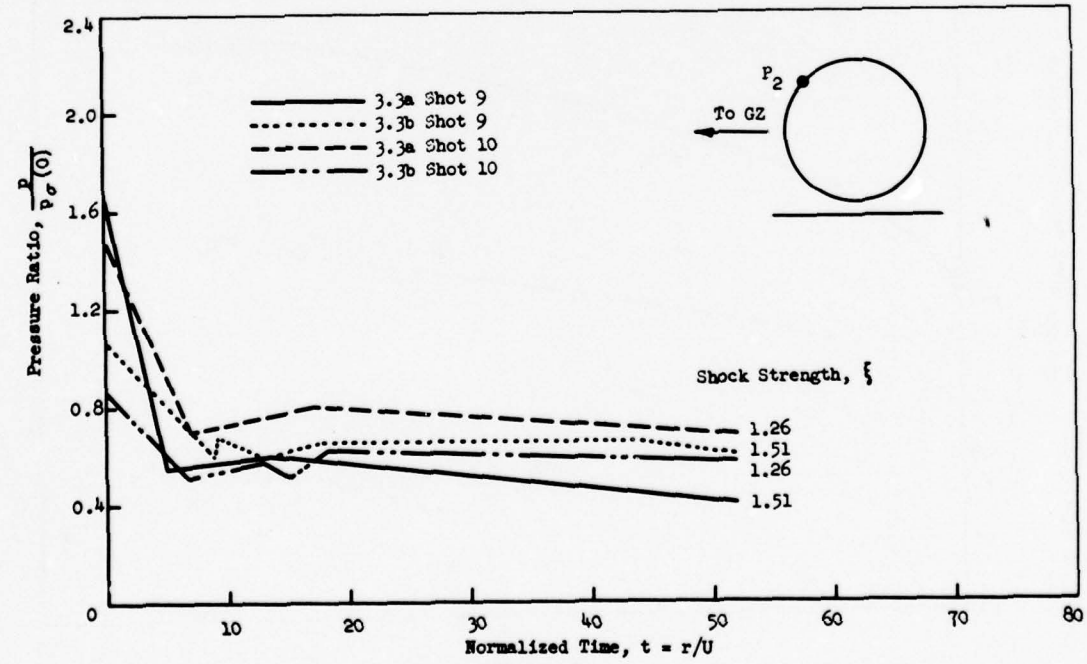

Fig. 5.16 Effect of Size, Gage P2 (Δ h/D = 0.5)

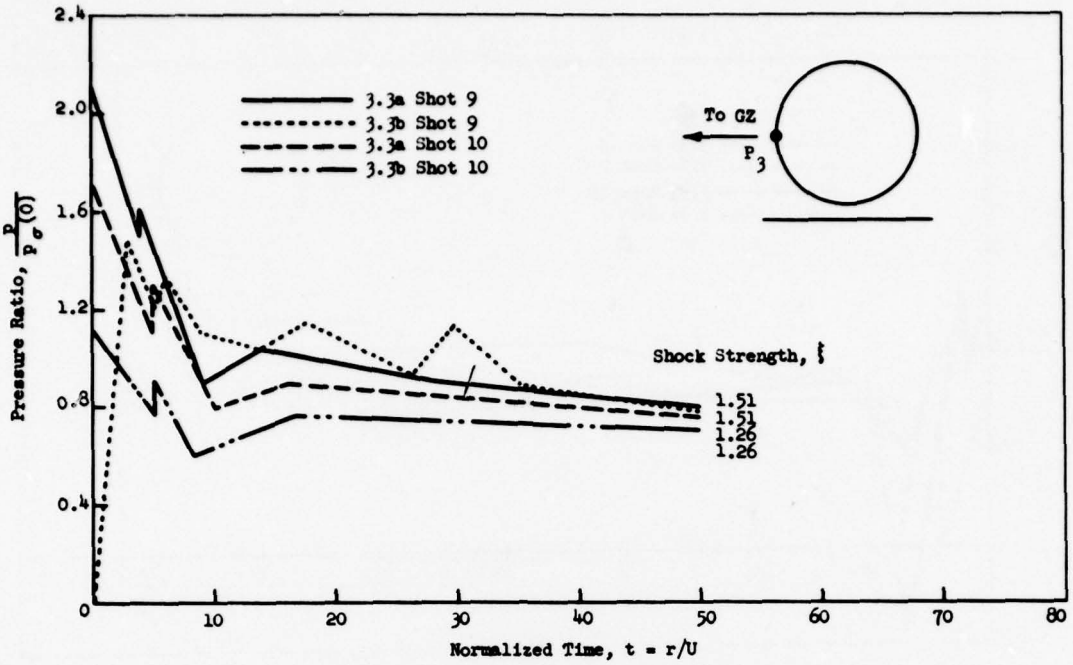

Fig. 5.17 Effect of Size, Gage P3 (Δ h/D = 0.5)

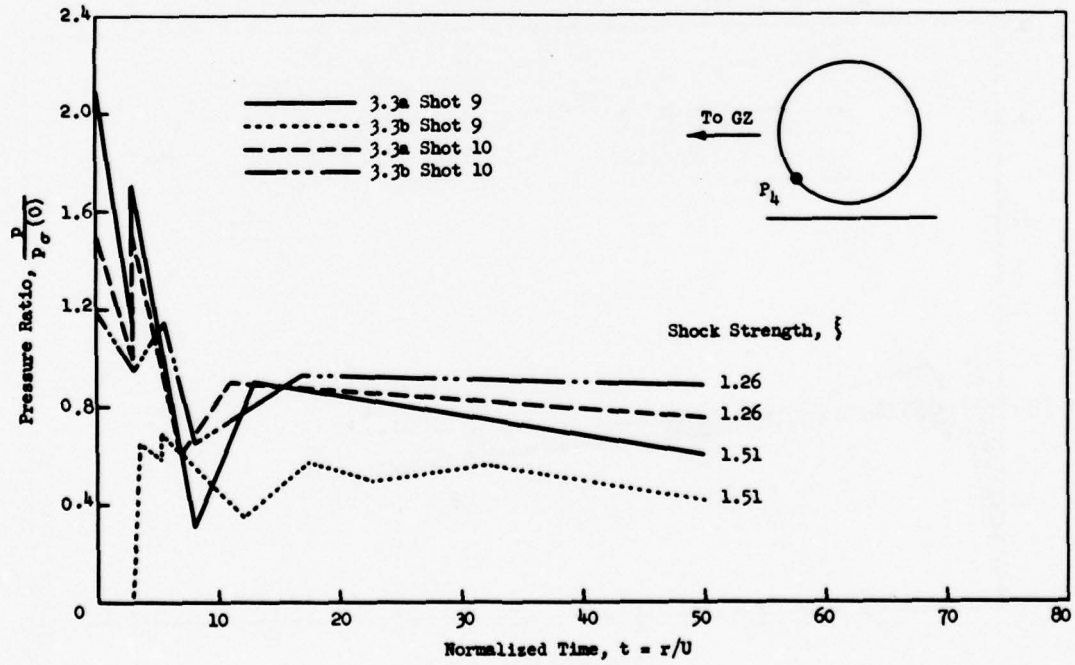

Fig. 5.18 Effect of Size, Gage P4 (Δ h/D = 0.5)

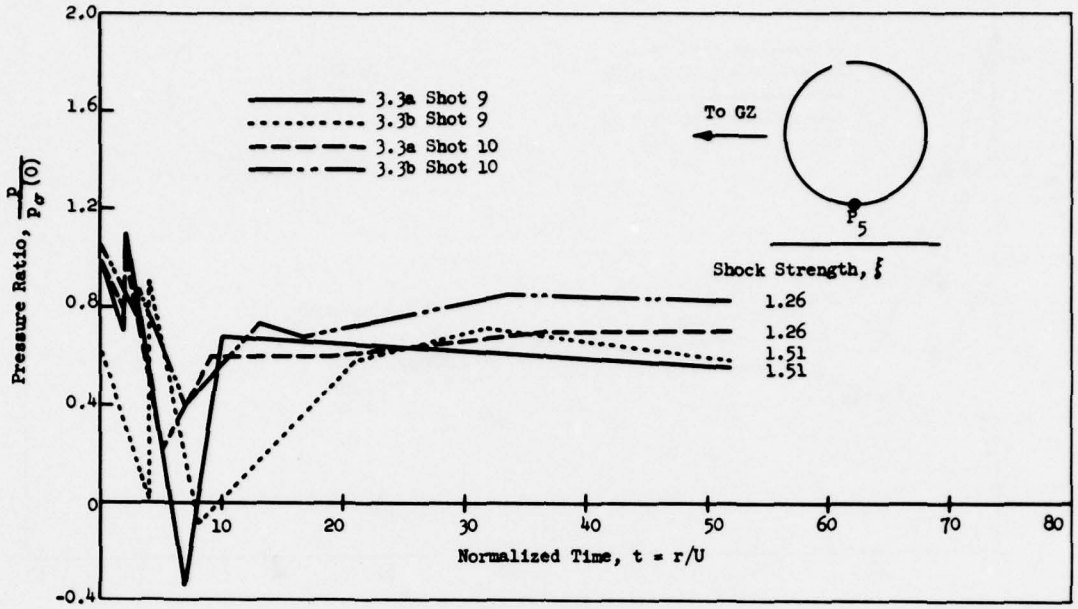

Fig. 5.19 Effect of Size, Gage P5 (Δ h/D = 0.5)

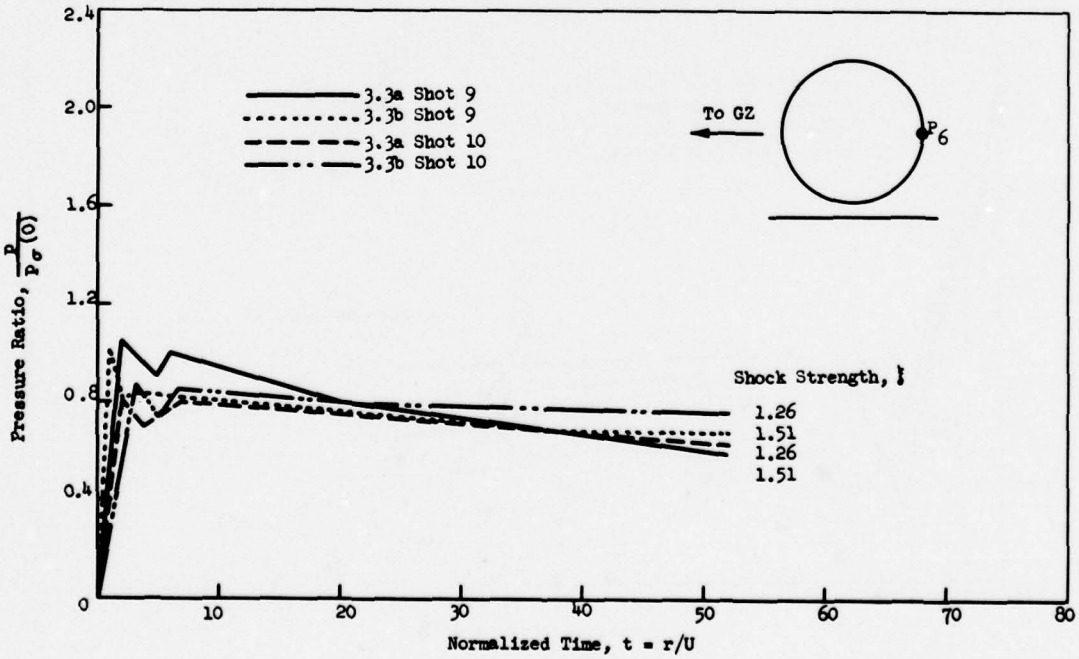

Fig. 5.20 Effect of Size, Gage P6 (Δ h/D = 0.5)

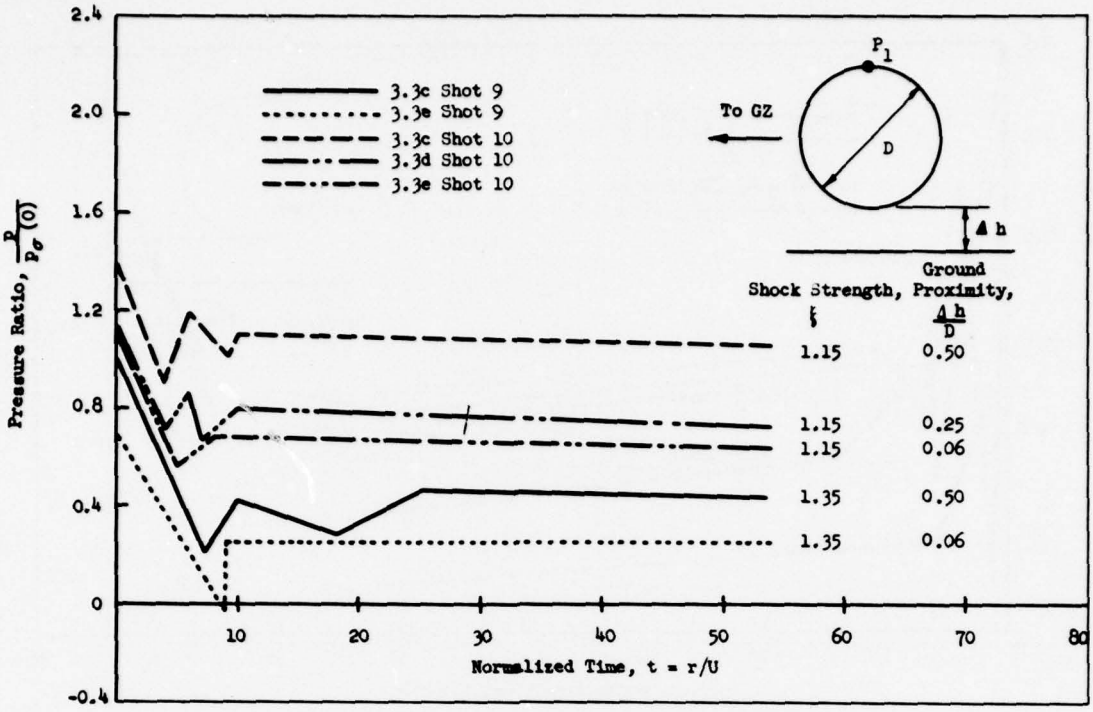

Fig. 5.21 Effect of Ground Proximity, Gage P1

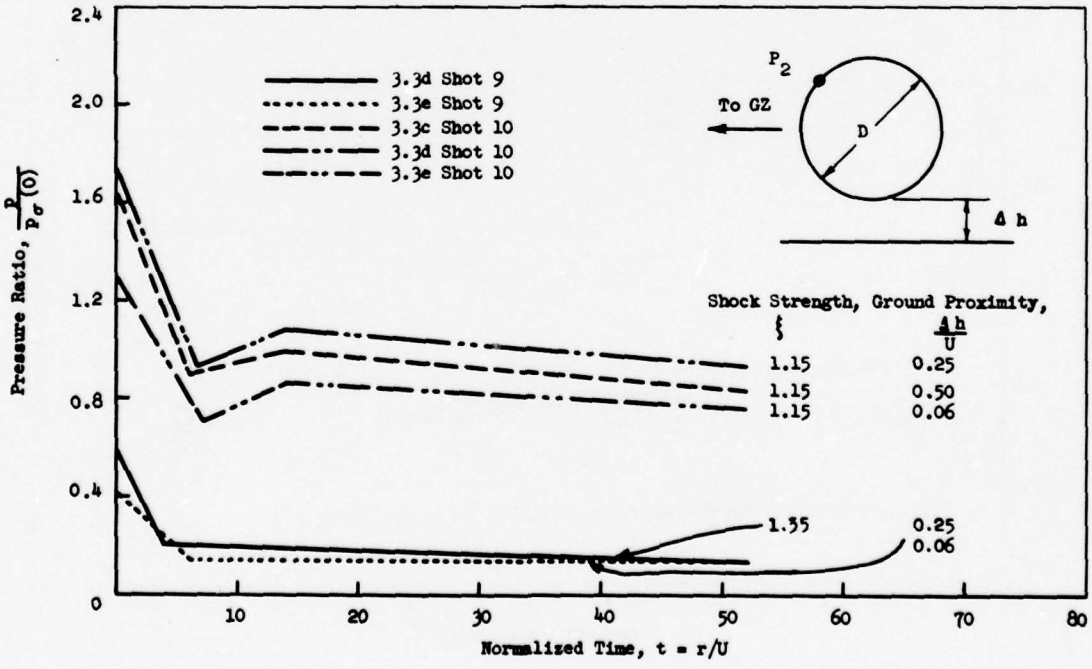

Fig. 5.22 Effect of Ground Proximity, Gage P2

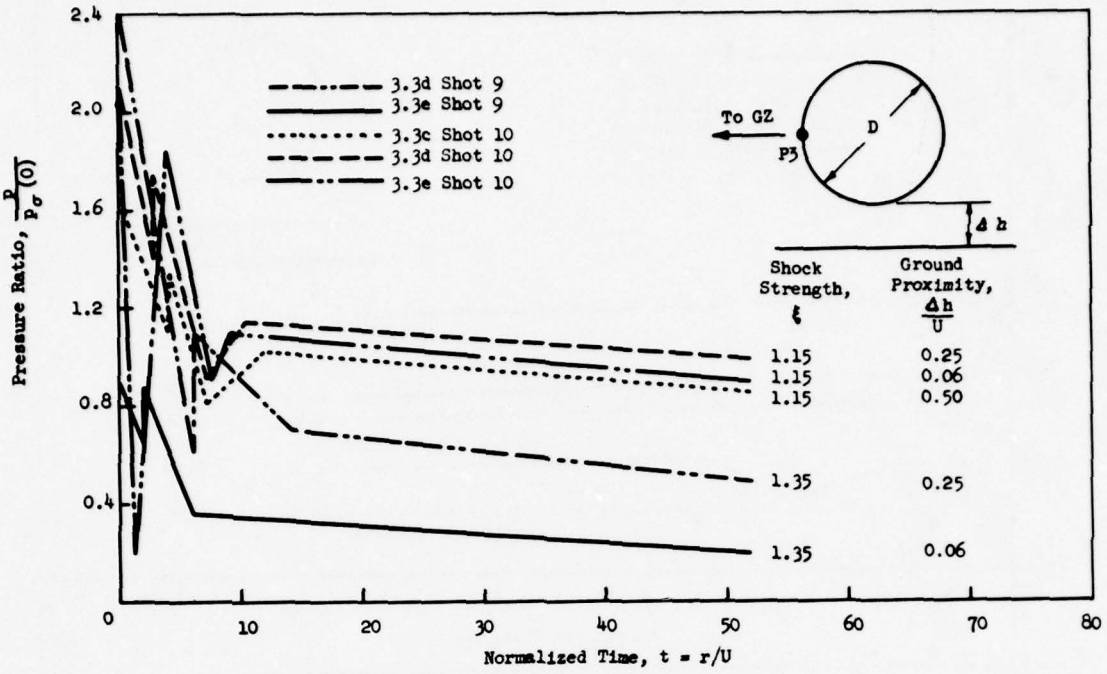

Fig. 5.23 Effect of Ground Proximity, Gage P3

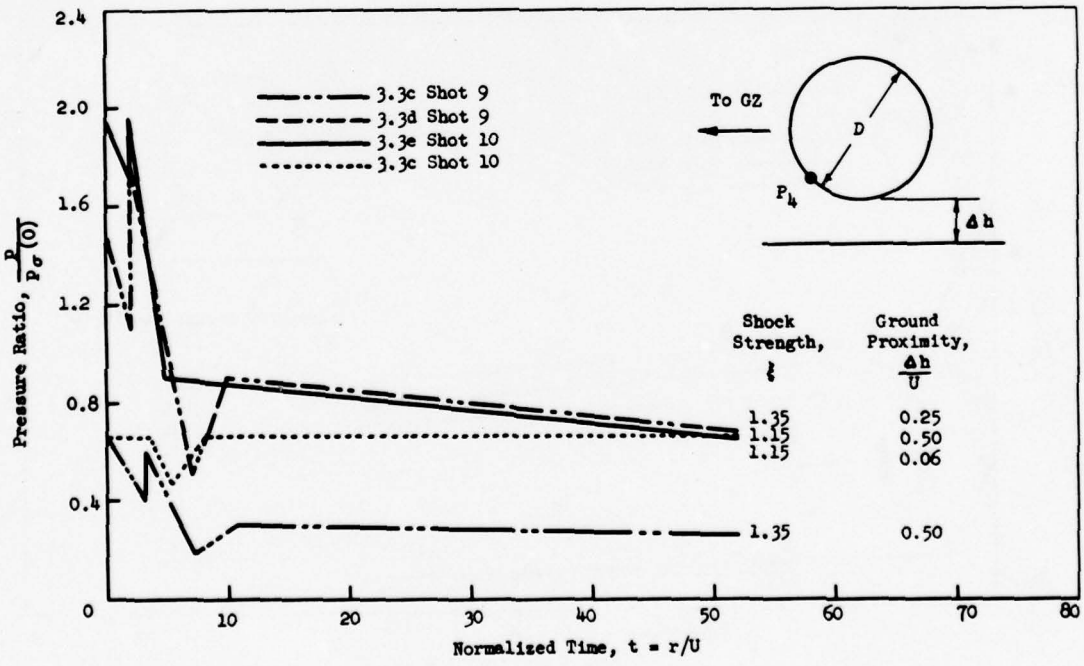

Fig. 5.24 Effect of Ground Proximity, Gage P4

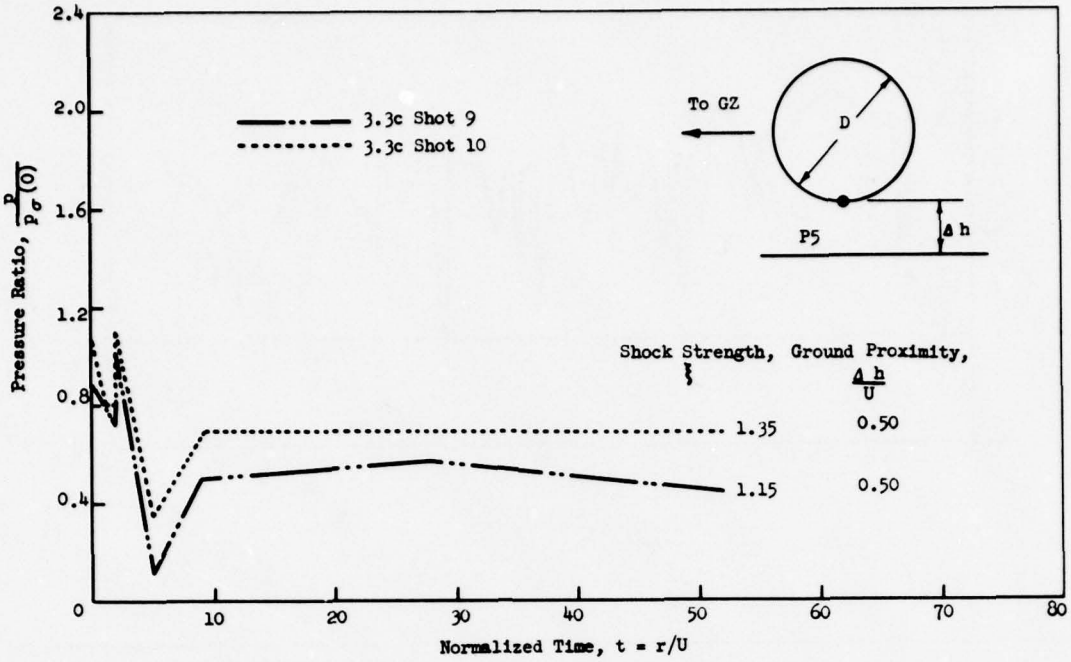

Fig. 5.25 Effect of Ground Proximity, Gage P5

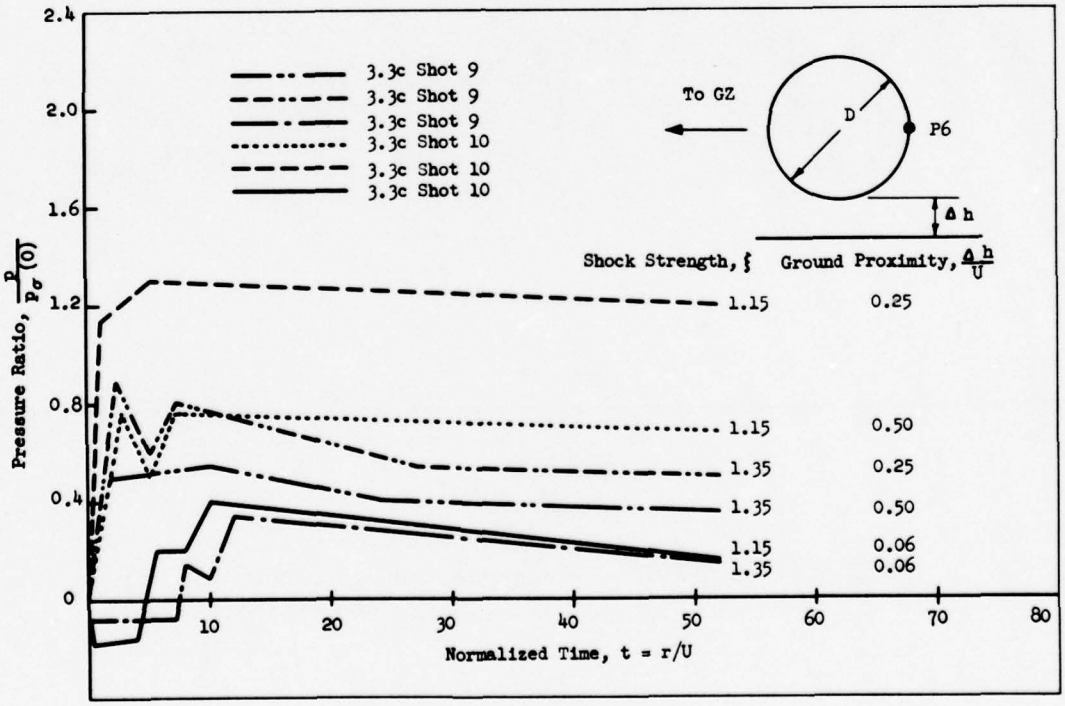

Fig. 5.26 Effect of Ground Proximity, Gage P6

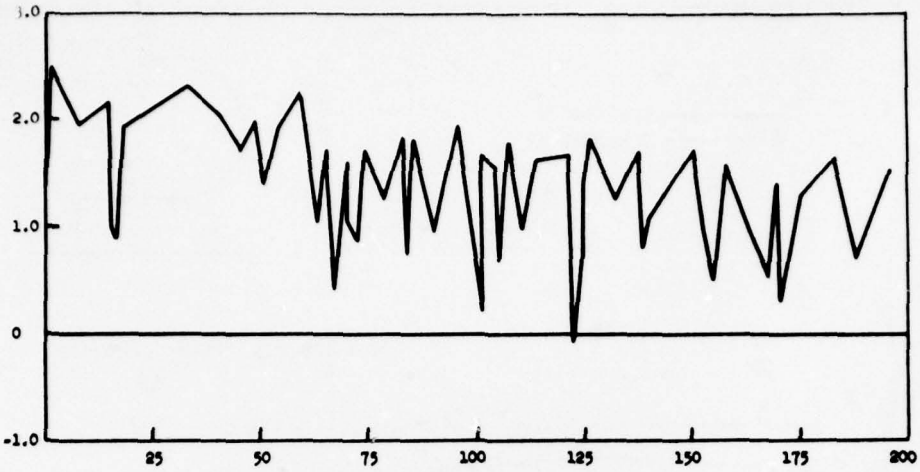

a. Tank 3.26bd, P1

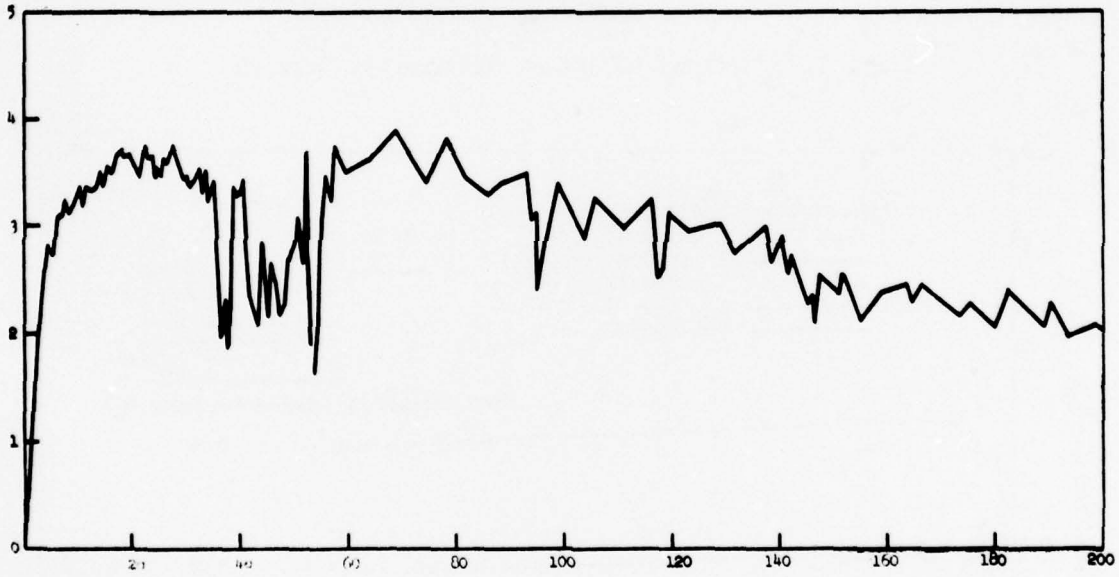

b. Tank 3.26bd, P10

Fig. 5.27 Linearized Pressure-Time Records on 3.26.1 Storage Tank (3.26bd), Fast Playback

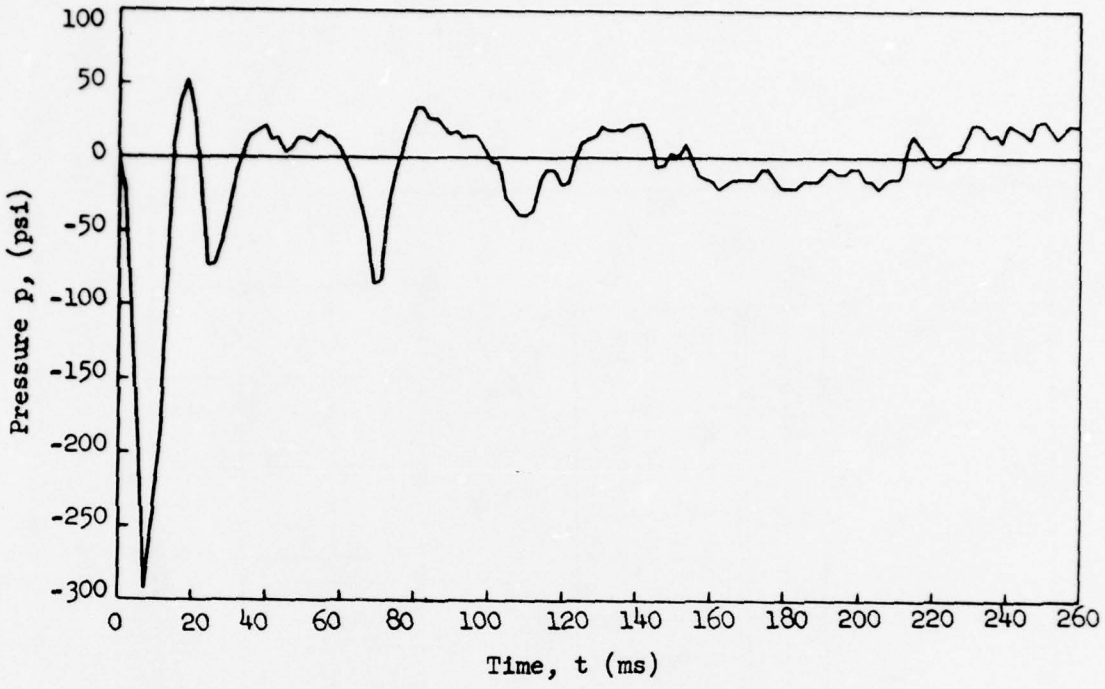

a. Cylinder 3.3d, Gage S1, Shot 9

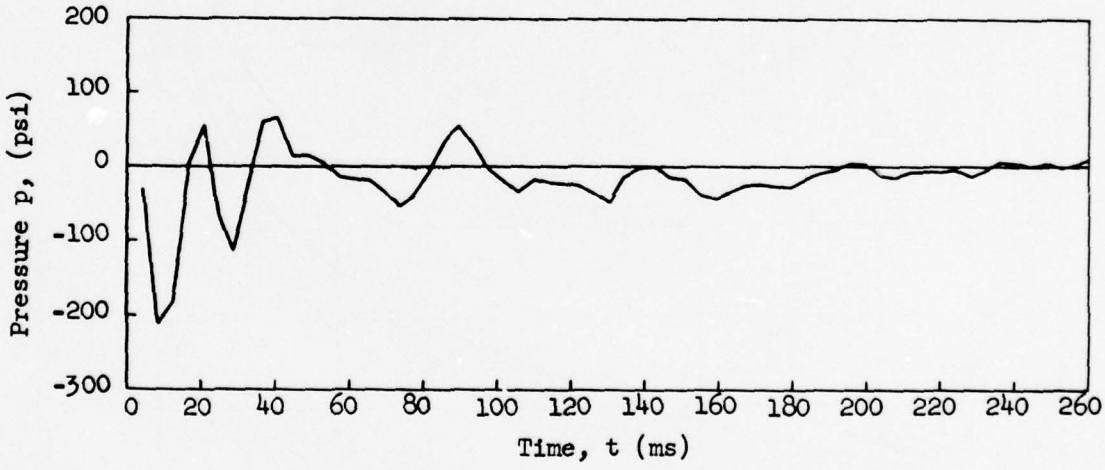

b. Cylinder 3.3e, Gage S2, Shot 10

Fig. 5.28 Typical Linearized Strain-Time Records

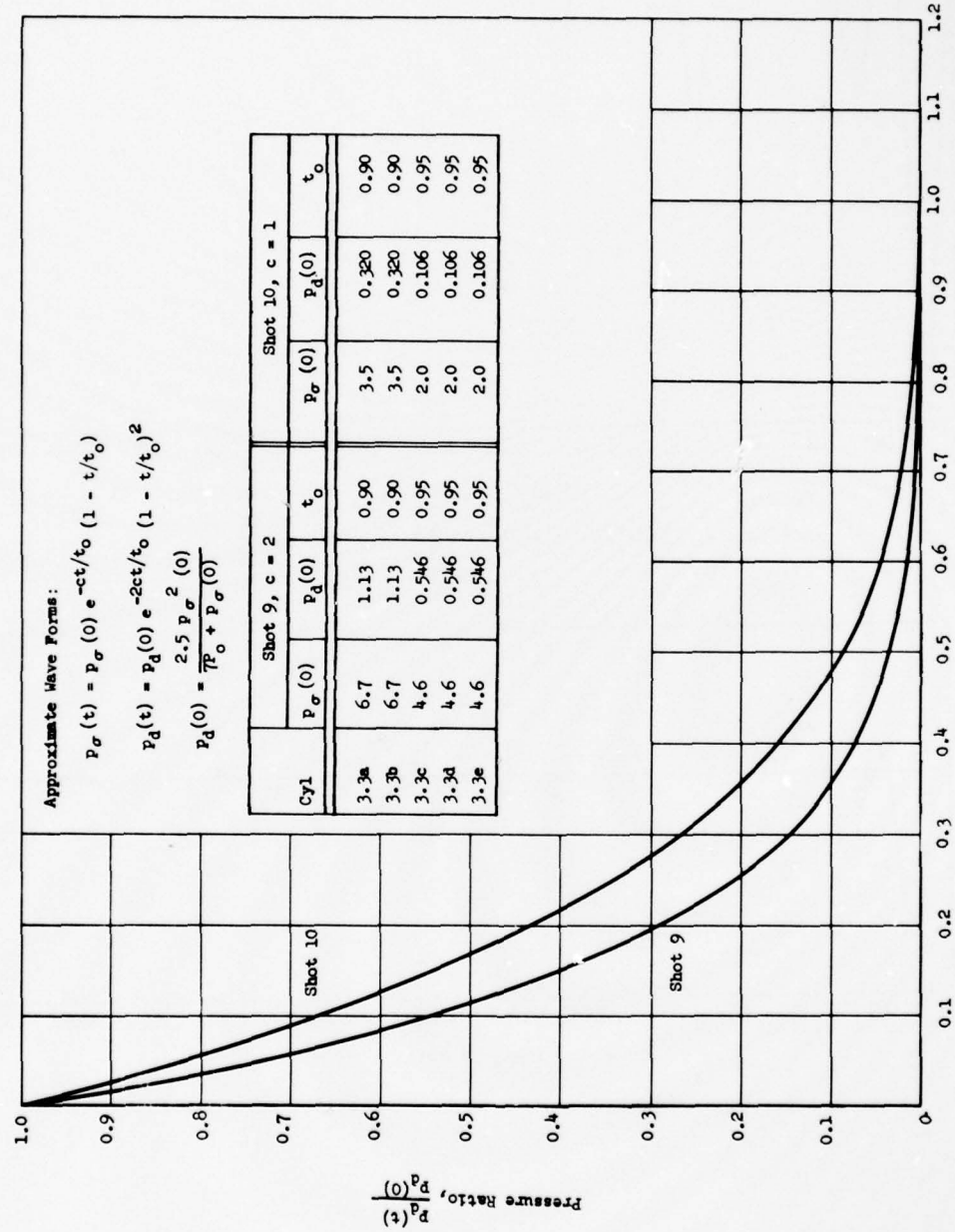

Cyl	Shot 9, c = 2			Shot 10, c = 1		
	$p_\sigma(0)$	$p_d(0)$	t_o	$p_\sigma(0)$	$p_d(0)$	t_o
3.3a	6.7	1.13	0.90	3.5	0.320	0.90
3.3b	6.7	1.13	0.90	3.5	0.320	0.90
3.3c	4.6	0.546	0.95	2.0	0.106	0.95
3.3d	4.6	0.546	0.95	2.0	0.106	0.95
3.3e	4.6	0.546	0.95	2.0	0.106	0.95

Fig. 5.29 Normalized Dynamic Pressure-Time Curves (Shots 9 and 10), Approximate Wave Forms

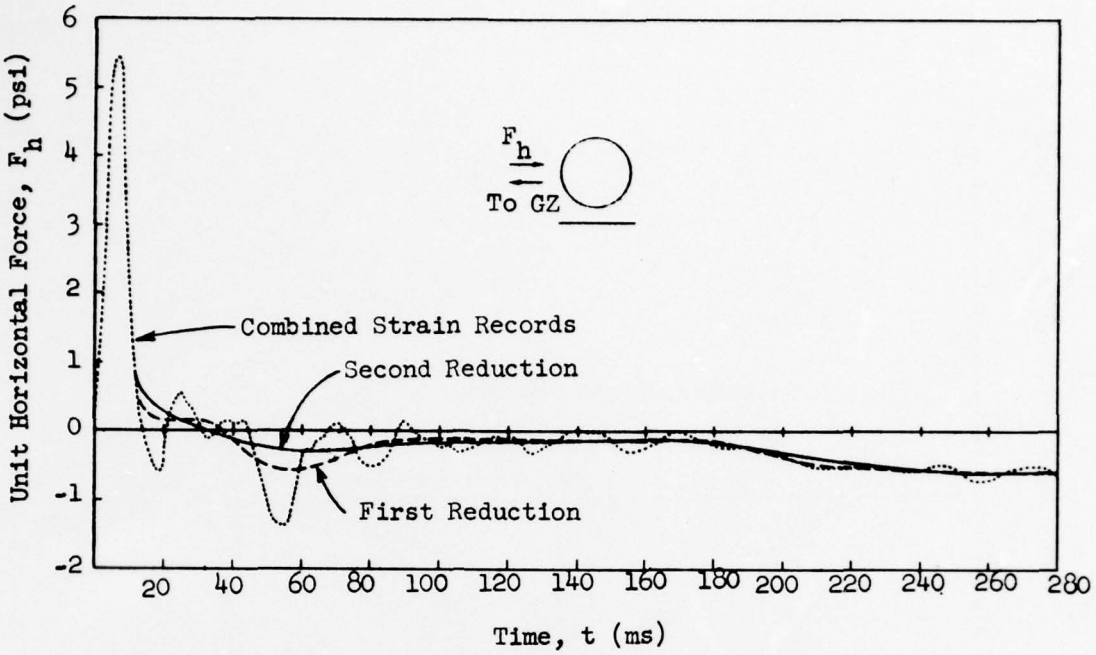

a. Horizontal Force

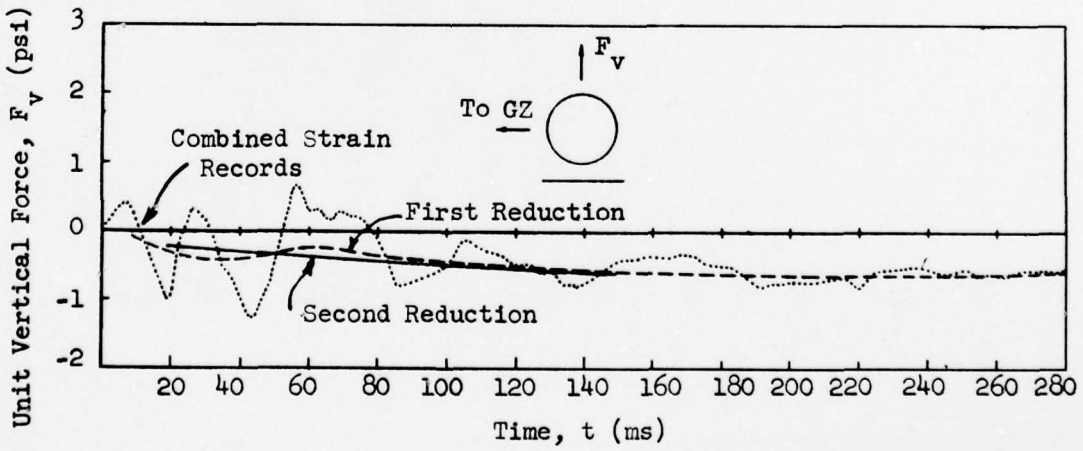

b. Vertical Force

Fig. 5.30 Horizontal and Vertical Force-Time Curves (3.3c, Shot 9)

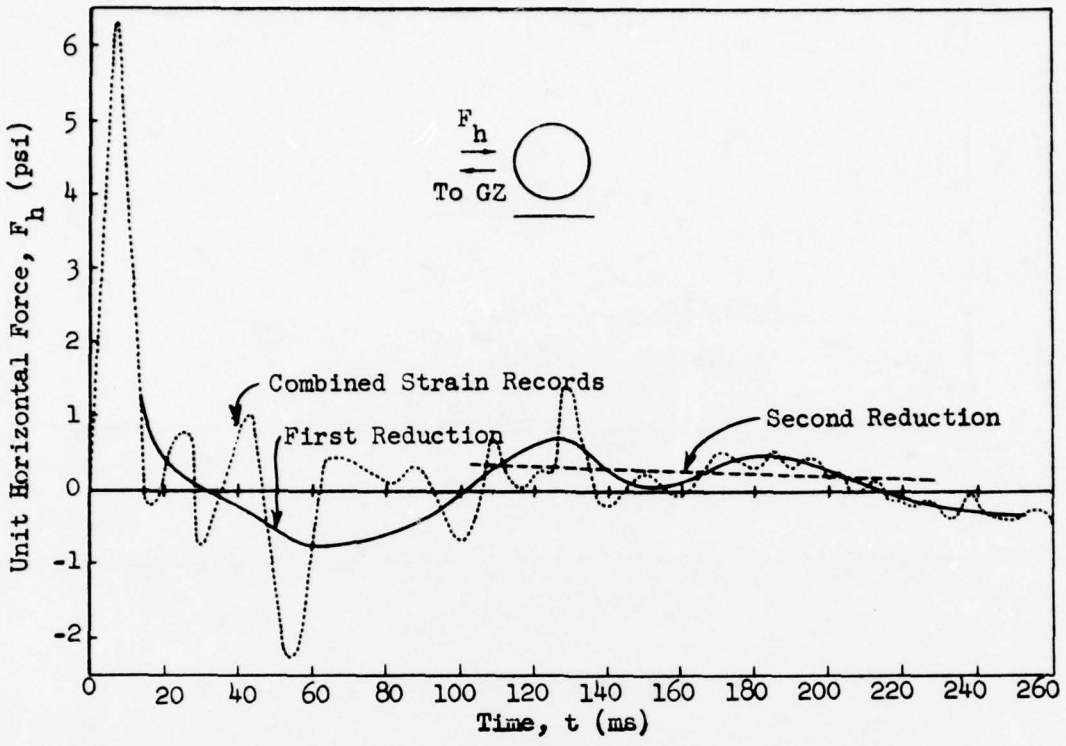

a. Horizontal

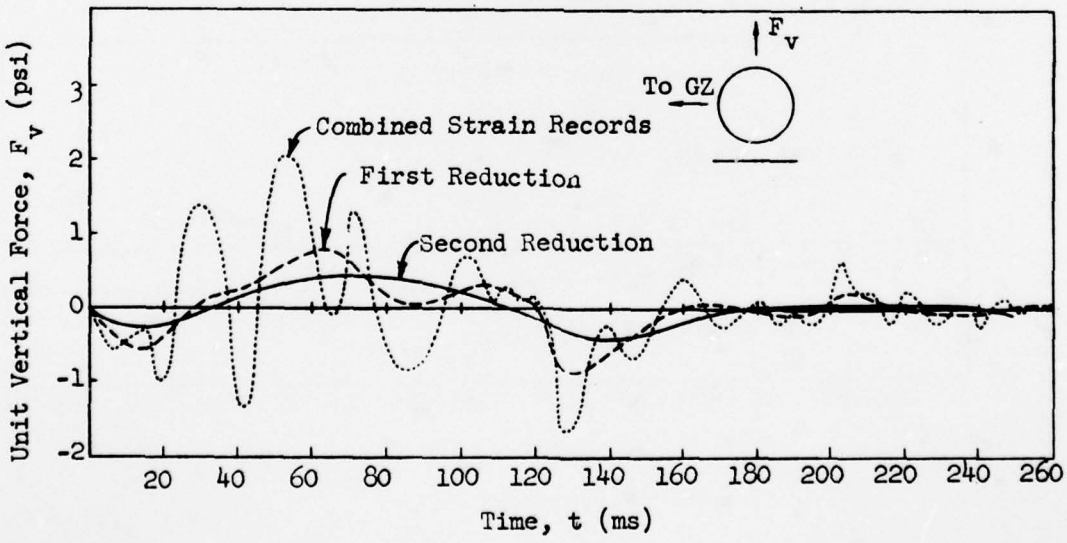

b. Vertical

Fig. 5.31 Horizontal and Vertical Force-Time Curves (3.3d, Shot 9)

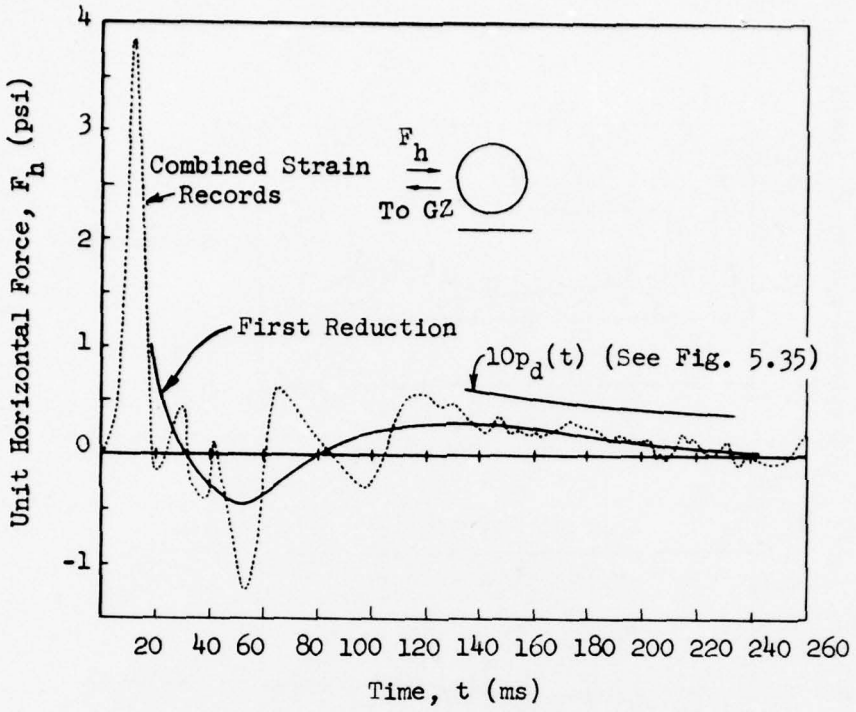

a. Horizontal

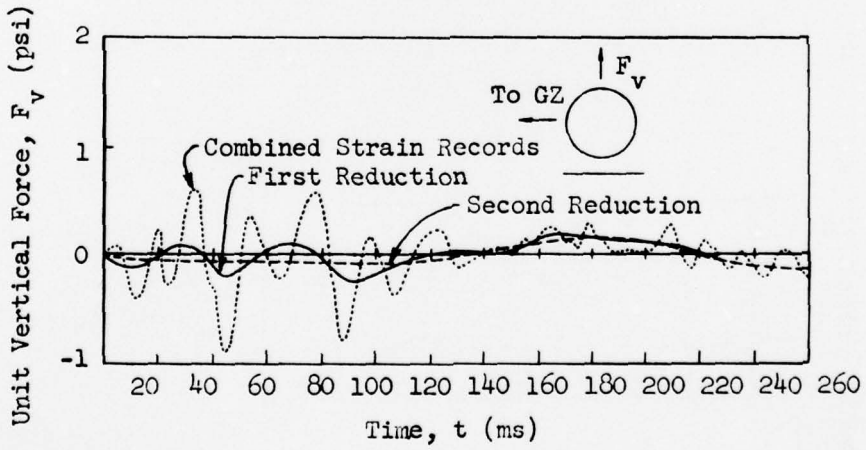

b. Vertical

Fig. 5.32 Horizontal and Vertical Force-Time Curves (3.3d, Shot 10)

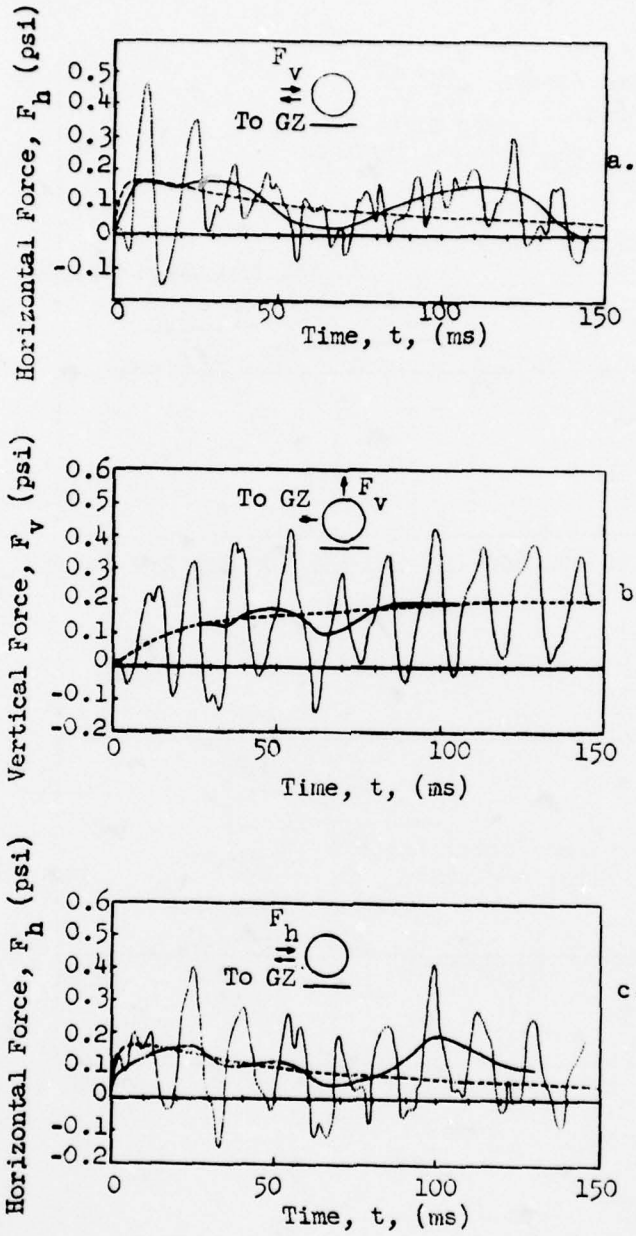

g. 5.33 Horizontal and Vertical Force-Time Curves (3.3a, Shot 10)

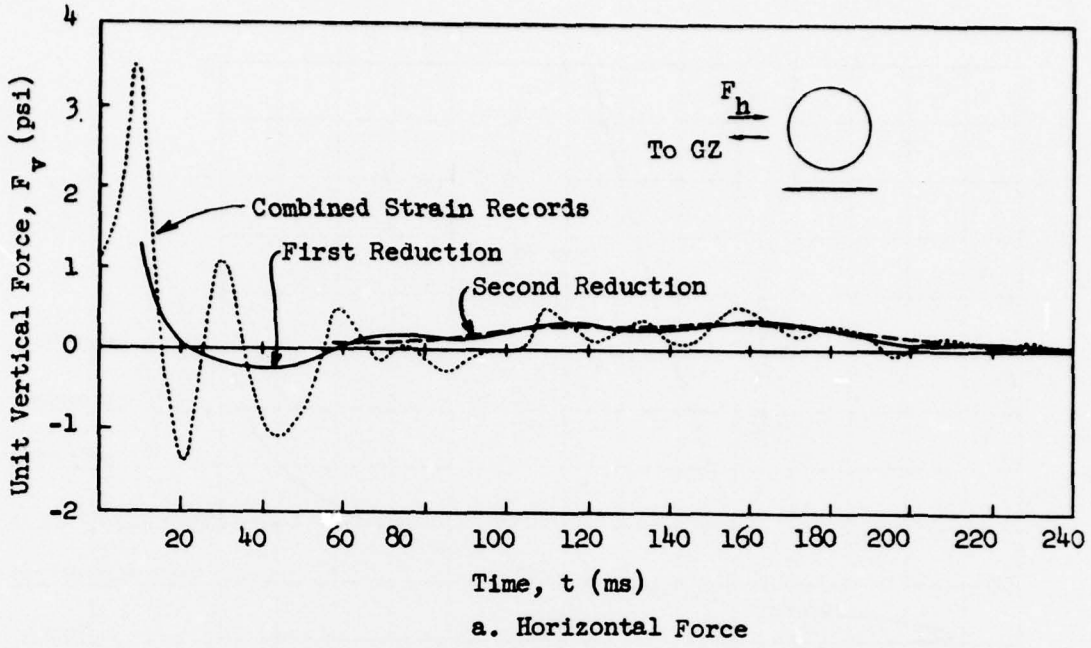

a. Horizontal Force

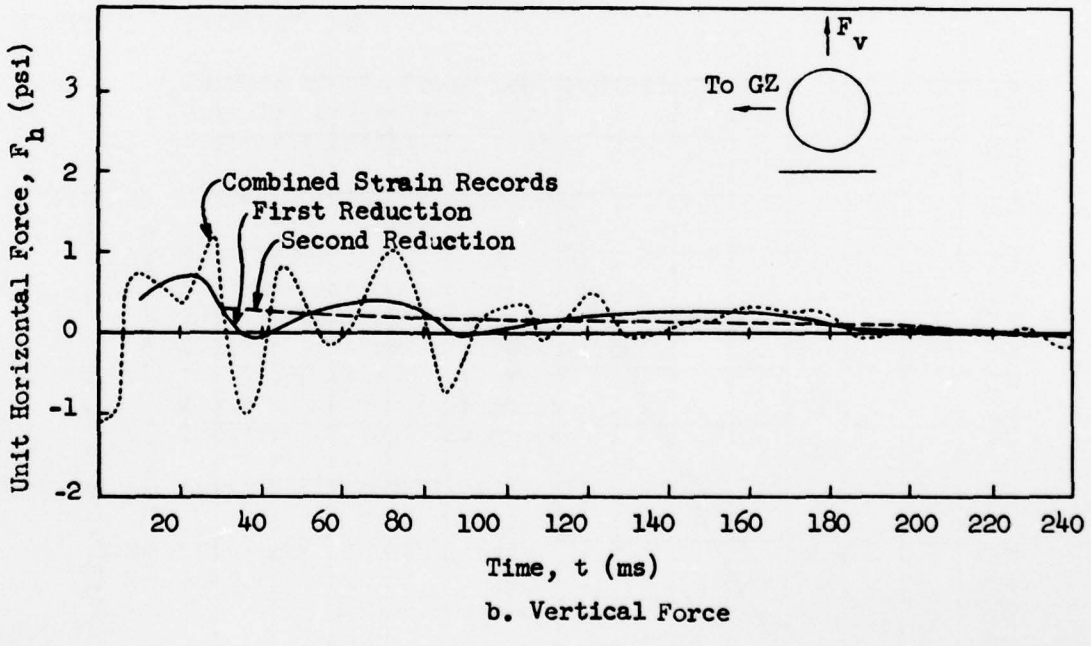

b. Vertical Force

Fig. 5.34 Horizontal and Vertical Force-Time Curves (3.3e, Shot 10)

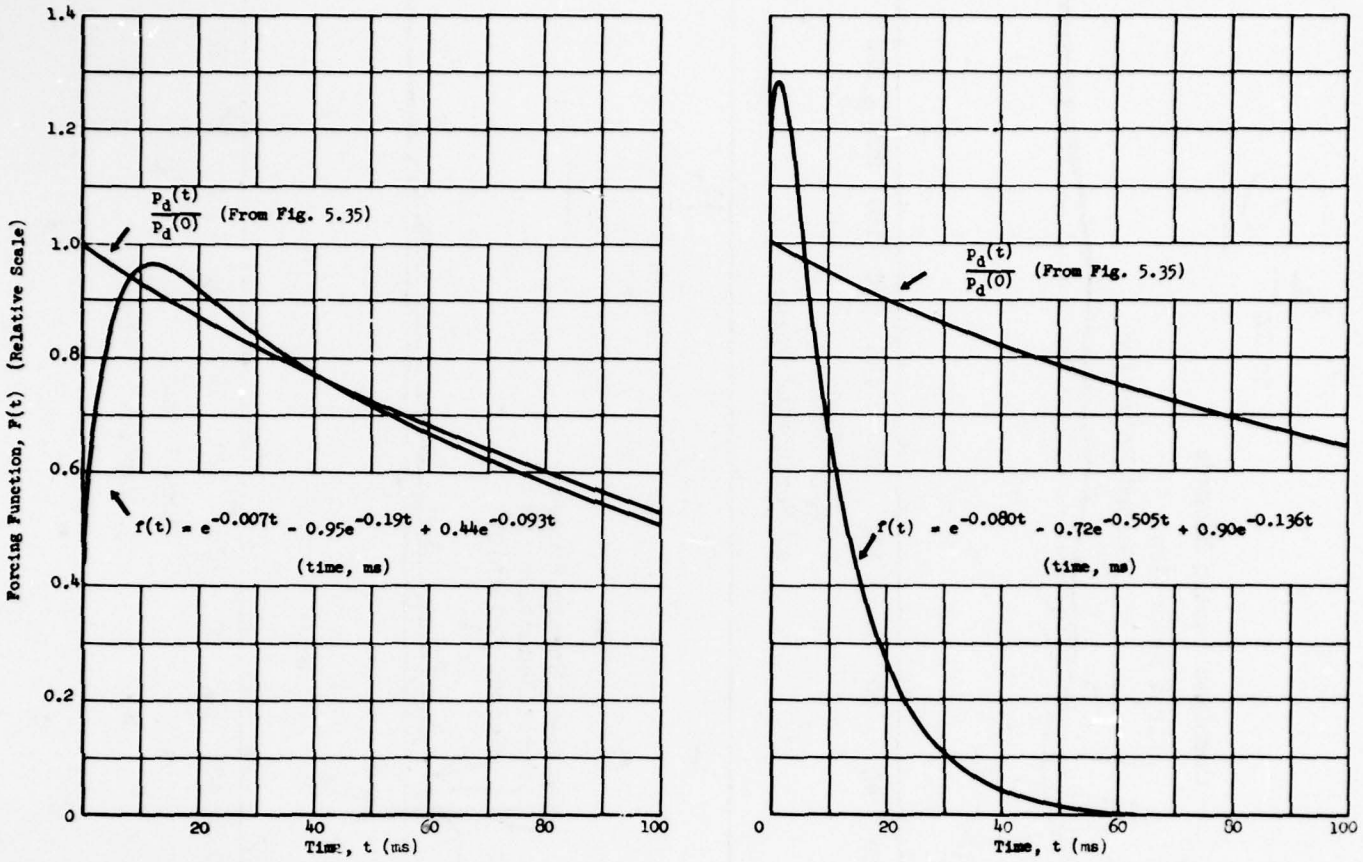

a. Cylinder 3. c, Gage S1, Shot 9

b. Cylinder 3.3e, Gage S2, Shot 10

Fig. 5.35 Results of Transient Analysis, Strain Records 3.3eS1, Shot 9, and 3.3eS2, Shot 10

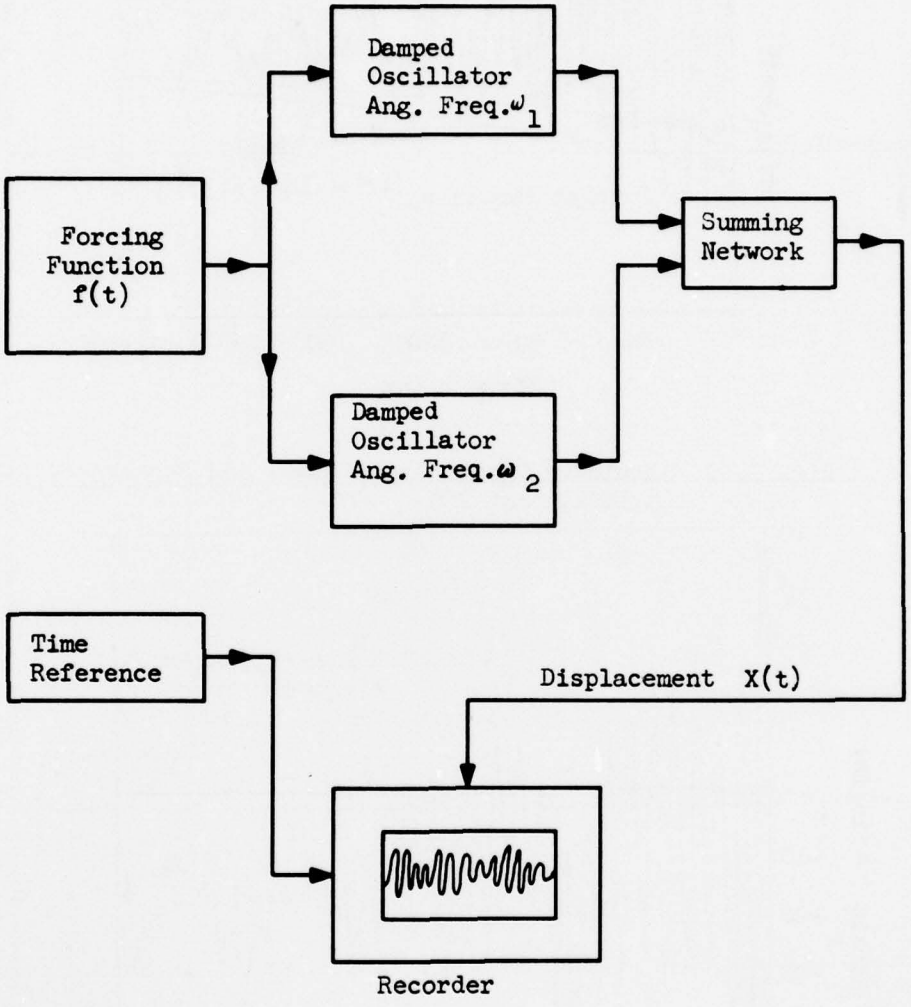

Fig. 5.36 Block Diagram for Simulated System Incorporating Two Frequencies

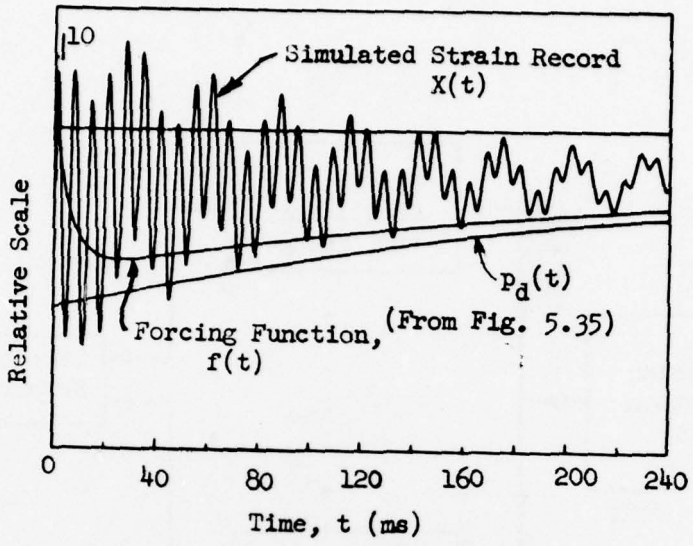

Fig. 5.37 Simulated Strain-Time Record and Forcing Function (3.3bS2, Shot 10)

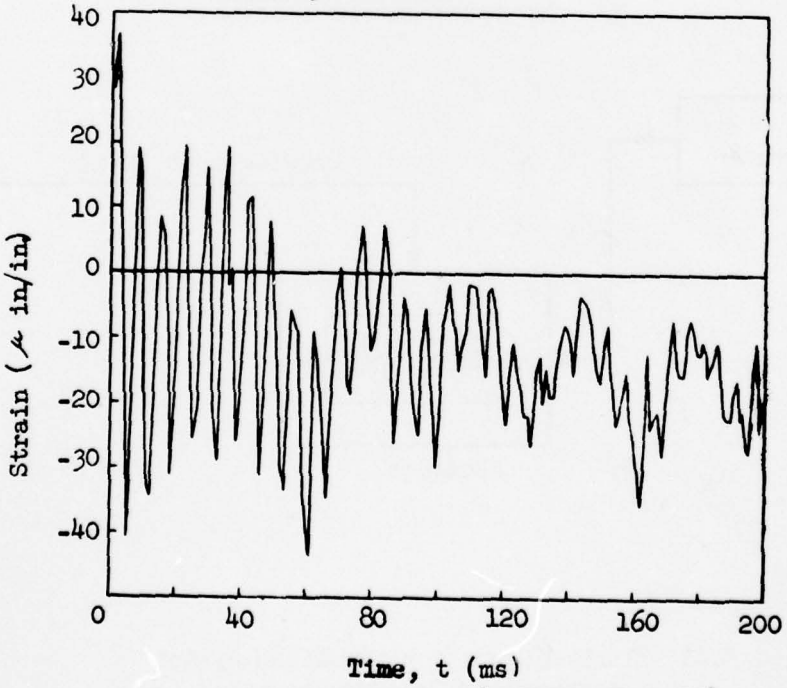

Fig. 5.38 Strain-Time Record (3.3bS2, Shot 10)

CHAPTER 6

CONCLUSIONS AND RECOMMENDATIONS

6.1 CONCLUSIONS

None of the specific test objectives listed in Chapter 2 have been completely satisfied as a result of the test data obtained, and in this respect the program must be termed unsuccessful. However, some information of value was obtained, and a great deal was learned concerning the complexities of a field test program such as this. The present section summarizes the results obtained and indicates the extent to which the various test objectives have been satisfied.

The test objective dealing with the effect of shock strength could not be realized from the pressure data since, for one reason or another, the data exhibited a randomness of behavior that effectively obscured any such effect. In addition, little quantitative information was obtained from the strain data.

Since the effect of shock strength could not be determined, the pressure data for the first 100 ms was averaged and further reduced to yield what is felt to be the best possible estimate of the loading on a cylinder one radius above the ground. While there exists some doubt as to the pressure scale (it is believed to be low), valuable information with respect to the time details of the loading was obtained. In particular, the build up and clearing times were found to be essentially the same as for a cylinder in free space, with the exception of the clearing time on the front face which was somewhat longer. The predicted clearing time on the front face of an isolated cylinder is between 4 and 5 r/U time units; the test results indicate a clearing time of between 8 and 10 r/U time units (r = radius of cylinder, U = speed of shock front).

The test objective dealing with the effect of size was to be achieved by comparing the loading on two geometrically similar cylinders which differed in absolute size by a factor of 4. The pressure data for these cylinders showed a considerable and generally random spread, and it was not possible to determine values of drag coefficients or even a qualitative trend in the loading due to any size effect. However, the pressure data did indicate that the time details of the loading scale as predicted with variation in size.

The test objective dealing with the effect of ground proximity could not be realized, inasmuch as four of the six critical pressure gage records (i.e., the gages on the undersurface of the cylinders) were either lost or were invalid. In addition, the other pertinent records are believed to be poor with respect to both magnitude and time details. However, some indication as to the effect of ground proximity was obtained from the strain data and from the loading on the cylinder one radius above the ground. In the last-mentioned loading a net upward vertical force of the order of the horizontal force was observed during the drag phase.

The test objective dealing with the effect of three-dimensionality was to have been achieved by comparison of the net load as determined by the strain gage data with the net (two-dimensional) load as determined from the pressure data. Inasmuch as the strain data provided virtually no quantitative results, this objective could not be satisfied. However, some useful information was obtained from the pressure gages on the Project 3.26.1 vertical cylindrical storage tank, which were analyzed in the present report. These data indicated that the finite size of the tank (the gages were close to the roof) did not affect the front face loading appreciably; the loading on the back side built up somewhat more rapidly than predicted for a two-dimensional cylinder, but this is not surprising.

The strain gage data did not provide anywhere near the information desired. While there exists some uncertainty as to the magnitudes of the recorded strain, the principal source of difficulty stemmed from an inability to properly interpret the data. The cylinder-support arrangement behaved as an extremely complicated dynamic system, and it was not feasible to compute analytically the response of this system to a known input. There are at least four principal frequencies evident in most records, and there is reason to believe that motion of the foundation in the soil took place and was picked up in the strain gages. By inspection alone, the appearance of the strain records was such as to yield only a very qualitative estimate of the forcing function.

The numerical data-reduction scheme, referred to as transient analysis and devised to interpret the strain data under just such circumstances, has proved unsatisfactory to date. This is believed due to two main causes. First, a reappraisal of the method indicates that its application to multi-degree-of-freedom systems is valid only where the input functions to the various modes are either zero or timewise proportional. While indications are that this requirement is violated in the present case, at least during the initial loading period, the applicability of the method is not sufficiently well understood to definitely rule out its use. The failure of the present application of the method probably can be explained more readily in terms of an inadequate representation of the numerical data by means of an exponential series — a step that is crucial to the success of the analysis. The implication here is that a much more refined job of curve-fitting is necessary which, in effect, may increase the computational problems enormously. Therefore, on the basis to present knowledge, it is not

possible to conclude definitely as to the feasibility of the method of transient analysis in the present application. However, indications now are that it may not be too practical a method even though under certain conditions, fundamentally sound.

An attempt was made to utilize the ARF analog computer in what can be termed a rapid trial-and-error approach to the problem of data interpretation. This work was not completed, and while no conclusive results were obtained, the method appeared to be a reasonable one and to have good potentialities.

It should be emphasized, however, that the entire subject of data reduction stemming from net force measurement systems deserves a more comprehensive research effort than could be given to it as a part of the present program. One cannot escape the fact that some method of data interpretation embodying, at least in principle, the philosophy of transient analysis is mandatory, unless the response of the system under consideration is such that the desired information can be obtained simply by inspection.

There are, of course, certain lessons to be learned from the experiment. It now appears most desirable to have obtained as much information as possible regarding the dynamic systems being tested. This would include pre- and post-test static pull tests of the cylinder (which would at least have checked out the strain gage system and calibration), as well as some sort of dynamic testing to determine the principal frequencies and damping of the system. Information of this type would have undoubtedly aided in the study and interpretation of the strain data. For, if the response of the cylinders to a known input could be obtained with sufficient accuracy, the determination of the forcing function from the strain data would have been enormously simplified.

In view of the unsuccessful application of transient analysis, and for lack of a better approach, an interpretation of the strain data was attempted on the basis of inspection and simple graphical suppression of the obvious harmonic components of the response. This approach yielded rather conflicting results which are not without some merit — if only to point out the inadequacy of the method, or of the strain data itself. In one lone case the horizontal component of applied load substantiated both an approximate dynamic pressure wave form and the steady-state drag coefficient, but there was no indication of any initial peak force. In other cases the peak force was evident and the wave form seemed reasonable, but the drag coefficients were unrealistically high. In still other cases, the rate of decay of the force differed significantly from the approximate dynamic pressure curve. The data from two cylinders indicated a vertical force that rose gradually to a value in excess of the dynamic pressure at that time; cylinders closer to the ground indicated a vertical force that oscillated about zero as a mean.

6.2 RECOMMENDATIONS

While the present test has been largely unsuccessful, it is believed that the original objectives are still valid ones. In view of the support lent the scaling of time details and, in some cases pressures, it is recommended that additional experimental investigations of the blast loading on cylinders be conducted on a model scale in a shock tube utilizing pressure, interferometric, and direct force measurements.

Much additional work remains to be done with respect to net force measurement systems, both as to physical design and interpretation of data. Despite the present unsuccessful utilization of the cylinder as a dynamometer with strain output, this approach has obvious advantages.1/ It is recommended, therefore, that a comprehensive study be initiated on the data-reduction problems associated with net force measurement systems. The objectives of this study would be to (a) devise methods of analysis, (b) specify the class of physical systems whose response will successfully permit the inverse solution, and (c) determine the type and quality of the necessary data to permit this solution. It is felt that particular consideration should be given to the analog computer technique of data analysis discussed in this report.

1/ Of course, other schemes can be thought of for the present test items (e.g., utilization of the cylinder as a ballistic pendulum with accelerometer output). However, the present dynamometer arrangement would be applicable to a wide variety of items.

APPENDIX A

TRANSIENT ANALYSIS

A.1 INTRODUCTION

In the present application, the prime data (i.e., the measured strains) do not represent in a direct sense the desired information (i.e., the net forces). In fact, the data obtained represent the response of a rather complicated dynamic system to an input which is itself the desired information. The dynamic system consists of aerodynamic, elastic, plastic, electronic, thermal and possibly stochastic components coupled in many and varied fashions. The problem at hand is to remove from the prime data the influence or contributions of these various components and of the system itself, leaving the desired information. Since it is difficult (probably impossible) to assess the exact contribution or influence that the dynamic system contributes to the prime data, a rational approach to the problem is to attempt to assess the contribution or influence of those components which could be expected to have the most pronounced effects. Due to lack of sufficient knowledge of the test conditions and the reliability and characteristics of the various recording and data-reduction instruments, the magnitude of the contributions of some of the above components cannot even be estimated. Nonetheless, it has been assumed that the major influence on the prime data stems from an elastic response of the cylinder-support system.

The following analysis, referred to as "transient analysis," is designed to remove the influence of the elastic components in the prime data, which is undoubtedly strongest, regardless of other effects. The analysis as applied here, represents the function or input required to produce the prime data as the response of an elastic model.

A.2 DERIVATION OF THE BASIC EQUATION

For the present application, the elastic model is assumed to be linear and possess several (but a finite number of) degrees of freedom. Its motion is then determined by a system of linear differential equations with constant coefficients. One such equation for each

degree of freedom occurs. Some of the possible degrees of freedom which might be effective are the rigid-body translation and rotation of the foundation, rigid-body motions of the cylinder, bending and axial vibrations of the cylinder supports, bending of the cylinder, torsional deflections of the cylinder, or vibrations of the cylinder as a shell. Regardless of the number of degrees of freedom present, the equations of elastic motion may be written in the form:

$$m_j \ddot{X}_j(t) + \sum_{i=1}^{N} a_{ij} \dot{X}_i(t) + \sum_{i=1}^{N} b_{ij} X_i(t) = f_j(t) \qquad (A.1)$$

$$j = 1, 2, \ldots N$$

where the a_{ij}, b_{ij}, and m_j are real constants, and $f_j(t)$ is the forcing term for the jth degree of freedom. $X_j(t)$ is the response of the jth degree of freedom represented by the jth mass, m_j. Equation A.1 is the most general system of equations for N degrees of freedom without inertial coupling. The constants a_{ij} and b_{ij} are the damping and elastic coupling coefficients, respectively, some of which may be zero.

For the present application, the forcing terms $f_j(t)$ arise primarily from the pressure acting on the cylinder. It is reasonable to assume that motion of the foundation, if it occurs, can result only from coupling with the cylinder motion. Thus, only those of Equation A.1 corresponding to masses m_j associated with motion of the cylinder are nonhomogeneous (i.e., $f_j(t) \neq 0$).

The masses m_j associated with the motion of the cylinder are of two types; namely, total mass corresponding to rigid-body motions, or generalized modal masses for the bending or shell vibrations. The forcing terms for each of these result from either the integrated pressure over the cylinder alone or the integrated pressure times a modal deflection curve over the cylinder. If the pressure is assumed to be nearly constant in the axial direction along the cylinder, these forcing terms will be essentially proportional to one another at each instant of time so that their time histories will be similar. In effect Equation A.1 will contain the same righthand members up to a constant factor, which may be zero.

In this case, Equation A.1 becomes,

$$m_j \ddot{X}_j(t) + \sum_{i=1}^{N} a_{ij} \dot{X}_i(t) + \sum_{i=1}^{N} b_{ij} X_i(t) = C_j f(t) \qquad (A.2)$$

$$j = 1, 2 \ldots N$$

AD-A073 477 WRIGHT AIR DEVELOPMENT CENTER WRIGHT-PATTERSON AFB OH F/G 18/3
OPERATION UPSHOT-KNOTHOLE NEVADA PROVING GROUND, MARCH-JUNE 195--ETC(U)
OCT 55 E SEVIN

UNCLASSIFIED WADC-TR-55-420 DASA-WT-722 NL

2 OF 2

AD A073 477

END
DATE FILMED
10-79
DDC

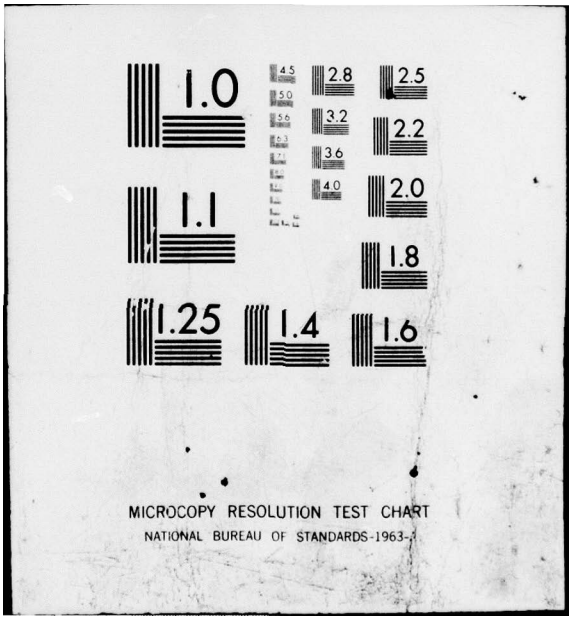
1.0
1.1
1.25
1.4
1.6
1.8
2.0
2.2
2.5
2.8
3.2
3.6
4.0
4.5
5.0
5.6
6.3
MICROCOPY RESOLUTION TEST CHART
NATIONAL BUREAU OF STANDARDS-1963-

It is well-known (see Vibration Problems in Engineering by S. Timoshenko) that the response $X_j(t)$, Equation A.1, subject to homogeneous initial conditions, can be given by a sum of Duhamel-type integrals as:

$$X_j(t) = \sum_{k=1}^{N} \int_0^t f_k(\tau) h_{kj}(t - \tau) d\tau \qquad (A.3)$$

where the h_{kj} are referred to as transfer functions and, for a fixed (k,j), represent the impulsive response in the jth degree of freedom to a unit impulse applied in the kth degree. In other words, $h_{kj}(t)$ is the solution, $X_j(t)$, of the corresponding homogeneous system of equations

$$m_j \ddot{X}_j(t) + \sum_{i=1}^{N} a_{ij} \dot{X}_i(t) + \sum_{i=1}^{N} b_{ij} X_i(t) = 0 \qquad (A.4)$$

$$j = 1, 2, \ldots N$$

subjected to the inhomogeneous initial conditions

$$X_j(0) = \dot{X}_j(0) = 0 \qquad j \neq k$$

$$X_k(0) = 0, \dot{X}_k(0) = 1$$

Such a solution $X_j(t) = h_{kj}(t)$ is known to be a linear combination of exponential functions (in general, complex)1/ of the form (see Vibration Problems in Engineering by S. Timoshenko).

$$h_{kj}(t) = \sum_{n=-N}^{N} \alpha_n^{kj} e^{\lambda_n t} \qquad (A.5)$$

where λ_n, $(n = 0, \pm 1, \ldots \pm N)$ are the 2N roots of the characteristic equation (system of equations)

$$m_j \lambda^2 + \sum_{i=1}^{N} a_{ij} \lambda + \sum_{i=1}^{N} b_{ij} = 0$$

$$j = 1, 2, \ldots N$$

If Equation A.5 is substituted in Equation A.3, there results:

$$X_j(t) = \sum_{k=1}^{N} \int_0^t f_k(\tau) \sum_{n=-N}^{N} \alpha_n^{kj} e^{\lambda_n (t - \tau)} d\tau \qquad (A.6)$$

1/ It is assumed here that the 2N characteristic roots are distinct.

If, in addition, the $f_k(t)$ are timewise proportional so that

$$f_k(t) = C_k f(t) \tag{A.6a}$$

as in Equation A.2, then, Equation A.6 may be written,

$$X_j(t) = \int_0^t f(\tau) \sum_{k=1}^{N} \sum_{n=-N}^{N} C_k \alpha_n^{hj} e^{\lambda_n (t-\tau)} \, d\tau$$

$$X_j(t) = \int_0^t f(\tau) \sum_{n=-N}^{N} \beta_n^j e^{\lambda_n (t-\tau)} \, d\tau$$

$$X_j(t) = \int_0^t f(\tau) \, h_j(t-\tau) \, d\tau \tag{A.7}$$

where:

$$\left.\begin{aligned} \beta_n^j &= \sum_{k=1}^{N} C_k \alpha_n^{kj} \\ h_j(t) &= \sum_{n=-N}^{N} \beta_n^j e^{\lambda_n t} \end{aligned}\right\} \tag{A.7a}$$

It is seen that the quantity $h_j(t-\tau)$ in Equation A.7 is precisely the form of the transfer functions $h_{kj}(t)$ in Equation A.3 (independent of k, however) and is a linear combination of exponential functions involving only the characteristic roots of the system. Equation A.7 is the desired basic equation and may be used to obtain the unknown forcing function $f(t)$ from a known response $X_j(t)$. The quantity $f(t)$ actually represents only the shape of the forcing function, since it is defined up to the constant factors C_j of Equation A.2.

The problem of uniqueness and the effect of "errors" in the response curve $X_j(t)$ as they affect the solution for $f(t)$ obtained, will be discussed at the appropriate steps in the subsequent analysis, It will be seen that the uniqueness problem essentially reduces to a problem in curve-fitting and may be treated in several ways.

A.3 SOLUTION OF THE BASIC EQUATION

Equation A.7 can be solved by a variety of methods, none of which, however, leads to a unique solution for the forcing function $f(t)$. For the present application it is assumed that $f(t)$ can be represented by exponential functions in the form:

$$f(t) = F_1 e^{\alpha_1 t} + \ldots F_K e^{\alpha_K t} \tag{A.8}$$

$$= \sum_{i=1}^{K} F_i e^{\alpha_i t}$$

where the F_i and α_i are constants. The number (K) of terms in Equation A.8 will be determined by the complexity of the actual forcing function or, at least, the complexity required of $f(t)$ in order to produce the known response $X(t)$. It should be mentioned that the form of Equation A.8 in no way restricts the generality of application.

If Equation A.8 is substituted into Equation A.7, and Equation A.7a is used, there results upon integration:

$$X_j(t) = \sum_{i=1}^{K} A_i e^{\alpha_i t} - \sum_{n=-N}^{N} B_n e^{\lambda_n t} \tag{A.9}$$

where,

$$\left.\begin{aligned} A_i &= \left[\sum_{n=-N}^{N} \frac{\beta_n^j}{\alpha_i - \lambda_n}\right] F_i \\ B_n &= \left[\sum_{i=1}^{K} \frac{F_i}{\alpha_i - \lambda_n}\right] \beta_n^j \end{aligned}\right\} \tag{A.10}$$

It is assumed here that $\alpha_i \neq \lambda_n$ for each i and n, since otherwise a resonance condition would result, which certainly does not happen in the physical case considered here. Equation A.9 gives $X_j(t)$ as a sum of exponential functions, and the present problem reduces to that of fitting such a sum to the prime data representing $X_j(t)$ for a discrete set of times, t.

A curve-fitting scheme results in the constants, A_i, α_i, B_n, and λ_n (real and complex, in general) which, in turn, may be used to compute the desired F_i through Equation A.10. Actually, Equation A.10 will also yield the β_n^j which, however, are not of direct concern in the present application. With the α_i, A_i, B_n, and λ_n known, Equation A.10 constitutes a system of $2N+K$ equations in the $2N+K$ unknowns, β_n^j and F_i. With the α_i and F_i determined, the desired forcing function is then given by Equation A.8. Actually, a little more information is assumed here; namely, that not only the constants α_i, A_i, B_n, and λ_n are obtained from the curve-fitting, but that the sets of A_i's and α_i's can be distinguished from the set of B_n's and λ_n's. Otherwise, the structure of Equation A.10 would not be determined so that, a unique forcing function could not be constructed through Equation A.8. In the present application, the distinction between the two classes of terms in Equation A.9 can be made through

the exponents α_i and λ_n themselves. Since Equation A.1 can be assumed to be stable, none of the characteristic roots λ_n can be pure real. On the other hand, it is assumed that the forcing function $f(t)$ contains no harmonic components so that a realistic curve-fitting scheme should yield only real exponentials α_i for $f(t)$ in Equation A.8. In brief, the nonreal exponents obtained from curve-fitting are associated with the transfer function

$$h_j(t) = \sum_{n=-N}^{N} \beta_n^j e^{\lambda_n t}$$

and give the λ_n, while any real exponents obtained are associated with the forcing function

$$f(t) = \sum_{i=1}^{K} F_i e^{\alpha_i t} .$$

The appropriateness of this choice of association can be asserted only after some study is made of the effect of errors, etc., of the prime data on the computed exponentials. It would be desirable, of course, to obtain the natural frequencies of the system either analytically or experimentally independent of the above analysis, since then they could be identified in Equation A.9 and $f(t)$ could then contain harmonics without affecting the above solution.

A.4 CURVE-FITTING

Equation A.9 may be written in the form:

$$X(t) = \sum_{k=1}^{M} C_k e^{\gamma_k t} \qquad \text{(A.11)}$$

where the C_k and γ_k are in general complex numbers, and where the subscript j has been dropped, since the only concern is with the response of but one component of the system. Curve-fitting consists of finding those values for C_k and γ_k such that $X(t)$ as given by Equation A.11 best fits the given prime data.

Method A. The most direct method of curve-fitting is accomplished by visual inspection of plots of the prime data itself. A discussion of this method and the results of its use in the present application are presented in Section 5.1.2.

Method B. A second method consists of rather standard technique from the theory contained in the calculus of finite differences (see The Calculus of Observations by Whittaker, E. and Robinson, A.). It is assumed now that the prime data are given in equal interval tabular form.

Let the interval of tabulation of the function $X(t)$ be Δ, and designate $X(t)$ at the time when

$$t = n\Delta \qquad n = 0, 1, \ldots, P$$

as X_n. The assumed form of $X(t)$ (Equation A.11) may then be written as

$$X_n = \sum_{k=1}^{M} C_k \lambda_k^n \tag{A.12}$$

where

$$\lambda_k = e^{\gamma_k \Delta} \tag{A.12a}$$

This method of curve-fitting rests upon the observation that Equation A.12 is the solution to a linear finite difference equation with constant coefficients. This finite difference equation may be written for each consecutive group of $(L + 1)$ tabulated values of X_n as

$$\sum_{\ell=0}^{L} D_\ell X_{n+\ell} = 0 \tag{A.13}$$

where $D_L = 1$ and the remaining D's are to be determined. If $(P + 1)$ is the total number of tabulated values of X_n, Equation A.13 may be written $(P - L + 1)$ times, each equation corresponding to each of the values of n in the range

$$n = 0, 1, 2, \ldots, (P - L)$$

Consider the resulting set of simultaneous equations

$$\left.\begin{aligned} D_0X_0 + D_1X_1 + \ldots + D_{L-1}X_{L-1} &= -X_L \\ D_0X_1 + D_1X_2 + \ldots &= -X_{L+1} \\ \ldots & \\ \ldots & \\ D_0X_{P-L} + D_1X_{P-L} + \ldots &= -X_P \end{aligned}\right\} \tag{A.14}$$

where the X_n's are known from the tabulated function $X(t)$. This set of simultaneous equations consists of $(P - L + 1)$ equations in the $(L + 1)$ unknown D's. A solution to the system of equations is possible if $P \geq 2L$. When L, the number of exponential terms used to approximate $X(t)$, is chosen equal to $P/2$, the system has a unique solution if the determinant of the coefficients of X_n is nonzero. Normally, this condition exists and the unknown D's are determined by ordinary methods (see The Calculus of Observations by Whittaker, E. and Robinson, A.) and are used to form the characteristic equation which is the polynomial

$$0 = D_0 + D_1 \lambda + D_2 \lambda^2 + \ldots + D_{L-1} \lambda^{L-1} + \lambda^L \qquad \text{(A.15)}$$

The roots of Equation A.15 are the λ_k's referred to in Equation A.12 and, hence, may be used to determine the γ_k's which, in turn, are used to form the approximate representation of $X(t)$.

The actual determination of the γ_k's is considered now, since the roots of Equation A.15 may be positive, negative, or complex. Regardless of the type of root, λ_k can be written as

$$\lambda_k = |\lambda_k| \, e^{-i\theta} \qquad (i = \sqrt{-1})$$

where θ is equal to zero or pi (π) if λ_k is positive or negative, respectively. If λ_k is a complex root, θ is the Cauchy principle angle and lies between $-\pi$ and π. If λ_k is positive,

$$\gamma_k = \frac{1}{\Delta} \log \lambda_k \qquad \text{(A.16a)}$$

If λ_k is negative,

$$\gamma_k = \frac{1}{\Delta} \log (-\lambda_k) + \frac{i\pi}{\Delta} \qquad \text{(A.16b)}$$

In the latter case the imaginary part of γ_k is dropped, since it introduces an extraneous frequency whose period is 2Δ. The conclusion that this frequency is extraneous is based upon the observation that it is dependent only upon the choice of the tabulation

interval and, therefore, may be changed to any value by a suitable choice of interval.2/ Thus, for all real values of λ_k

$$\gamma_k = \frac{1}{\Delta} \log \lambda_k \tag{A.17a}$$

If λ_k is complex, it must be one of a conjugate pair and both pairs are contained in

$$\gamma_k = \frac{1}{\Delta} \log \lambda_k \pm \frac{i\theta}{\Delta} \tag{A.17b}$$

Having obtained the γ_k's from Equations A.17a and A.17b, the C_k's may be obtained from Equation A.12 in combination with the initial conditions. These conditions are satisfied if

$$\sum_{k=1}^{M} C_k = 0 \tag{A.18}$$

and

$$\sum_{k=1}^{M} \gamma_k C_k = 0 \tag{A.19}$$

2/ An alternate method of dropping the frequency induced by the negative roots is to consider only the even terms in Equation A.12. Equation A.12 becomes

$$X_{2n} = \sum_{k=1}^{M} C_k (\lambda_k^2)^n$$

And Equation A.12a becomes

$$(\lambda_k^2) = e^{\gamma_k (2\Delta)}$$

from which

$$\gamma_k = \frac{1}{2\Delta} \log (\lambda_k^2)$$

and X(t) again has the form of Equation A.12 where the extraneous frequency corresponding to π/Δ is not present.

Since Equation A.12 is to be satisfied for each tabulated value of X(t), there results the following P equations in (L - 2) unknowns,

$$\left.\begin{aligned} C_1\lambda_1 + C_2\lambda_2 + \ldots + C_L\lambda_L &= X_1 \\ C_1\lambda_1^2 + C_2\lambda_2^2 + \ldots + C_L\lambda_L^2 &= X_2 \\ &\vdots \\ C_1\lambda_1^P + C_2\lambda_2^P + \ldots \quad C_L\lambda_L^P &= X_P \end{aligned}\right\} \qquad (A.20)$$

where Equations A.18 and A.19 are to be used to eliminate two of the C_k's. The above system of equations is overdeterminate and usually inconsistent, since a finite number of terms is used to approximate X(t). The method of least squares is used to determine the most probable set of (L - 2) equations in the (L - 2) unknowns (see Numerical Mathematical Analysis, by J. B. Scarborough) and then this set of equations is solved for the C_k's.3/

Method C. A third method of curve-fitting utilizes an analog computer, and represents a rapid trial-and-error process. A discussion of this method is presented in Section 5.1.3.

A.5 DISCUSSION OF APPLICATION OF TRANSIENT ANALYSIS (METHOD B)

The application of transient analysis as described in Method B consists of the following steps:

a) The frequencies and exponents occurring in the expansion of the response curves (prime data) are determined by analogy with finite difference equations. The prime data is interpreted as representing the solution of a system of linear finite difference equations. The characteristic equation (polynomial) for this system of difference equations is constructed using the prime data and solved to obtain the characteristic roots. These roots, in turn, are taken as the desired frequencies and exponents of the response curve expansion.

b) Having obtained the frequencies and exponents of the response curve expansion, the amplitudes associated with each of the exponential terms are then determined by a straightforward least squares fit to the prime data.

c) With the expansion of the response curve determined, the forcing function is then associated with the real exponential terms and is obtained through Equation A.10.

3/ If $L < P/2$, the method of least squares is used to reduce the equations to a determinate number.

The success of the application of transient analysis to the predicting of actual forcing functions hinges upon several reasonable but crucial assumptions. First, and of utmost importance, is the assumption that the dynamic system producing the response curves be essentially linear. Just what magnitude of nonlinear effects such as stochastic errors, or baseline shifts are tolerable is not known at present, and indeed represents a major area of required investigation before any net force measurement technique of the present type can be evaluated. The effect of errors (known or unknown) in the prime data affect the analysis most critically in step a) above. In fact, if the frequencies and exponents determined in step a) are realistic, the success of the entire analysis appears to rest only upon the identification made in step c), which will be discussed presently. One criticism of the procedure in step a) for determining the all-important frequencies and exponents appears immediately as the result of using the prime data itself. Since these data in the present application are known to contain various types of errors, it would be desirable to incorporate some data-smoothing process prior to the application of transient analysis. There are several types of data-smoothing techniques available with various degrees of reliability and meaningfulness to the present application, but the most promising appears to be the use of the autocorrelation function. For the latter application, step a) would use the autocorrelation function defined as

$$\bar{X}(t) = \frac{1}{T} \int_0^T X(\tau)X(t + \tau)\, d\tau \qquad (A.21)$$

instead of the prime data, X(t), itself.4/

The autocorrelation function $\bar{X}(t)$ contains the same frequencies and exponentials as does the prime data, X(t), and smooths the data by eliminating stochastic and/or bias errors. This smoothing technique is being tried and tested at present in other and similar applications (see Operation TEAPOT Project 3.2, Study of Drag Loading on Structures in and out of the Precursor Zone, WT-1124). Of course, the analogy technique applied in step a) does itself perform some sort of averaging on the data fed in. Just what the nature of this averaging is, is not known at present. A perturbation study of the effect on the exponents and frequencies as determined by step a) is necessary before a realistic evaluation of transient analysis can be made. Because of the complications involved, such a study would, no doubt, have to be carried on in the sphere of numerical experimentation.

Step b) determines a "best fit" of the prime data. The fit obtained itself is, in many respects, a measure of the reliability of transient analysis in the present application. However, a realistic criteria for "goodness" of fit has not yet been established; at least, not in terms of the reliability or meaningfulness of the forcing function

4/ The fixed interval T is taken approximately as representing the extent of the data available.

so obtained. A point-by-point check on the fit may not be too meaningful, since the analysis, to be successful, must, of necessity, ignore "errors" in the prime data and pick out only pertinent information. However, the method of least squares as applied in step b) appears, at present, to have the most reliable characteristics for curve-fitting as applied in this application.

The procedure of step c) is based on the assumption that the forcing function is represented, or "sufficiently well" represented, by a sum of real exponentials. Just what is "sufficiently well" to assure success of transient analysis has not yet been determined. The limits of reliability could most likely (and probably have to) be determined by numerical experimentation, also.

Finally, the assumption that all forcing functions are timewise proportional needs to be considered. The first question to be answered is whether the forcing functions considered are essentially proportional or not. The second question to be answered is what is "sufficiently proportional" in terms of success of the application of transient analysis. Thirdly (since the first two questions have not as yet been answered), what happens to transient analysis if the forcing functions are not essentially timewise proportional? In particular, does the forcing function obtained by applying transient analysis in this latter case have any significance or yield any real information? Of these three questions, only the third can be answered (to some degree at least) at the present time.

In answer to the question of what happens if the forcing functions are not timewise proportional, the analysis of the preceding sections is repeated in brief as follows:
Equation A.6 is written in the form

$$X(t) = \sum_{k=1}^{N} \int_0^t f_k(\tau) \sum_{n=-N}^{N} \alpha_n^k e^{\lambda_n (t-\tau)} \, d\tau \qquad (A.22)$$

where the index j has been dropped, since the only concern is the response in a single degree of freedom. The forcing function $f_k(t)$ is written in the form

$$f_k(t) = \sum_{i=1}^{K} F_i^k e^{\alpha_i t} \qquad (A.23)$$

where the α_i range over all exponentials appearing in any of the degrees of freedom, so that some of the F_i^k may be zero. With Equation A.23 substituted in Equation A.22 and the integration performed, there results the equation:

$$X(t) = \sum_{i=1}^{K} \left[\sum_{k=1}^{N} \sum_{n=-N}^{N} \frac{F_i^k \alpha_n^k}{\alpha_i - \lambda_n} \right] e^{\alpha_i t} - \sum_{n=-N}^{N} \left[\sum_{k=1}^{N} \sum_{i=1}^{K} \frac{F_i \alpha_n^k}{\alpha_i - \lambda_n} \right] e^{\lambda_n t}$$

$$= \sum_{i=1}^{K} A_i e^{\alpha_i t} - \sum_{n=-N}^{N} B_n e^{\lambda_n t} \qquad \text{(A.24)}$$

which is precisely the same form as Equation A.9. However, the A_i and B_n are related to the forcing coefficients F_i^k and the transfer function coefficients α_n^k by

$$\left.\begin{aligned} A_i &= \sum_{k=1}^{N} \sum_{n=-N}^{N} \frac{F_i^k \alpha_n^k}{\alpha_i - \lambda_n} \\ B_n &= \sum_{k=1}^{N} \sum_{i=1}^{K} \frac{F_i^k \alpha_n^k}{\alpha_i - \lambda_n} \end{aligned}\right\} \qquad \text{(A.25)}$$

which are the counterparts of Equations A.10. The relationships between Equations A.10 and A.25 result in (dropping the index j)

$$\sum_{k=1}^{N} F_i^k \alpha_n^k = \beta_n F_i \qquad \text{(A.26)}$$

$$n = \pm 1, \pm 2, \ldots \pm N$$

$$i = 1, 2, \ldots K$$

Hence, the curve-fitting of step b) may be applied to Equation A.24 resulting in the A_i, α_i, B_n and λ_n which, in turn, are used in Equation A.10 to determine the β_n and F_i. However, step c) is not, in general, valid since the F_i are not the actual forcing function coefficients. In fact, there is no longer a single forcing function in question, but one for each degree of freedom. The actual forcing function coefficients F_i^k are related to the β_n and F_i by Equation A.26. However, in Equation A.26 only the β_n and F_i are known, while both sets of F_i^k and α_n^k are unknown. Since there are (2N) x K equations in Equation A.26 and (2N) x K x N unknowns, Equation A.26 does not, in general, determine the actual forcing function coefficients F_i^k uniquely and an infinitude of solution may be constructed. It should be mentioned, however, that some information about the forcing functions has already been determined in step b); namely, <u>all</u> the exponents α_i appearing in <u>any</u> of forcing

functions $f_k(t)$ have been determined, and Equation A.26 represents a number (even though, in general, not enough), of necessary conditions on the coefficients F_i^k. Certain auxiliary information about either or both the dynamic system or forcing functions obtained analytically or experimentally together with Equation A.26 can, in certain instances, determine a unique set of coefficients F_i^k. For example, if curve-fitting results in but one real exponential, transient analysis yields a unique forcing function (in a trial way, of course).

It is interesting to see how the assumption of timewise proportionality of forcing functions, together with Equation A.26, yields a unique solution (as it must, by previous considerations).

The assumption of proportionality is equivalent to Equations A.24, A.6a and A.8:

$$F_i^k = C_k F_i \quad \text{for each} \quad i \quad \text{and} \quad k \tag{A.27}$$

so that Equation A.26 may be written

$$\sum_{k=1}^{N} C_k F_i \alpha_n^k = \left[\sum_{k=1}^{N} C_k \alpha_n^k \right] F_i = \beta_n F_i \tag{A.28}$$

$$n = \pm 1, \pm 2, \ldots \pm N$$

$$i = 1, 2, \ldots K$$

which identifies the F_i, as well as the

$$\beta_n = \sum_{k=1}^{N} C_k \alpha_n^k$$

of Equation A.7a[5] uniquely, since the right members of Equation A.28 are known. In effect the assumption of proportionality uncouples Equation A.26 (which is generally coupled in the independent indices i and n) into two independent sets of equations

$$F_i = F_i \; ; \; i = 1, 2, \ldots, K$$

and

$$\sum_{k=1}^{N} C_k \alpha_n^k = \beta_n; \quad n = \pm 1, \pm 2, \ldots \pm N$$

5/ Dropping the index j.

Less drastic assumptions regarding the forcing functions or transfer functions could be expected to yield additional information about the forcing functions. For example, if Equation A.26 is summed with respect to i, there results

$$\sum_{k=1}^{N} \left[\sum_{i=1}^{K} F_i^k \right] \alpha_n^k = \beta_n \left[\sum_{i=1}^{K} F_i \right] \tag{A.29}$$

The inner sum

$$\sum_{i=1}^{K} F_i^k$$

is clearly (see Equation A.23) the quantity $f_k(0)$ which is the magnitude of the forcing function in the kth component at time $t = 0$. Hence, Equation A.29 may be written:

$$\sum_{k=1}^{N} f_k(0) \alpha_n^k = \beta_n \sum_{i=1}^{N} F_i \tag{A.30}$$

$$n = \pm 1, \pm 2, \ldots, \pm N$$

It is possible that at least the relative magnitudes (if not the absolute magnitudes) of the $f_k(0)$ can be estimated from theory, etc., so that Equation A.30 could be used to yield additional independent conditions on the unknowns of Equation A.26. If the absolute magnitudes of the $f_i^k(0)$ are known, Equation A.30 yields 2N additional equations. If only their relative magnitudes are known, 2N-1 additional equations result.

Another possibility is that some of the F_i^k may be known from other considerations, in effect reducing the number of unknowns in Equation A.26. For example, some degrees of freedom may not admit a forcing function and are known to be excited only through coupling with other degrees. Hence, the corresponding F_i^k are zero. Certain timewise proportionality conditions may also exist between certain degrees of freedom, such as the set of all bending modes, further reducing the number of unknowns.

BIBLIOGRAPHY

Operation UPSHOT-KNOTHOLE, Project 3.1, Tests on the Loading of Building and Equipment Shapes, by E. Gallagher and T. Schiffman, WT-721. SECRET-RESTRICTED DATA

Operation UPSHOT-KNOTHOLE, Project 3.26.1, Tests of the Effects on POL Installations, by E. Sevin and F. B. Porzel, WT-736. SECRET-RESTRICTED DATA

Operation UPSHOT-KNOTHOLE, Project 3.28.1, Structures Instrumentation, Ballistic Research Laboratories, WT-738.

Operation UPSHOT-KNOTHOLE, Project 3.4, Tests on the Loading of Truss Systems Common to Open-Framed Structures, by E. Sevin, WT-723. CONFIDENTIAL-RESTRICTED DATA

Operation UPSHOT-KNOTHOLE, Summary Report of the Technical Director, by E. B. Doll, WT-782. SECRET-RESTRICTED DATA

Armour Research Foundation, Air Force Structures Program 3.3 of Operation JANGLE, Contract No. AF33(038)-20054, Final Report, WT-405 Vol. I, November, 1952. SECRET

Operation TEAPOT, Air Force Project 3.2, Study of Drag Loading of Structures in and out of the Precursor Zone, WT-1124. TO BE PUBLISHED

Armour Research Foundation, Planning Program for Air Force Structures Tests, Final Report, Part I, Oil Storage and Equipment Tests, Contract No. AF33(038)-30029, October, 1952. SECRET

Armour Research Foundation, Planning Program for Air Force Structures Tests, Final Report, Part V, Regular Reflection on Cubical Structures, Contract No. AF33(038)-30029, March, 1953. SECRET

Armour Research Foundation, Planning Program for Air Force Structures Tests, Final Report, Part VI, Tests on Horizontal Cylinders, Contract No. AF33(038)-30029. SECRET

Bleakney, W., The Diffraction of Shock Waves Around Obstacles and the Resulting Transient Loading of Structures, Physics Department, Princeton University, Technical Report II-3, March, 1950.

Hoerner, S. F., Aerodynamic Drag, The Otterbein Press, 1951.

Love, A. E. H., Mathematical Theory of Elasticity, Fourth Ed., Dover Publications, New York, 1944.

Roberts, A. M., Elastic Structures Under Rapidly Applied Loading - III, Mechanical World and Engineering Record, May 15, 1936, Vol. XCIX, No. 2574.

Scarborough, J. B., Numerical Mathematical Analysis, The Johns Hopkins Press, 1950.

Timoshenko, S., Vibration Problems in Engineering, D. Van Nostrand Co. Inc., New York, 1937.

Whittaker, E. and Robinson, A., The Calculus of Observations, Fourth Ed., Blockie and Son Ltd., London, 1944.

DISTRIBUTION

Military Distribution Categories 5-21 and 5-60

ARMY ACTIVITIES

1 Asst. Chief of Staff, G-3, D/A, Washington 25, D.C. ATTN: Dep. CofS, G-3 (RR&SW)
2 Chief of Research and Development, D/A, Washington 25, D.C. ATTN: Special Weapons and Air Defense Division
3 Chief of Ordnance, D/A, Washington 25, D.C. ATTN: ORDTX-AR
4- 6 Chief Signal Officer, D/A, P&O Division, Washington 25, D.C. ATTN: SIGOP
7 The Surgeon General, D/A, Washington 25, D.C. ATTN: Chief, R&D Division
8- 9 Chief Chemical Officer, D/A, Washington 25, D.C.
10 The Quartermaster General, D/A, Washington 25, D.C. ATTN: Research and Development Div.
11- 15 Chief of Engineers, D/A, Washington 25, D.C. ATTN: ENGNB
16 Chief of Transportation, Military Planning and Intelligence Div., Washington 25, D.C.
17- 19 Commanding General, Continental Army Command, Ft. Monroe, Va.
20 President, Board #1, Headquarters, Continental Army Command, Ft. Sill, Okla.
21 President, Board #2, Headquarters, Continental Army Command, Ft. Knox, Ky.
22 President, Board #3, Headquarters, Continental Army Command, Ft. Benning, Ga.
23 President, Board #4, Headquarters, Continental Army Command, Ft. Bliss, Tex.
24 Commanding General, U.S. Army Caribbean, Ft. Amador, C.Z. ATTN: Cml. Off.
25 Commander-in-Chief, European Command, APO 128, c/o PM, New York, N.Y.
26- 27 Commander-in-Chief, Far East Command, APO 500, c/o PM, San Francisco, Calif. ATTN: ACofS, J-3
28- 29 Commanding General, U.S. Army Europe, APO 403, c/o PM, New York, N.Y. ATTN: OPOT Div., Combat Dev. Br.
30- 31 Commandant, Command and General Staff College, Ft. Leavenworth, Kan. ATTN: ALLLS(AS)
32 Commandant, The Artillery and Guided Missile School, Ft. Sill, Okla.
33 Secretary, The Antiaircraft Artillery and Guided Missile School, Ft. Bliss, Texas. ATTN: Maj. George L. Alexander, Dept. of Tactics and Combined Arms
34 Commanding General, Medical Field Service School, Brooke Army Medical Center, Ft. Sam Houston, Tex.
35 Director, Special Weapons Development Office, Headquarters, CONARC, Ft. Bliss, Tex. ATTN: Lt. Arthur Jaskierny
36 Commandant, Army Medical Service Graduate School, Walter Reed Army Medical Center, Washington 25, D.C.
37 Superintendent, U.S. Military Academy, West Point, N.Y. ATTN: Prof. of Ordnance
38 Commandant, Chemical Corps School, Chemical Corps Training Command, Ft. McClellan, Ala.
39 Commanding General, Research and Engineering Command, Army Chemical Center, Md. ATTN: Deputy for RW and Non-Toxic Material
40- 41 Commanding General, Aberdeen Proving Grounds, Md. (inner envelope) ATTN: RD Control Officer (for Director, Ballistics Research Laboratory)
42- 44 Commanding General, The Engineer Center, Ft. Belvoir, Va. ATTN: Asst. Commandant, Engineer School
45 Commanding Officer, Engineer Research and Development Laboratory, Ft. Belvoir, Va. ATTN: Chief, Technical Intelligence Branch
46 Commanding Officer, Picatinny Arsenal, Dover, N.J. ATTN: ORDBB-TK
47 Commanding Officer, Army Medical Research Laboratory, Ft. Knox, Ky.
48- 49 Commanding Officer, Chemical Corps Chemical and Radiological Laboratory, Army Chemical Center, Md. ATTN: Tech. Library
50 Commanding Officer, Transportation R&D Station, Ft. Eustis, Va.
51 Director, Technical Documents Center, Evans Signal Laboratory, Belmar, N.J.
52 Director, Waterways Experiment Station, PO Box 631, Vicksburg, Miss. ATTN: Library
53 Director, Armed Forces Institute of Pathology, 7th and Independence Avenue, S.W., Washington 25, D.C.
54 Director, Operations Research Office, Johns Hopkins University, 7100 Connecticut Ave., Chevy Chase, Md. Washington 15, D.C.
55- 56 Commanding General, Quartermaster Research and Development Command, Quartermaster Research and Development Center Natick, Mass. ATTN: CBR Liaison Officer
57- 63 Technical Information Service, Oak Ridge, Tenn. (Surplus)

NAVY ACTIVITIES

64- 65 Chief of Naval Operations, D/N, Washington 25, D.C. ATTN: OP-36
66 Chief of Naval Operations, D/N, Washington 25, D.C. ATTN: OP-03EG
67 Director of Naval Intelligence, D/N, Washington 25, D.C. ATTN: OP-922V
68 Chief, Bureau of Medicine and Surgery, D/N, Washington 25, D.C. ATTN: Special Weapons Defense Div.
69 Chief, Bureau of Ordnance, D/N, Washington 25, D.C.
70 Chief, Bureau of Ships, D/N, Washington 25, D.C. ATTN: Code 348
71 Chief, Bureau of Yards and Docks, D/N, Washington 25, D.C. ATTN: D-440
72 Chief, Bureau of Supplies and Accounts, D/N, Washington 25, D.C.
73- 74 Chief, Bureau of Aeronautics, D/N, Washington 25, D.C.
75 Chief of Naval Research, Department of the Navy Washington 25, D.C. ATTN: Code 811
76 Commander-in-Chief, U.S. Pacific Fleet, Fleet Post Office, San Francisco, Calif.
77 Commander-in-Chief, U.S. Atlantic Fleet, U.S. Naval Base, Norfolk 11, Va.
78- 81 Commandant, U.S. Marine Corps, Washington 25, D.C. ATTN: Code AO3H
82 President, U.S. Naval War College, Newport, R.I.
83 Superintendent, U.S. Naval Postgraduate School, Monterey, Calif.
84 Commanding Officer, U.S. Naval Schools Command, U.S. Naval Station, Treasure Island, San Francisco, Calif.
85 Commanding Officer, U.S. Fleet Training Center, Naval Base, Norfolk 11, Va. ATTN: Special Weapons School
86- 87 Commanding Officer, U.S. Fleet Training Center, Naval Station, San Diego 36, Calif. ATTN: (SPWP School)
88 Commanding Officer, Air Development Squadron 5, VX-5, U.S. Naval Air Station, Moffett Field, Calif.
89 Commanding Officer, U.S. Naval Damage Control Training Center, Naval Base, Philadelphia 12, Pa. ATTN: ABC Defense Course
90 Commanding Officer, U.S. Naval Unit, Chemical Corps School, Army Chemical Training Center, Ft. McClellan, Ala.
91 Commander, U.S. Naval Ordnance Laboratory, Silver Spring 19, Md. ATTN: EE

92 Commander, U.S. Naval Ordnance Laboratory, Silver Spring 19, Md. ATTN: EH
93 Commander, U.S. Naval Ordnance Laboratory, Silver Spring 19, Md. ATTN: R
94 Commander, U.S. Naval Ordnance Test Station, Inyokern, China Lake, Calif.
95 Officer-in-Charge, U.S. Naval Civil Engineering Res. and Evaluation Lab., U.S. Naval Construction Battalion Center, Port Hueneme, Calif. ATTN: Code 753
96 Commanding Officer, U.S. Naval Medical Research Inst., National Naval Medical Center, Bethesda 14, Md.
97 Director, Naval Air Experimental Station, Air Material Center, U.S. Naval Base, Philadelphia, Penn.
98 Director, U.S. Naval Research Laboratory, Washington 25, D.C. ATTN: Code 2029
99 Commanding Officer and Director, U.S. Navy Electronics Laboratory, San Diego 52, Calif. ATTN: Code 4223
100-101 Commanding Officer, U.S. Naval Radiological Defense Laboratory, San Francisco 24, Calif. ATTN: Technical Information Division
102-103 Commanding Officer and Director, David W. Taylor Model Basin, Washington 7, D.C. ATTN: Library
104 Commander, U.S. Naval Air Development Center, Johnsville, Pa.
105 Director, Office of Naval Research Branch Office, 1000 Geary St., San Francisco, Calif.
106-111 Technical Information Service, Oak Ridge, Tenn. (Surplus)

AIR FORCE ACTIVITIES

112 Asst. for Atomic Energy, Headquarters, USAF, Washington 25, D.C. ATTN: DCS/O
113 Director of Operations, Headquarters, USAF, Washington 25, D.C. ATTN: Operations Analysis
114 Director of Plans, Headquarters, USAF, Washington 25, D.C. ATTN: War Plans Div.
115 Director of Research and Development, Headquarters, USAF, Washington 25, D.C. ATTN: Combat Components Div.
116-117 Director of Intelligence, Headquarters, USAF, Washington 25, D.C. ATTN: AFOIN-IB2
118 The Surgeon General, Headquarters, USAF, Washington 25, D.C. ATTN: Bio. Def. Br., Pre. Med. Div.
119 Deputy Chief of Staff, Intelligence, Headquarters, U.S. Air Forces Europe, APO 633, c/o PM, New York, N.Y. ATTN: Directorate of Air Targets
120 Commander, 497th Reconnaissance Technical Squadron (Augmented), APO 633, c/o PM, New York, N.Y.
121 Commander, Far East Air Forces, APO 925, c/o PM, San Francisco, Calif.
122 Commander-in-Chief, Strategic Air Command, Offutt Air Force Base, Omaha, Nebraska. ATTN: Special Weapons Branch, Inspector Div., Inspector General
123 Commander, Tactical Air Command, Langley AFB, Va. ATTN: Documents Security Branch
124 Commander, Air Defense Command, Ent AFB, Colo.
125-126 Commander, Wright Air Development Center, Wright-Patterson AFB, Dayton, O. ATTN: WCRRN, Blast Effects Research
127 Commander, Air Training Command, Scott AFB, Belleville, Ill. ATTN: DCS/O GTP
128 Assistant Chief of Staff, Installations, Headquarters, USAF, Washington 25, D.C. ATTN: AFCIE-E
129 Commander, Air Research and Development Command, PO Box 1395, Baltimore, Md. ATTN: RDDN
130 Commander, Air Proving Ground Command, Eglin AFB, Fla. ATTN: AG/TRB
131-132 Director, Air University Library, Maxwell AFB, Ala.
133-140 Commander, Flying Training Air Force, Waco, Tex. ATTN: Director of Observer Training
141 Commander, Crew Training Air Force, Randolph Field, Tex. ATTN: 2CTS, DCS/O
142 Commander, Headquarters, Technical Training Air Force, Gulfport, Miss. ATTN: TA&D
143-144 Commandant, Air Force School of Aviation Medicine, Randolph AFB, Tex.
145-150 Commander, Wright Air Development Center, Wright-Patterson AFB, Dayton, O. ATTN: WCOSI
151-152 Commander, Air Force Cambridge Research Center, LG Hanscom Field, Bedford, Mass. Attn: CRQST-2
153-155 Commander, Air Force Special Weapons Center, Kirtland AFB, N. Mex. ATTN: Library
156 Commandant, USAF Institute of Technology, Wright-Patterson AFB, Dayton, O. ATTN: Resident College
157 Commander, Lowry AFB, Denver, Colo. ATTN: Department of Armament Training
158 Commander, 1009th Special Weapons Squadron, Headquarters, USAF, Washington 25, D.C.
159-160 The RAND Corporation, 1700 Main Street, Santa Monica, Calif. ATTN: Nuclear Energy Division
161 Commander, Second Air Force, Barksdale AFB, Louisiana. ATTN: Operations Analysis Office
162 Commander, Eighth Air Force, Westover AFB, Mass. ATTN: Operations Analysis Office
163 Commander, Fifteenth Air Force, March AFB, Calif. ATTN: Operations Analysis Office
164-170 Technical Information Service, Oak Ridge, Tenn. (Surplus)

OTHER DEPARTMENT OF DEFENSE ACTIVITIES

171 Asst. Secretary of Defense, Research and Development, D/D, Washington 25, D.C. ATTN: Tech. Library
172 U.S. Documents Officer, Office of the U.S. National Military Representative, SHAPE, APO 55, New York, N.Y.
173 Director, Weapons Systems Evaluation Group, OSD, Rm 2E1006, Pentagon, Washington 25, D.C.
174 Armed Services Explosives Safety Board, D/D, Building T-7, Gravelly Point, Washington 25, D.C.
175 Commandant, Armed Forces Staff College, Norfolk 11, Va. ATTN: Secretary
176-181 Commanding General, Field Command, Armed Forces Special Weapons Project, PO Box 5100, Albuquerque, N. Mex.
182-183 Commanding General, Field Command, Armed Forces, Special Weapons Project, PO Box 5100, Albuquerque, N. Mex. ATTN: Technical Training Group
184-192 Chief, Armed Forces Special Weapons Project, Washington 25, D.C. ATTN: Documents Library Branch
193 Office of the Technical Director, Directorate of Effects Tests, Field Command, AFSWP, PO Box 577, Menlo Park, Calif. ATTN: Dr. E. B. Doll
194-200 Technical Information Service, Oak Ridge, Tenn. (Surplus)

ATOMIC ENERGY COMMISSION ACTIVITIES

201-203 U.S. Atomic Energy Commission, Classified Technical Library, 1901 Constitution Ave., Washington 25, D.C. ATTN: Mrs. J. M. O'Leary (For DMA)
204-205 Los Alamos Scientific Laboratory, Report Library, PO Box 1663, Los Alamos, N. Mex. ATTN: Helen Redman
206-210 Sandia Corporation, Classified Document Division, Sandia Base, Albuquerque, N. Mex. ATTN: Martin Lucero
211-213 University of California Radiation Laboratory, PO Box 808, Livermore, Calif. ATTN: Margaret Edlund
214 Weapon Data Section, Technical Information Service, Oak Ridge, Tenn.
215-274 Technical Information Service, Oak Ridge, Tenn. (Surplus)